Analysis of fetal heart rate variability from non-invasive electrocardiography recordings

Document Version:
Publisher's PDF, also known as Version of Record (includes final page, issue and volume numbers)

Please check the document version of this publication:

• A submitted manuscript is the version of the article upon submission and before peer-review. There can be important differences between the submitted version and the official published version of record. People interested in the research are advised to contact the author for the final version of the publication, or visit the DOI to the publisher's website.
• The final author version and the galley proof are versions of the publication after peer review.
• The final published version features the final layout of the paper including the volume, issue and page numbers.

[Link to publication](#)

Analysis of fetal heart rate variability from non-invasive electrocardiography recordings

Guy Warmerdam

Analysis of fetal heart rate variability from non-invasive electrocardiography recordings

Guy Warmerdam

Analysis of fetal heart rate variability from non-invasive electrocardiography recordings

PROEFSCHRIFT

ter verkrijging van de graad van doctor aan de Technische Universiteit Eindhoven, op gezag van de rector magnificus prof.dr.ir. F.P.T. Baaijens, voor een commissie aangewezen door het College voor Promoties, in het openbaar te verdedigen op maandag 30 april 2018 om 13:30 uur

door

Guy Johannes Jacobus Warmerdam

geboren te Nijmegen

Dit proefschrift is goedgekeurd door de promotoren en de samenstelling van de promotiecommissie is als volgt:

voorzitter:	prof.dr.ir. A.B. Smolders
1^e promotor:	prof.dr.ir. J.W.M. Bergmans
2^e promotor:	prof.dr. S.G. Oei
copromotoren:	dr.ir. R. Vullings
	dr. J.O.E.H. Van Laar (Máxima Medisch Centrum)
leden:	prof.dr. R. Barbieri (Politecnico di Milano)
	prof.dr. D. Ayres-de-Campos (Universidade de Lisboa)
	dr.ir. P.J.A. Harpe
adviseur:	dr. L. Schmitt (Grünenthal Group)

Analysis of fetal heart rate variability from non-invasive electro-cardiography recordings

Each year, over 6 millions deaths occur worldwide that are related to obstetric events. One of the major sources for obstetric complications is fetal oxygen deficiency during labor. Monitoring of the fetal condition is essential to allow for timely clinical intervention and prevent damaging of the central organs of the fetus. The technique that is currently used for fetal monitoring, i.e. cardiotocography (CTG), monitors changes in the fetal heart rate in response to uterine contractions. However, interpretation of the CTG suffers from a high false alarm rate. This means that an abnormal CTG can also be encountered for healthy fetuses, leading to unnecessary operative deliveries. Although there are techniques that provide complementary information to CTG, these are often obtrusive, and can only be used after sufficient cervical dilatation and rupturing of the fetal membranes. This limits their use in clinical practice. Hence, additional unobtrusive information about the fetal condition is needed.

One of the most important features to assess in fetal monitoring is fetal heart rate variability (HRV). As the fetal heart rate is regulated by the autonomic nervous system, variations in the fetal heart rate can indirectly provide information about fetal distress. Despite the importance of fetal HRV, unobtrusive fetal heart information is generally obtained using Doppler ultrasound, which has the drawback that it does not provide accurate, beat-to-beat, fetal heart rate information. This makes fetal heart rate from Doppler ultrasound less suited for analysis of fetal HRV. Alternatively, beat-to-beat fetal heart rate information can be obtained unobtrusively from the non-invasive fetal electrocardiogram (ECG), that is recorded by electrodes on the maternal abdomen. Besides a more accurate fetal heart rate estimation, analysis of fetal ECG morphology can also provide information about the fetal condition. Unfortunately, the non-invasiveness comes at the cost of a low signal-to-noise ratio (SNR) of the fetal ECG. In this thesis, we aim to advance the use of the non-invasive fetal ECG as a monitoring technique. To this end, the signal quality of the non-invasive fetal ECG is improved and the potential of beat-to-beat fetal HRV analysis for detection of fetal distress is examined.

First, the power line interference (PLI) is suppressed to enhance the quality of the fetal ECG. Filtering PLI from ECG recordings can lead to significant distortion of the ECG and mask clinically relevant features in ECG waveform morphology. This is particularly true for filtering PLI from fetal ECG recordings, as the PLI frequency strongly overlaps with the frequency content of the fetal ECG. The adaptive smoothing filter that is proposed in this thesis to suppress

the PLI leads to minimal distortion of the ECG waveform. The proposed method is demonstrated to have a superior quality ECG after PLI suppression compared to other PLI filters.

After PLI suppression, a method is developed for reliable detection of the fetal heart rate. Detecting fetal heart rate from non-invasive fetal ECG recordings is challenging due to the low SNR. The fetal ECG signal is strongly attenuated by the tissue layers between the fetal heart and the abdominal electrodes. As a result, electrical interferences often have a larger amplitude than the fetal ECG. Moreover, as the fetal ECG waveform that is recorded by the abdominal electrodes depends on the orientation of the fetus within the abdomen, changes in fetal orientation can result in changes in the fetal ECG waveform. To overcome these difficulties, our method for heart rate detection combines predictive models of the ECG waveform and heart rate in a probabilistic framework. The developed method outperforms other methods that have been proposed in the literature, and provides reliable fetal heart rate information even for low and varying SNR conditions.

In the second part of this thesis, beat-to-beat fetal heart rate is used to address some of the major challenges related to analysis of fetal HRV. During labor, uterine contractions can cause fluctuations in the intrauterine pressure that can strongly influence the fetal cardiovascular system and thus fetal HRV. It is shown that the use of contraction-dependent HRV features increases the diagnostic value of HRV analysis for the detection of fetal distress. Next to the influence from varying uterine pressure, fetal HRV also depends on maturation of the autonomic nervous system and can be influenced by some types of medications. In two prospective cohort studies, the effect of maturation and medication on fetal HRV is examined using non-invasive fetal ECG recordings.

The clinical application of the non-invasive fetal ECG is still in its infancy. The work presented in this thesis has hopefully brought the non-invasive fetal ECG one step closer to clinical use.

SAMENVATTING

Analyse van foetale hartritmevariabiliteit uit niet-invasieve electrocardiogram metingen

Elk jaar overlijden er wereldwijd meer dan 6 miljoen kinderen als gevolg van complicaties in de zwangerschap. Een van de belangrijkste oorzaken voor deze complicaties is foetaal zuurstoftekort tijdens de bevalling. Het bewaken van de foetale conditie is van essentieel belang om tijdig medisch ingrijpen mogelijk te maken en schade aan de centrale organen van de foetus te voorkomen. De bestaande technologie voor foetale bewaking, cardiotocografie (CTG), meet veranderingen in het foetale hartritme als reactie op weeën. Interpretatie van het CTG is echter lastig en leidt vaak tot onterecht alarmerende conclusies. Dit komt doordat abnormale CTG patronen ook voor kunnen komen in gevallen waar geen sprake is van foetale nood. Deze verkeerde interpretatie kan leiden tot onnodig medisch ingrijpen. Naast het CTG zijn er technieken die aanvullende informatie geven over de foetale conditie, maar deze technieken zijn vaak belastend voor moeder en kind en kunnen pas worden gebruikt bij voldoende ontsluiting en nadat de vliezen zijn gebroken. Dit beperkt het gebruik van deze technieken in de klinische praktijk. Er is daarom aanvullende informatie nodig over de foetale conditie die op een niet-belastende manier kan worden verkregen.

Een belangrijke bron van informatie voor foetale bewaking is foetale hartritmevariabiliteit (HRV). Omdat het foetale hartritme wordt aangestuurd door het autonome zenuwstelsel, kunnen variaties in het foetale hartritme indirect iets zeggen over foetale nood. De huidige manier om het foetale hartritme op een niet-belastende, uitwendige, wijze te meten is door middel van Doppler ultrageluid. Het nadeel hiervan is echter dat Doppler ultrageluid relatief onnauwkeurige informatie geeft over het foetale hartritme. Als alternatief is het mogelijk om het foetale hartritme te verkrijgen uit het niet-invasieve foetale electrocardiogram (ECG), dat wordt gemeten met elektrodes op de buik van de moeder. Naast een nauwkeurig foetaal hartritme, geeft deze techniek mogelijk nog extra informatie over de foetale conditie door analyse van de foetale ECG-golfvorm. Helaas gaat het niet-invasieve karakter ten koste van de signaalkwaliteit van het foetale ECG. Met dit proefschrift willen we het gebruik van het niet-invasieve foetale ECG als bewakingstechniek bevorderen. Hiervoor worden methodes ontwikkeld om de signaalkwaliteit van het niet-invasieve foetale ECG te verbeteren en wordt onderzoek gedaan naar de potentie van analyse van foetale HRV voor het detecteren van foetale nood.

Eerst worden verstoringen door het spanningsnet (PLI; power line interference) onderdrukt om de signaalkwaliteit van het niet-invasieve foetale ECG te

verbeteren. Het onderdrukken van PLI in ECG metingen kan leiden tot substantiële vervormingen van het ECG en kan daarmee klinisch relevante informatie van de ECG-golfvorm maskeren. Dit geldt in het bijzonder voor het onderdrukken van PLI in het foetale ECG, omdat de frequentie van het spanningsnet sterk overlapt met de frequentie inhoud van het foetale ECG. De adaptieve methode voor het onderdrukken van de PLI die in dit proefschrift is beschreven geeft minimale verstoringen van de ECG-golfvorm. In een vergelijking met bestaande methodes voor PLI-onderdrukking wordt aangetoond dat de kwaliteit van het ECG na PLI-onderdrukking met de ontwikkelde methode superieur is.

Na onderdrukking van de PLI is een methode ontwikkeld voor betrouwbare detectie van het foetale hartritme. Het detecteren van het foetale hartritme in niet-invasieve foetale ECG metingen is een uitdaging vanwege de lage signaalkwaliteit. Het signaal van het foetale ECG wordt sterk verzwakt door de verschillende weefsels tussen het foetale hart en de elektrodes op de buik van de moeder. Door deze verzwakking hebben elektrische verstoringen vaak een grotere amplitude dan het foetale ECG. Daarnaast is de golfvorm van het foetale ECG gemeten op de buik van de moeder afhankelijk van de houding van de foetus in de baarmoeder. Veranderingen in deze houding kunnen leiden tot veranderingen in de golfvorm van het foetale ECG. Om deze moeilijkheden te ondervangen, combineert de ontwikkelde methode voor detectie van het hartritme voorspellende modellen van het foetale ECG en hartritme. De methode werkt aantoonbaar beter dan bestaande methodes die in de literatuur worden beschreven en geeft zelfs voor lage en variërende signaalkwaliteit betrouwbare informatie van het foetale hartritme.

In het tweede deel van dit proefschrift worden enkele van de belangrijkste problemen bij het analyseren van foetale HRV onderzocht. Tijdens de bevalling veroorzaken weeën een sterk variërende druk in de baarmoeder. Deze veranderingen in druk kunnen een grote invloed hebben op het foetale cardiovasculaire systeem en daarmee op foetale HRV. Er wordt aangetoond dat de diagnostische waarde van analyse van HRV voor het detecteren van foetale nood toeneemt door maten voor HRV te gebruiken die afhangen van de activiteit van de baarmoeder. Naast de invloed van variërende druk in de baarmoeder, wordt foetale HRV ook beïnvloed door de ontwikkeling van het autonome zenuwstelsel en door toediening van verschillende medicijnen. In twee prospectieve studies wordt de invloed van ontwikkeling van het zenuwstelsel en toediening van medicatie op foetale HRV onderzocht.

Het gebruik van het niet-invasieve foetale ECG in de kliniek staat nog in de kinderschoenen. Hopelijk brengt het werk dat in dit proefschrift wordt beschreven het niet-invasieve foetale ECG een stap dichter bij klinische toepassing.

CONTENTS

ABBREVIATIONS

ANS	Autonomic nervous system
AUC	Area under the ROC curve
AV	Atrioventricular (node)
BMI	Body mass index
BPM	Beats per minute
CTG	Cardiotocography
CWT	Continuous Wavelet Transform
DFA	Detrended Fluctuation Analysis
DSP	Digital signal processor
ECG	Electrocardiogram
EHG	Electrohysterogram
EMG	Electromyogram
FBS	Fetal blood sampling
FHR	Fetal heart rate
FIR	Finite impulse response
GA	Genetic Algorithm
HRV	Heart rate variability
IAC	Improved Adaptive Canceller
IIR	Infinite impulse response
IUPC	Intra-uterine pressure catheter
KF	Kalman filter
KS	Kalman smoother
LMS	Least-mean-square
MAP	Maximum *a posteriori*
MPS	Multiplications per sample
PLI	Power line interference
PRSA	Phase Rectified Signal Averaging
rbf	Radial base function
RMS	Root mean square
ROC	Receiver operating characteristic
SA	Sinoatrial (node)
SD	Standard deviation
Se	Sensitivity
SNR	Signal-to-noise ratio

Sp	Specificity
STFT	Short Term Fourier Transform
SVM	Support Vector Machine
UA	Uterine activity
US	Ultrasound
VCG	Vectorcardiogram
wG	Weeks of gestation

1

INTRODUCTION

1.1 Motivation

One of the most difficult periods in fetal life is labor. During this critical period, the fetus is exposed to temporary oxygen deficiency [1]. Generally, a healthy fetus is capable of handling this kind of stress and will develop normally. However, in case of severe or prolonged oxygen deficiency, the fetus might be unable to respond and low oxygen concentration can occur in the central organs (a state called asphyxia) [2]. The World Health Organisation estimated that 4 million neonatal deaths occur every year [3], of which 0.9 million are related to birth asphyxia [4]. Additionally, one third of the 3.3 million fetal deaths that occur every year happens during labor [3]. Perinatal mortality (deaths that occur during obstetric events or the first week of life) is five times more common in low-income countries compared to high income countries [3]. To allow for timely intervention before asphyxia develops, it is of vital importance to accurately monitor the fetal condition during labor.

The introduction of cardiotocography (CTG) in the 1960s has enabled continuous fetal monitoring [5]. CTG simultaneously records the fetal heart rate (FHR) and uterine activity (UA). CTG allows clinicians to evaluate the fetal response to the stress caused by uterine contractions and it is currently the main source of information to assess fetal distress [6, 7]. In Fig. 1.1, an example is shown of a CTG recording. Although CTG is the current standard for fetal monitoring, its diagnostic value is limited [8, 9]. CTG patterns are interpreted visually, but the inter- and intra-observer variability of CTG interpretation is high [10]. Moreover, the specificity of CTG interpretation is low and the introduction of the CTG has led to an increase in the rate of unnecessary operative deliveries, without improvement in fetal outcome [7, 9].

There are several diagnostic tools complementary to CTG that clinicians can use during labor [11]. The most important include fetal blood sampling (FBS) [12] and continuous analysis of the fetal electrocardiogram (ECG) [13, 14]. In FBS, a small droplet of fetal blood is obtained and analyzed to acquire information about the fetal acid-base balance, which is related to the oxygen concentration in the fetal blood. However, FBS only provides instantaneous information and requires repeated measurements if the CTG remains abnormal. Besides the instantaneous information of FBS, continuous analysis of the fetal ECG waveform is provided by the STAN® (Neoventa Medical, Mölndal, Sweden). The

ECG reflects the electrical activity of the heart and STAN focuses on a specific segment of the ECG, the ST-segment, that might change under influence of fetal distress [15–17]. STAN records the fetal ECG invasively from an electrode attached to the fetal scalp. Although initial results of using STAN to improve fetal outcome seemed promising [18, 19], subsequent trials could not reproduce these findings [20–23]. Moreover, the STAN guidelines state that STAN alarms should be ignored when the CTG is reassuring [24, 25]. Because of the high inter- and intra-observer variability of CTG interpretation, this dependency of STAN on CTG interpretation restricts the success of STAN.

In addition to the limited diagnostic value of FBS and STAN [26, 27], both techniques are invasive. Hence, there is a small risk of serious complications such as haemorrhage and infections [12, 28]. Furthermore, FBS and STAN can only be used after the fetal membranes have ruptured, meaning that these techniques cannot be used during pregnancy or in case of threatening pre-term labor. Therefore, there is a need for a non-invasive method that provides more reliable information about the fetal condition.

In clinical practice, visual interpretation of fetal heart rate variability (HRV) is one of the most important aspects in CTG monitoring [7]. Since the heart rate is regulated by the autonomic nervous system (ANS), the presence of variations in the heart rate indicates autonomic regulation and can indirectly provide information on fetal distress [29–32]. In recent studies, interest is shown in computerized analysis of fetal HRV [31–39]. Computerized HRV analysis can quantify aspects of HRV that are not directly visible from the heart rate signal, such as beat-to-beat heart rate variations. However, the FHR is commonly determined by Doppler ultrasound (US) [40]. Despite being non-invasive, Doppler US requires autocorrelation techniques to determine the FHR and the FHR is averaged over several heartbeats [41]. Although the error that is introduced by averaging of the FHR has little influence on visual interpretation of fetal HRV, the averaging makes FHR from Doppler US less suited for computerized analysis of fetal HRV [42].

As an alternative to FHR from Doppler US, beat-to-beat FHR can be obtained unobtrusively from the non-invasive fetal ECG, which is recorded by electrodes on the maternal abdomen [43–46]. In addition to a more accurate estimation of the FHR, the non-invasive fetal ECG also provides information that could be used for analysis of fetal ECG morphology [13, 15, 19, 47]. Unfortunately, the non-invasiveness comes at the expense of a typically low signal-to-noise ratio (SNR) [40]. Moreover, fetal movements can cause variations in the waveform of the non-invasive fetal ECG, further complicating the detection and analysis of the fetal ECG [48–50]. The difficulty to extract the non-invasive fetal ECG limits its use in the clinic.
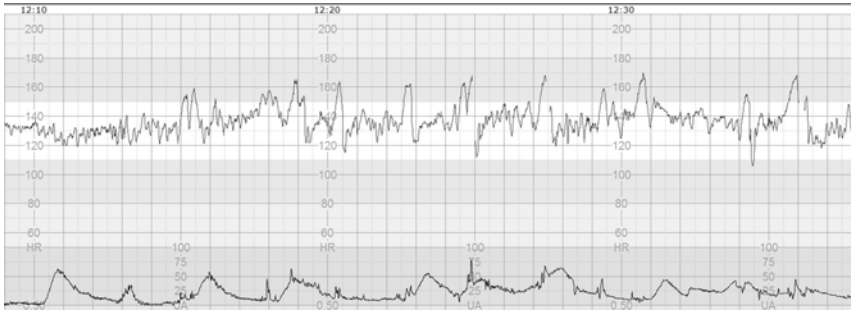
Figure 1.1: Example of a CTG. The FHR and UA are shown in the upper and lower line, respectively.

1.2 Goals of this thesis

From the previous section it becomes clear that computerized analysis of fetal HRV has great promise as an additional diagnostic tool to assess the fetal condition. However, its application in clinical practice is hampered by the fact that no beat-to-beat FHR is currently available throughout the pregnancy, or is unreliable due to difficulties to extract the beat-to-beat FHR unobtrusively. Besides, most HRV features that have been presented in the literature are validated for adults in controlled experiments only. For the fetus it is not possible to control external conditions. In particular during labor, uterine contractions can strongly influence the fetal cardiovascular system and thus fetal HRV [1, 51, 52].

Several developments are required before fetal HRV can be used in clinical practice. The accomplishment of some of these developments is addressed in this thesis and explained in two distinctive parts: I) development of new processing techniques that enable reliable extraction of beat-to-beat FHR from non-invasive fetal ECG recordings and II) the use of fetal HRV analysis for the detection of fetal distress during labor.

1.3 Thesis outline

The physiological and technical background on fetal monitoring that is relevant for this thesis is provided in **Chapter 2**. After the background, the first part of this thesis deals with the signal processing steps that have been developed for reliable FHR detection from non-invasive fetal ECG recordings. In **Chapter 3**, a new method is provided for suppression of the power line interference (PLI). Filtering of the PLI can be seen as a pre-processing step that is required before FHR detection and analysis of fetal ECG morphology can be performed. To prevent distortion of the fetal ECG waveform, a Kalman smoother with adaptive noise estimation has been developed.

Chapter 4 presents a method for FHR detection in non-invasive fetal ECG recordings. The FHR detection uses predictive models for FHR, fetal ECG morphology, and interferences. The models are integrated within a hierarchical Bayesian framework to account for the non-stationary nature of non-invasive fetal ECG recordings. Moreover, we have extended this framework to a multi-channel approach, because the non-invasive fetal ECG is typically recorded using multiple electrodes.

The second part of this thesis addresses some of the challenges related to analysis of fetal HRV. During labor, uterine contractions influence the fetal cardiovascular system, which results in non-stationarities in the fetal HRV. In **Chapter 5** we show that separating contractions from rest periods increases the diagnostic value of fetal HRV features for the detection of fetal distress during labor. Then, in **Chapter 6** we use classification algorithms to show that the detection rate of fetal distress based on HRV analysis can indeed be improved by combining information from HRV features that are calculated without distinguishing contractions and information from contraction-dependent HRV features.

Besides influence of uterine contractions, fetal HRV is also influenced by maturation of the ANS and several types of medication. Using non-invasive fetal ECG recordings, we examined the effect of gestational age on fetal HRV in **Chapter 7**. The effect of corticosteroids, medication that is often used in case of threatening preterm labor, on fetal HRV is examined in **Chapter 8**.

The main findings of this thesis are summarized in **Chapter 9**. This chapter also includes a discussion on promising future research directions. Note that Chapters 3-8 are either published or submitted for publication. Each of these chapters is written to be self-contained, causing some overlap between these chapters.

1.4 List of publications

Journal papers

JP-1 **Warmerdam G.J.J.**, Vullings R., Schmitt L., Van Laar J.O.E.H., and Bergmans J.W.M., Hierarchical Bayesian framework for fetal R-peak detection, using ECG waveform and heart rate information. *Submitted.*

JP-2 Hulsenboom A.D.J., **Warmerdam, G.J.J.**, Weijers J., Van Laar J.O.E.H., Oei S.G., Blijham P.J., Vullings R., Delhaas T., The effect of head orientation and electrode placement on ECG waveform in underwater ECG measurement. *Submitted.*

JP-3 Lempersz C., Van Laar J.O.E.H., Clur S.B., Verdurmen K.M.J., **Warmerdam G.J.J.**, Van der Post J., Blom N.A., Delhaas T., Oei S.G., Vullings R., The standardized Fetal Electrocardiogram and its potential use in the detection of Fetal Congenital Heart disease. *Submitted.*

JP-4 **Warmerdam, G.J.J.**, Vullings R., Van Laar J.O.E.H., Van der Hout-Van der Jagt B., Bergmans J.W.M., Schmitt L., Oei S.G., Detection rate of fetal distress using contraction-dependent fetal heart rate variability analysis. *Accepted for publication in Phys. Meas.*

JP-5 Verdurmen K.M.J., **Warmerdam G.J.J.**, Lempersz C., Hulsenboom A.D.J., Renckens J., Dieleman J., Vullings R., Van Laar J.O.E.H., Oei S.G., The influence of betamethasone on fetal heart rate variability, obtained by noninvasive fetal electrocardiogram recordings. *Accepted for publication in Early Hum. Dev.*

JP-6 **Warmerdam G.J.J.**, Vullings R., Schmitt L., Van Laar J.O.E.H., and Bergmans J.W.M., A fixed-lag Kalman smoother to filter power line interference in electrocardiogram recordings. IEEE. Trans. Biomed. Eng. 2017, 64(8): 1852-1861.

JP-7 **Warmerdam G.J.J.**, Vullings R., Van Laar J.O.E.H., Van der Hout-Van der Jagt M.B., Bergmans J.W.M., Schmitt L., Oei S.G., Using uterine activity to improve fetal heart rate variability analysis for detection of asphyxia during labor. Phys. Meas. 2016, 37: 387-400.

JP-8 Van Laar J.O.E.H., **Warmerdam G.J.J.**, Verdurmen K.M.J., Vullings R., Peters C.H.L., Houterman S., Wijn P.F.F., Andriessen P., Van Pul C., Oei S.G., Fetal heart rate variability in frequency-domain during pregnancy, obtained from noninvasive electrocardiogram recordings. Acta Obstet Gynecol Scand. 2014, 93: 93-101.

Conference proceedings

CP-1 Verdurmen K.M.J., **Warmerdam G.J.J.**, Lempersz C., Hulsenboom A.D.J., Renckens J., Dieleman J.P., Vullings R., Van Laar J.O.E.H., Oei S.G., The influence of betamethasone of fetal heart rate variability, obtained by noninvasive fetal electrocardiogram recordings. European Congress on Intrapartum Care, 25-27 May 20017,Stockholm, Sweden.

CP-2 **Warmerdam G.J.J.**, Vullings R., Van Laar J.O.E.H, Bergmans J.W.M., Schmitt L., Hierarchical Bayesian framework for fetal R-peak detection using QRS waveform and heart rate information. Biomedica, 9-10 May 2017, Eindhoven, The Netherlands.

CP-3 **Warmerdam G.J.J.**, Vullings R., Van Laar J.O.E.H., Van der Hout M.B., Bergmans J.W.M., Schmitt L., Oei S.G., Selective heart rate variability analysis to account for uterine activity during labor and improve classification of fetal distress. 38th Annual International Conference of the IEEE EMBS, 16-20 August 2016, Orlando, Florida.

CP-4 **Warmerdam G.J.J.**, Vullings R., Van Laar J.O.E.H., Van der Hout M.B., Bergmans J.W.M., Schmitt L., Oei S.G., Fetal heart rate variability analysis for detection of asphyxia can be improved by including uterine activity information. 14th National Day on Biomedical Engineering, 26-27 November 2015, Brussels, Belgium.

CP-5 **Warmerdam G.J.J.**, Vullings R., Bergmans J.W.M., Oei S.G., Estimating the error in spectral analysis of fetal heart rate variability. 5th Dutch Biomedical Engineering Conference, 22-23 January 2015, Egmond aan Zee, The Netherlands.

CP-6 **Warmerdam G.J.J.**, Vullings R., Bergmans J.W.M., Oei S.G., Reliability of spectral analysis of fetal heart rate variability. 36th Annual International Conference of the IEEE EMBS, 26-30 August 2014, Chicago, Illinois.

CP-7 Verdurmen K.M.J., Van Laar J.O.E.H., **Warmerdam G.J.J.**, Oei S.G., Fetal heart rate variability during pregnancy. European Congress of Perinatal Medicine, 4-7 June 2014, Florence, Italy.

CP-8 **Warmerdam G.J.J.**, Vullings, R., Oei, S.G., Wijn, P.F.F., Automated detection of premature atrial contractions in non-invasive fetal electrocardiogram recordings: a case report. Meeting Abstract: The 3rd International Congress on Cardiac Problems in Pregnancy, 20-23 February 2014, Venice, Italy.

CP-9 **Warmerdam G.J.J.**, Vullings R., Van Laar J.O.E.H., Van der Hout-Van der Jagt B., Bergmans J.W.M., Schmitt L., Oei S.G., Accounting for uterine activity improves fetal heart rate variability analysis for detection of fetal distress. IEEE SBE Symposium Advancing Healthcare, 18 February 2014, Eindhoven, The Netherlands.

CP-10 **Warmerdam G.J.J.**, Vullings R., Van Pul C., Andriessen P., Oei S.G., Wijn P.F.F., QRS classification and spatial combination for robust heart rate detection in low-quality fetal ECG recordings. 35th Annual International Conference of the IEEE EMBS, 03-07 July 2013, Osaka, Japan.

CP-11 Verdurmen K.M.J., Van Laar J.O.E.H., **Warmerdam G.J.J.**, Oei S.G., Fetal heart rate variability during pregnancy. Symposium on Advances in Perinatal Monitoring, 24 April 2013, Eindhoven, The Netherlands.

2 | BACKGROUND

2.1 Physiology of the fetal heart

2.1.1 Contraction of the heart

The main function of the heart is to provide vital organs and peripheral tissue with blood. The adult heart consists of two separate pumps: the right side of the heart pumps oxygen-depleted blood through the lungs (pulmonary circulation) and the left side of the heart pumps oxygenated blood through the peripheral organs (systemic circulation) (Fig. 2.1a) [53]. Each side of the heart consists of two chambers to regulate blood flow into the heart (the atria) and outflow from the heart to the pulmonary or systemic circulation (the ventricles).

The contraction of the cardiac muscle originates from the conversion of electrical impulses (action potentials) into mechanical activity of the cardiac muscle cells [53, 54]. A specialized nervous system conducts the action potentials rapidly throughout the muscular layer of the heart (the myocardium, Fig. 2.1a). The action potentials that cause cardiac contraction are generated by self-excitation. Since pacemaker cells located in the sinoatrial (SA) node have the highest self-excitation rate, these cells determine the heart rate. From the SA node, the action potentials first propagate through the atria, causing contraction of the atria. The action potentials cannot directly cross from the atria to the ventricles. First, the action potentials need to propagate through the atrioventricular (AV) node and the bundle of His. After the bundle of His, the nerve fibers split into the left and right bundle branches that end in the left and right ventricles respectively.

When this system functions normally, a delay in propagation is caused by the AV node and the bundle of His, and the atria contract before the ventricular contraction [53]. This allows the atria to empty their content into the ventricles and ensures that the ventricles are filled before they pump the blood into the pulmonary and systemic circulation. Another purpose of this system is that it allows all parts of the ventricles to contract simultaneously, optimizing the effective pressure generated by the ventricles [53].

The fetal circulation differs from the adult circulation because the oxygen intake and the carbon-dioxide secretion take place in the placenta instead of the lungs [55–57]. In the fetal circulation, the right ventricle does not pump the blood through the pulmonary circulation alone. Instead, both ventricles pump blood through the entire body [57]. To enable this, two interconnections exists in
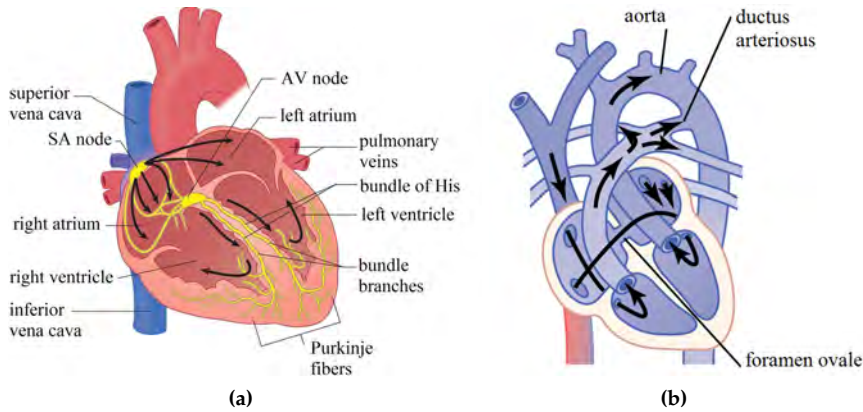
Figure 2.1: (a) Schematic illustration of the anatomy of the adult heart and cardiac conduction system. Adapted from [58]. (b) Schematic illustration of the fetal heart. Adapted from [53].

the fetal circulation. The foramen ovale links the atria and the ductus arteriosus links the outgoing arteries of both ventricles, as illustrated in Fig. [57]. Despite the difference between the adult and fetal circulation, the propagation of action potentials through the fetal heart is similar to that of adults.

2.1.2 The electrocardiogram

At cellular level, a potential difference exists between the intracellular and extracellular fluid of the cardiac muscle cells that is mainly controlled by the concentrations of sodium (Na^+), potassium (K^+) and calcium (Ca^{2+}) ions on each side of the cell membrane [53, 54]. The membrane potential is negative when the cells are in rest. In the occurrence of an action potential, a cycle is initiated that activates the cell. First, the membrane potential increases due to a rapid influx of Na^+, inverting the membrane potential to positive (called *depolarization*). Then, the membrane potential remains at a plateau level due to the exchange of K^+ and Ca^{2+}. Finally, the membrane potential returns to its rest value due to persisting outflow of K^+ (called *repolarization*).

The action potentials propagate from cell to cell by increasing the membrane potential of neighboring rest cells and initiating the depolarization in these cells[54]. Due to this cell-to-cell activation, the action potential can propagate in any given direction through the cardiac muscle. Moreover, action potentials propagate rather uniformly through the cardiac muscle and adjacent cells depolarize virtually simultaneously, creating depolarization waves through the heart (Fig. 2.2a) [53]. The wavefront is a collection of electrical dipoles.

Since the tissue surrounding the cardiac muscle acts as a conductor, it allows the electrical currents that are generated by the individual dipoles to spread

(a)   (b)
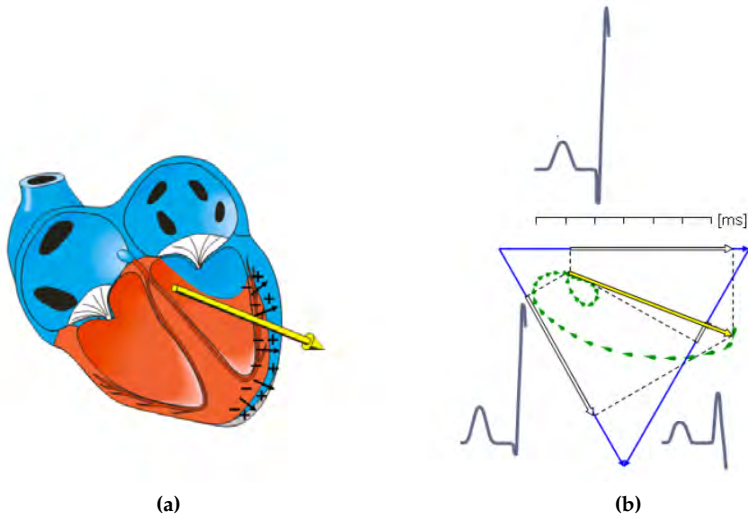
Figure 2.2: (a) Illustration of the dipole wavefront during a ventricular contraction. Red indicates cardiac tissue that is contracting and blue indicates cardiac tissue that is relaxed. A dipole wave exists at the boundary between contracting and relaxed tissue. The direction of the dipole field vector is indicated by the yellow arrow. (b) The two-dimensional illustration of the VCG (green) and the projection of the dipole field vector onto the leads of the Einthoven triangle. Adapted from [62].

through the cardiac tissue [54, 59]. At the body surface, the electric field that is generated from the coherent activation of cells at the dipole wavefront results in measurable potential differences. The electrical activity can be approximated (in first order) by a single field vector [60, 61]. The path that is described by this vector over time in the three-dimensional space is called the vectorcardiogram (VCG) [62].

The potential differences can be measured with electrodes on the skin. The projection of the three-dimensional field vector onto the lead vector of two electrodes is called the ECG [53, 61]. An example of the VCG projections onto the lead vectors of the traditional Einthoven triangle is displayed in Fig. 2.2b [63]. The ECG signal of a single cardiac cycle typically consists of a P-, QRS-, and T-wave, as schematically illustrated in Fig. 2.3 [53]. The P-wave is associated with the depolarization of the atria and the QRS-complex with depolarization of the ventricles. The T-wave is associated with the repolarization of the ventricles. Note that repolarization of the atria cannot be distinguished in the ECG because it occurs simultaneously with the depolarization of the ventricles.
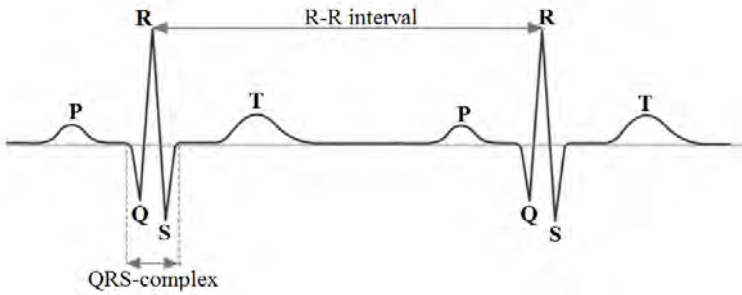
Figure 2.3: Typical ECG signal.

2.2 Autonomic regulation

To ensure that the heart provides the required cardiac output and arterial pressure to deliver sufficient blood flow to the body tissues, the heart is regulated by the ANS [53]. The ANS controls the activity of the heart by alternating the contractility of the heart and the rate at which the heart contracts. During fetal life, adjusting the contractility of the heart only plays a moderate role and the cardiac output is mainly dependent on changes in the fetal heart rate [64]. In this thesis we are therefore mostly interested in the ANS regulation of the fetal heart rate.

2.2.1 Autonomic cardiac regulation

The ANS controls the heart through the sympathetic nervous system and the parasympathetic nervous system (Fig. 2.4) [53, 65]. Stimulation of the sympathetic nervous system increases the heart rate, while stimulation of the parasympathetic nervous system decreases the heart rate. The change in heart rate is usually a combination of variations in sympathetic and parasympathetic activity.

The nerve endings of the parasympathetic nerves are mainly located at the SA and AV nodes. Stimulation of the parasympathetic nerves to the heart causes the hormone acethylcholine (ACh) to be released at the nerve endings. ACh increases the permeability of K^+ in the membranes of the cardiac cells, causing the rest membrane potential to become more negative than normal [53]. Hence, more time is required before the membrane potential of the cells within the SA node reach the threshold potential that is required for self-excitation, slowing down the heart rate. The effect of parasympathetic stimulation decays relatively quick, because the SA and AV node contain an enzyme that breaks down ACh. This mechanism enables the parasympathetic nervous system to control the heart rate on a beat-to-beat basis.
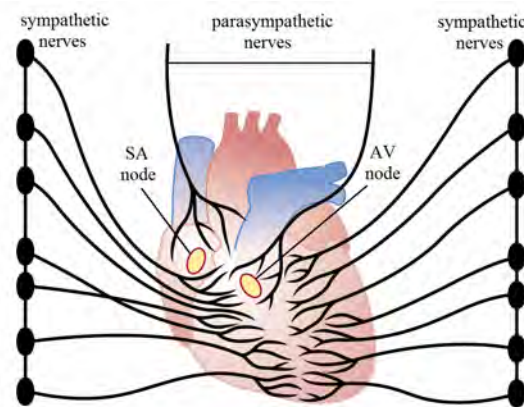
Figure 2.4: Sympathetic and parasympathetic nerves in the heart. Adapted from [53].

The nerve endings of the sympathetic nerves are distributed to all parts of the heart. Stimulation of the sympathetic nerves releases the hormone norepinephrine at the sympathetic nerve endings. It is believed that norepinephrine increases the permeability of Na^+ and Ca^{2+} [53]. In contrast to parasympathetic stimulation, this increases the resting membrane potential of the cardiac cells in the SA node, which increases the self-excitation rate and thus the heart rate. Furthermore, the increase in Na^+ and Ca^{2+} permeability reduces the conduction time for the action potentials to travel from the atria to the ventricles. Since the release and decay of norepinephrine is relatively slow, the effect of sympathetic stimulation is slow compared to the beat-to-beat regulation of the parasympathetic nervous system [30].

2.2.2 Autonomic reflex mechanisms

The ANS regulates the cardiovascular system through reflex mechanisms [53]. The most important of these reflex mechanisms are the baroreceptor reflex and the chemoreceptor reflex. Humoral influences and thermoregulation induce long term regulation (very low frequent fluctuation) of heart rate [66, 67]. The influence of these factors on heart rate are beyond the scope of this thesis and are not further discussed in this chapter.

Baroreceptor reflex The best known mechanism to control the arterial pressure is the baroreceptor reflex [53]. This reflex is initiated by stretch receptors (baroreceptors) that are located in the walls of the carotic arteries and aortic arch. An increase in arterial pressure stretches the arterial walls and activates the baroreceptors. In response, the ANS sends nervous signals to the circulation to reduce the arterial pressure back to a normal value, e.g. by decreasing the heart rate or the systemic resistance. Besides the baroreceptor reflex, the arterial

pressure is regulated by several interrelated reflex mechanisms (e.g. Brainbridge reflex or respiratory sinus arrhythmia). Since these other mechanisms are less pronounced for the fetus, they are not further discussed.

Chemoreceptor reflex   The chemoreceptor reflex regulates the respiratory activity in a similar way as the baroreceptor reflex controls the arterial pressure [53]. The chemoreceptor reflex is initiated by chemoreceptors that are located in the carotid and aortic arteries. The chemoreceptors are activated when the arterial oxygen concentration falls below normal. For adults, activation of the chemoreceptors leads to an increase in respiration. The fetal response to changes in oxygen concentration differs from that of adults (as discussed in Section 2.2.3), because the fetal oxygen supply does not come from the lungs.

2.2.3   Fetal response to oxygen deficiency

In the fetal circulation, the placenta serves as the lungs of the fetus and it allows oxygen to diffuse from the maternal circulation to the fetal circulation [68]. The fetus is connected to the placenta through the umbilical cord. Deoxygenated blood is transported from the fetus to the placenta, while oxygenated blood flows from the placenta to the fetus. The oxygenated blood then passes the fetal heart, from where the blood is pumped to the rest of the body tissues. Finally, the oxygen is used in the body tissues and cells to produce energy through a process called aerobic metabolism.

During labor, uterine contractions can cause a temporal block of oxygen supply to the fetus [1]. Although maternal placental blood flow is normally high, in case of a strong contraction it can occur that the maternal blood flow to the placenta is reduced. In this case the fetus has to rely on its own oxygen storage. Besides reduced maternal placental blood flow, fetal oxygen supply can also be interrupted if the umbilical cord is occluded due to an increase in intrauterine pressure that is caused by uterine contractions. For moderate contractions during the first stage of labor (the stage of cervical dilation), a connective tissue that surround the blood vessels in the umbilical cord can protect the cord vessels. However, during the second stage of labor (the stage of active pushing) it can occur that intrauterine pressure becomes so high that the connective tissue can no longer oppose this pressure and that the umbilical blood flow is blocked.

In the absence of oxygen, aerobic metabolism can be supported by anaerobic metabolism [53]. During anaerobic metabolism, glucose reserves are utilized to produce energy without oxygen. It is important to note that anaerobic metabolism only produces a fraction of the energy that is produced during normal aerobic metabolism and there is a risk of damaging the tissues. During aerobic and anaerobic metabolism hydrogen ions are produced as waste product. Normally, these hydrogen ions are buffered by carbon dioxide and haemoglobin [53]. However, in case the fetus has depleted its buffering capacity, the free hydrogen ions will cause an increase in the acidity of the blood (measured by the

pH of the blood). After birth, the pH is therefore often used as a measure to determine the severity of the oxygen deficiency that was suffered by the fetus [22, 69].

Throughout pregnancy, the fetus develops mechanisms that protect it against oxygen deficiency. These mechanisms, amongst others, involve activation of the baroreceptor reflex and chemoreceptor reflex [70]. If the umbilical cord is occluded, this will initially increase the systemic resistance in the fetal cardiovascular system, causing an increase in fetal blood pressure and activation of the baroreceptor reflex. Besides, the oxygen concentration in the fetal blood will also decrease because the fetal oxygen supply is blocked, which activates the chemoreceptors.

There are three stages of oxygen deficiency that can be distinguished [1]. During the initial stage of oxygen deficiency, called hypoxemia, the oxygen concentration is only decreased in the arterial blood and not in the body tissues. In response, fetal activity is reduced while oxygen uptake in the placenta is optimized. As the oxygen concentration further decreases, the fetus ensures that the oxygen concentration in the central organs (the heart, brain, and adrenals) remains in tact by reducing the blood flow to the peripheral tissues [71, 72]. This stage is called hypoxia, in which low oxygen concentration requires anaerobic metabolism in the peripheral tissues, possibly damaging the peripheral tissue [73]. Because the central organs are protected during hypoxia, the effect on fetal outcome is limited. For even lower levels of oxygen concentration, anaerobic metabolism may also occur in the central organs, which is referred to asphyxia, and there is a risk of damaging the central organs [2]. The ability of the fetus to respond to oxygen deficiency strongly depends on the development of the protective mechanisms. If these mechanisms have already been used or have not been fully developed (i.e. due to prematurity), the oxygen deficiency can lead to fetal morbidity and mortality [74–76].

2.2.4 Fetal autonomic development

The control of FHR by the fetal ANS changes throughout the pregnancy due to maturation of the fetal ANS [77–79]. Early in the pregnancy, the heart has not yet been fully developed and the heart is autoregulated [80, 81]. Sheep studies have shown that the sympathetic nervous system becomes functional prior to the parasympathetic nervous system and dominates the cardiovascular control [82, 83].

Besides maturation of the ANS and fetal heart, also the fetal activity changes as the fetus develops. Where in the first trimester fetal body movements occur randomly over time, in the second half of the pregnancy these movements become clustered in rest-activity cycles [84–86]. These rest-activity episodes eventually result in behavioral states that are associated with fetal heart rate patterns and eye movements. Four behavioral states can be distinguished [87]. The first state (1F) is called quiet sleep and little fetal movement occurs. During this stage, the

fetal heart rate is stable and changes in the fetal heart rate are relatively small. The second state (2F) is active sleep (or REM-sleep), in which repeated body movements and continuous eye movements can be observed. During 2F, large changes in fetal heart rate can been seen. The final two states are quiet awake and active awake. These states are of lesser importance since they occur less frequently [85, 88].

2.3 Heart rate variability

Computerized analysis of HRV aims to quantify the functional state of the autonomic cardiovascular regulation [30]. Already in the seventies, studies found that reduced HRV is associated with an increased risk of mortality after myocardial infarction [89]. Since then, the use of HRV analysis expanded from cardiac applications [90, 91] to a diversity of other pathological conditions, including neurological disorders such as diabetes [92, 93]. Recently, several studies have used computerized analysis of fetal HRV to predict fetal distress [31, 32, 34–39].

From Sections 2.1 and 2.2 it becomes clear that the cardiovascular system is a complex system and the heart rate is only one of the variables that the ANS uses to regulate the cardiovascular system. The variety of factors that can influence the cardiovascular control (e.g. mental load or physical load) makes the heart rate signal difficult to analyze. Moreover, for long recordings, notable changes in the cardiovascular system may have occurred due to internal influences (e.g. hormones) or changes in the exterior environment. Over the years, various HRV features have been developed that quantify different aspects of the cardiovascular control [94, 95]. This section will briefly discuss several of these features. For a more detailed description of the HRV features that were used in this study the reader is referred to Chapter 5.

HRV analysis is generally based on the RR-interval signals, the sequence of intervals between successive R-peaks in the ECG (see Fig. 2.3) [30]. It should be noted that, in theory, true HRV would be measured by the interval between the onset of two successive P-waves (P-P interval), because the P-P intervals are related to rhythms of the SA node that initiate the cardiac cycle. However, the small amplitude of the P-wave makes accurate detection of the P-P interval difficult and detection of the RR-interval is more reliable in practice. Fortunately, changes in RR-intervals and PP-intervals are highly similar [96].

The most straightforward measures for HRV analysis are statistical features that are obtained from the RR-intervals directly [30]. These can generally be divided into two classes of features: features that are derived directly from the RR-intervals and those that are derived from the differences between RR-intervals. Features that focus on the overall R-R signal reflect both sympathetic and parasympathetic regulation. Features that are obtained from the differences between RR-intervals are mostly sensitive to beat-to-beat variations and mainly reflect parasympathetic regulation [97].

As explained in Section 2.2.2, the heart rate is regulated by the interplay of several feedback mechanisms that each have their own intrinsic delay [53]. As a consequence of the delays in these feedback mechanisms, periodic variations are observed in the heart rate that can be related to different regulatory mechanisms. To quantify these periodicities, spectral analysis of HRV can be used. The frequency bands of this spectral analysis can be chosen to reflect sympathetic and parasympathetic activity [29]. As the effect of sympathetic regulation is relatively slow compared to the parasympathetic regulation, low frequency oscillations are related to both sympathetic and parasympathetic regulation, while high frequency oscillations are related to parasympathetic regulation alone [29].

Often complicated and irregular variations are seen in the heart rate since there are many factors that influence the cardiovascular system[95]. These irregular variations are not well explained by spectral analysis. Because the heart rate is one of the main tools for ANS regulation of the cardiovascular system, the occurrence of irregularities in the heart rate is indicative of healthy autonomic regulation. The irregularity in the heart rate can be quantified by entropy measures [98, 99].

Besides quantifying HRV at a specific time scale (e.g. as is done with spectral analysis), other HRV features focus on the ability of the ANS to regulate the cardiovascular system on different time scales [100]. For example, diurnal rhythms determine HRV on a daily basis, hormones influence HRV on the scale of hours, while blood pressure is regulated in seconds to minutes. The relation between HRV on different time scales can be described by fractal analysis [38, 100].

It should be noted that many HRV features were originally developed for analyzing ideal and theoretical systems. Calculating these features for physiological time series such as the heart rate might not exactly describe the characteristic it was originally developed for. Yet, the features may still contain clinically relevant information.

2.4 Non-invasive fetal ECG

In clinical practice, fetal HRV is evaluated visually from CTG recordings. Doppler US is currently the most commonly used technique to record the FHR. The FHR is detected making use of the frequency shift (Doppler effect [101]) that is experienced by ultrasonic waves when they are reflected by moving parts of the fetal heart. Although Doppler US is a non-invasive technique to monitor the FHR, it is prone to signal loss as the US beam needs to be focused at the fetal heart. Movements of the transducer or fetal movements results in signal loss and requires manual repositioning of the transducer. Moreover, Doppler US is an imprecise method to determine the FHR and does not provide beat-to-beat FHR information. Inaccuracies in the detected FHR can occur because ultrasonic waves detect both movements of the valves and the walls of the fetal heart. Besides, autocorrelation techniques are used to determine the FHR. As a consequence, the

<div align="center">(a)   (b)</div>
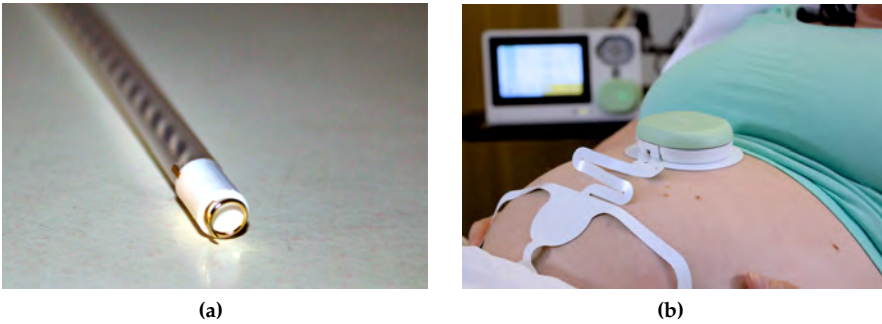
Figure 2.5: (a) Scalp electrode, adapted from [45]. (b) Non-invasive fetal ECG (Photo with permission from Nemo healthcare.)

FHR from Doppler US is averaged over several heartbeats, limiting its use for computerized analysis of fetal HRV [42].

To obtain the FHR on a beat-to-beat basis, the fetal ECG can be used. Another advantage of using the fetal ECG is that additional diagnostic information can be obtained through the study of ECG morphology [13, 15, 19, 47]. The fetal ECG is generally recorded invasively, using an electrode that is screwed into the fetal scalp (Fig. 2.5a) [102]. Despite having a good signal quality, the invasive fetal ECG can only be used after the fetal membranes have ruptured. Moreover, the signal is acquired using only a single differential electrode and the cardiac electric activity is thus projected onto a single specific lead axis [103]. This means that the three dimensional electric field information of the heart is lost and the ECG morphology will depend on the orientation of the fetal heart with respect to the electrode lead [104].

To overcome the limitations of the invasive fetal ECG, it is also possible to record the fetal ECG non-invasively with electrodes on the maternal abdomen (Fig. 2.5b) [43]. In contrast to the invasive scalp ECG, the non-invasive ECG can be recorded throughout the pregnancy.

Unfortunately, the non-invasiveness comes at the expense of typically low SNR. Before the fetal heart signal reaches the abdominal skin, the signal has to propagate through several layers of tissue that attenuate the electrical activity [105]. The larger the distance between the fetal heart and electrode, the more the fetal ECG will be attenuated. The overall conductivity of the layers of tissues changes throughout the gestation [106, 107]. In particular the development of the vernix caseosa strongly influences the signal strength [108]. The vernix caseosa is a protective layer that surrounds the fetus, develops from about 28 weeks of gestation, and starts to dissolve from about 32 weeks of gestation [109]. Because the vernix caseosa electrically isolates the fetus, it is very difficult the detect the fetal ECG during this period.
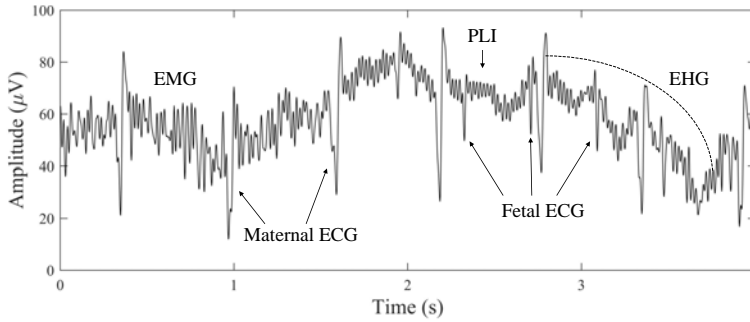
Figure 2.6: Example of a non-invasive fetal ECG signal. The interferences of the maternal ECG, EMG, EHG, and PLI are indicated.

Besides a low amplitude of the fetal ECG, the signal that is recorded by the abdominal electrodes is contaminated by electrical interferences, both physiological and non-physiological [110]. The most important of these interferences are the maternal ECG [111], PLI [112], abdominal muscle activity (electromyogram, EMG) [113], and activity from the uterine muscle (electrohysterogram, EHG) [114, 115]. An example of a signal that is recorded on the maternal abdomen is shown in Fig. 2.6. The amplitude of the interferences is often larger than the amplitude of the fetal ECG. The overlapping frequency content of the interferences with the frequency content of the fetal ECG makes suppression of these interferences challenging.

Finally, the position and orientation of the fetus within the abdomen are a priori unknown. To cover any fetal orientation, the non-invasive fetal ECG is typically recorded using an array of electrodes that are spread across the abdomen [116]. The SNR and fetal ECG waveform that is recorded by each electrode depends on the fetal position (i.e. distance to the electrode), orientation (i.e. projection of the electrical activity onto the electrode lead), and intermediate tissue [61, 117]. As the fetus moves, this can cause the SNR and fetal ECG waveform of a certain channel to change during a recording [48–50]. The use of the non-invasive ECG in clinical practice has been restricted to date due to the difficulty to extract the fetal ECG from the abdominal recordings.

In recent years, the non-invasive fetal ECG has been extensively studied [44, 118–128]. Most studies focused on suppression of the maternal ECG, which is the dominant interference. Many different techniques have been presented in the literature to suppress the maternal ECG. The most important techniques are template subtraction [118–120], adaptive filtering [121, 124], blind source separation [44, 122, 123, 125], or a combination of these techniques []. For a more extensive review of the different techniques the reader is referred to [126–128]. Since many of these techniques perform relatively well, we will not focus on suppression of the maternal ECG in this thesis. Instead, we will focus on the processing steps that follow after maternal ECG suppression.

PART I

Analysis of the non-invasive fetal electrocardiogram
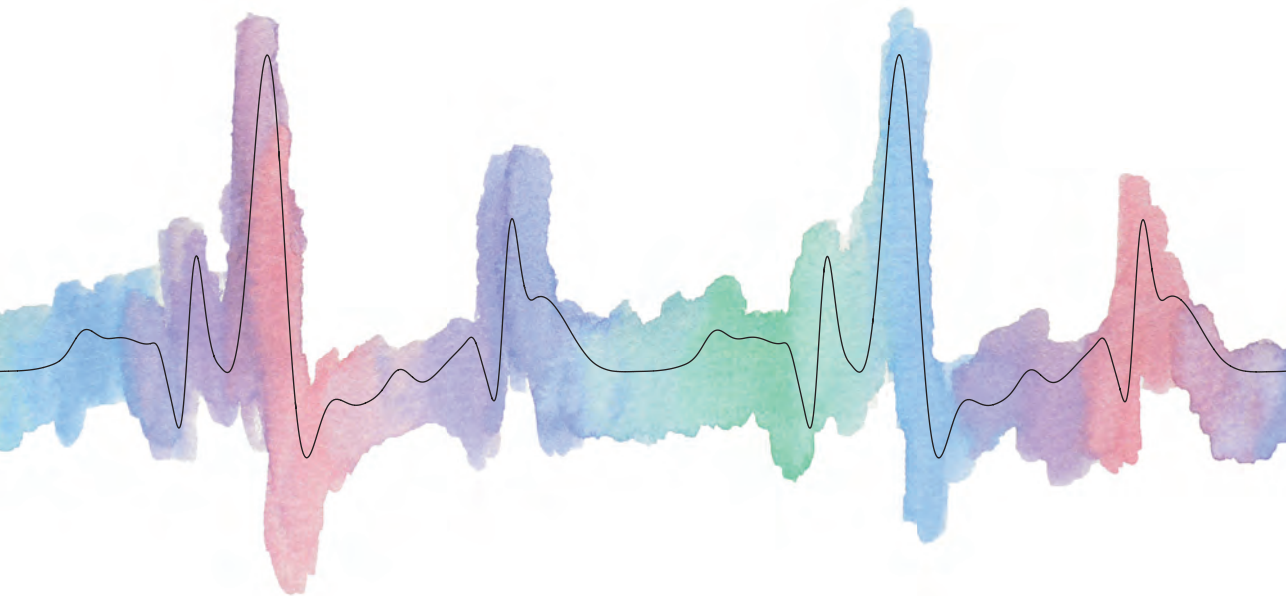
3

A FIXED-LAG KALMAN SMOOTHER TO FILTER POWER LINE INTERFERENCE IN ECG RECORDINGS

Abstract - Objective*: Filtering power line interference (PLI) from electrocardiogram (ECG) recordings can lead to significant distortions of the ECG and mask clinically relevant features in ECG waveform morphology. The objective of this study is to filter PLI from ECG recordings with minimal distortion of the ECG waveform.* Methods*: In this paper, we propose a fixed-lag Kalman smoother with adaptive noise estimation. The performance of this Kalman smoother in filtering PLI is compared to that of a fixed-bandwidth notch filter and several adaptive PLI filters that have been proposed in the literature. To evaluate the performance, we corrupted clean neonatal ECG recordings with various simulated PLI. Furthermore, examples are shown of filtering real PLI from an adult and a fetal ECG recording.* Results*: The fixed-lag Kalman smoother outperforms other PLI filters in terms of step response settling time (improvements that range from 0.1 s to 1 s) and signal-to-noise ratio (improvements that range from 17 dB to 23 dB). Our fixed-lag Kalman smoother can be used for semi real-time applications with a limited delay of 0.4 s.* Conclusion and significance*: The fixed-lag Kalman smoother presented in this study outperforms other methods for filtering PLI and leads to minimal distortion of the ECG waveform.*[1]

3.1 Introduction

Power line interference (PLI) is often a source of interference for biomedical signals such as electrocardiogram (ECG) recordings. Electric fields surrounding the power lines are picked up by the patient, the electric wires, and by the electrocardiograph itself. Differences in skin-electrode impedance of electrodes can lead to voltage differences measured at the electrodes which are then amplified at the output. Using a proper recording setup (e.g. cable shielding or amplifiers with a high common mode rejection) can reduce PLI, but this is often insufficient to fully suppress PLI. Especially with developments in sensor technology in the direction of less obtrusive sensors such as textile electrodes and capacitive electrodes [129], PLI can even exceed the ECG in amplitude. Despite that filtering PLI is a fairly mature domain [112, 121, 130–136], filtering PLI from ECG recordings remains a challenging task because the frequency content of the ECG (in particular the frequency content of the QRS complex) overlaps with the frequency of the PLI.

The classical approach for removing PLI is to use a fixed notch filter (e.g. an infinite impulse response (IIR) filter [137]), with unit gain at all frequencies except the PLI frequency. Typically, the impulse response of a notch filter shows some ringing [131], as presented in Fig. 3.1a. In case of a steep QRS complex, this ringing effect is also observed after filtering an ECG signal with the fixed notch filter. In particular for neonatal and fetal ECG, ringing can lead to significant disturbance of the ECG, as shown in Fig. 3.1b. The shorter duration of the QRS complex (typically 50 ms for neonates and 40 ms for fetuses) compared to the duration of the adult QRS complex (typically 80 ms) [138], leads to more overlap of the frequency content of the QRS complex with the frequency of the PLI. Note that since ringing is a response of the notch filter to a QRS complex, using a notch filter will always cause ringing, even in case there is little to no PLI.

As an alternative to notch filters with fixed parameters, several adaptive filters have been proposed in the literature [112, 121, 132–136]. Least-mean-square (LMS) adaptive algorithms were used in [112, 121, 132–134]. The first adaptive filters that were developed had the practical limitation that they required an externally recorded reference signal [121, 132, 133]. In contrast, an algorithm that required no additional reference signal was suggested by Ziarani et al. [134]. In [112], Martens et al. made improvements to the algorithm of Ziarani, resulting in a more stable filter. More recently, some researchers have used a Kalman filter (KF) [135] and extended KF [136] for PLI tracking and cancellation. Unlike LMS algorithms that use a fixed learning rate, KFs have the advantage that the learning rate of the filter is adapted to the signal-to-noise ratio (SNR).

Although most of these studies also consider the possibility of frequency deviations of the PLI, frequency deviations are only of the order $\pm$ 0.01 Hz in most developed countries according to the power system quality standards [139]. In contrast to the relatively stable frequency, the amplitude and phase of the PLI can significantly change, e.g. due to different patient positioning or impedance

changes. A linear KF was suggested by Sameni that combined variations in both amplitude and phase into the estimation of a single parameter [135]. This method has the advantage that it does not require *a priori* knowledge of the PLI amplitude and phase dynamics.

One of the main problems with adaptive filtering of PLI from ECG recordings is the interference of the QRS complex with the parameter estimation [112, 133]. While fast adaptation of model parameters is preferred in order to track changes in the PLI, using high learning rates will also allow model parameters to adapt to the QRS complex, hence leading to distortion of the ECG waveform. To prevent model parameters from adapting to the QRS complex, several studies have suggested to reduce the learning rate during a QRS complex or even set the learning rate to zero, either based on R-peak locations [133] or based on some general properties of the QRS complex [112]. Reducing the learning rate during a QRS complex has shown promising results. Unfortunately, in case of a time-varying PLI this approach leads to an error in the estimation of the PLI after a QRS complex.

In this study we suggest to use a Kalman smoother (KS) to improve estimation of the PLI. A smoother consists of a combination of two filters: one filter operates on past observations (called a forward filter), while the other filter operates on future observations (called a backward filter) [140]. Ideally, the forward and backward parameter estimation have uncorrelated errors and the combination of the two improves the parameter estimation [140, 141]. Besides the advantage of improving the parameter estimation, a KS also reduces the error made by the interference of QRS complexes with the parameter estimation. Because smoothing requires future information, a delay is generated in the estimation of the PLI. However, for most real-time applications a small delay is acceptable. We therefore propose a fixed-lag KS that estimates the PLI for some fixed delay [142].

The rest of this paper is organized as follows; in section 3.2.1 and 3.2.2 the linear KF and extension to a fixed-lag KS are discussed. Noise estimation that accounts for the interference of the ECG with the parameter estimation of the PLI is discussed in sections 4.2.1 and 3.2.4. Then section 6.2.1 discusses the data acquisition and simulation of the PLI that is used to validate the developed method. For validation we used neonatal ECG recordings, but the developed algorithm can equally be applied to adult and fetal ECG recordings, as is shown by two examples. Finally, our work is compared to several other algorithms proposed in the literature, and results and discussion are presented in sections 6.3 and 6.4.

3.2 Methods

3.2.1 Linear Kalman filter

Implementation of the linear KF is based on the work presented by Sameni [135]. This section summarizes the main concepts of the KF.
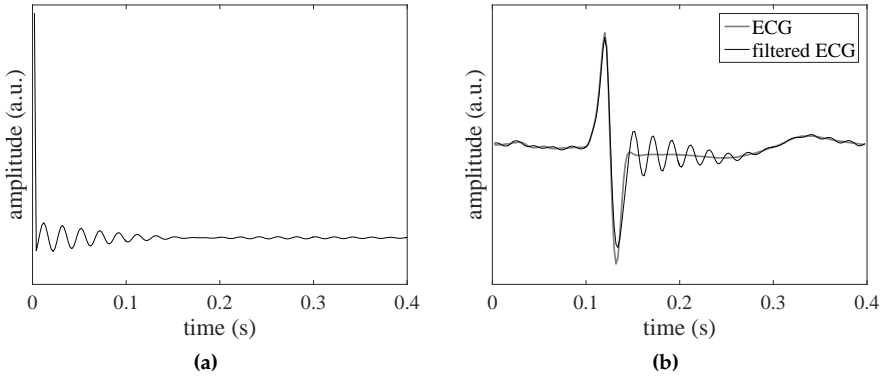
Figure 3.1: Effect of fixed-bandwidth notch filter. 3.1a Impulse response of a second order IIR notch filter. 3.1b Clean neonatal ECG signal before and after notch filtering.

The PLI is modeled as a periodic signal with frequency (f_0), amplitude (B), and phase (ϕ)

$$x_n = B\cos(\omega_0 n + \phi), \tag{3.1}$$

where $\omega_0 = 2\pi f_0/f_s$ is the angular frequency, n the time index, and f_s the sampling frequency. Using basic trigonometry, Eq. 3.1 can be rewritten into a recursive equation:

$$x_{n+1} + x_{n-1} = 2\cos(\omega_0)x_n. \tag{3.2}$$

To approximate variations in amplitude, phase, or frequency between x_{n+1} and x_n an additive random term w_n is used, which will be referred to as process noise. Although variations in phase and frequency are not additive, this approximation works well in practice since variations in phase and frequency are relatively small for PLI [139]. To obtain an analytically tractable solution for the parameter estimation, w_n is assumed to be a zero-mean Gaussian distribution with variance q_n. The PLI model can hence be expressed as

$$x_{n+1} + x_{n-1} = 2\cos(\omega_0)x_n + w_n. \tag{3.3}$$

The recorded signal (y_n) does not only consists of PLI, but contains a superposition of several other signals such as the ECG, the electromyogram (EMG), and noise. All non-PLI signals are represented by a random noise term v_n, which will be referred to as observation noise. The signal recorded at the electrodes is thus modeled as

$$y_n = x_n + v_n. \tag{3.4}$$

Because v_n is considered a combination of several signals, including measurement noise, we assumed v_n to have a zero-mean Gaussian distribution with

variance r_n. Note that since v_n also models the ECG, this assumption is only approximately true. However, in [142] it is shown that even in case of non Gaussian noise, a KF is the optimal linear estimator in the sense that it minimizes the mean square error.

Based on Eqs. 3.3 and 3.4 we can define a state-space model that describes the PLI as follows:

$$\begin{aligned}
x_{n+1} &= Ax_n + bw_n \\
y_{n+1} &= h^{\mathsf{T}}x_{n+1} + v_{n+1},
\end{aligned} \tag{3.5}$$

where $x_n = \begin{bmatrix} x_n \\ x_{n-1} \end{bmatrix}$, $A = \begin{bmatrix} 2\cos(\omega_0) & -1 \\ 1 & 0 \end{bmatrix}$, $b = \begin{bmatrix} 1 \\ 0 \end{bmatrix}$, and $h = \begin{bmatrix} 1 \\ 0 \end{bmatrix}$.

Given observations y_{n+1}, our aim is to estimate the parameter x_{n+1}. The first element of the estimate of x_{n+1} is then our estimation of the PLI at time $n+1$. Due to the uncertainties in the state-space model described by Eq. 4.6, a probabilistic approach can be used to solve the PLI estimation problem. In this case we are interested in x_{n+1} that maximizes the *posterior* probability density function $p(x_{n+1}|y_{n+1}, I)$, with $I = \{A, b, h, q_n, r_n\}$.

According to Bayes' rule, we can describe the PLI parameter estimation problem as

$$p(x_{n+1}|y_{n+1}, I) = \frac{p(y_{n+1}|x_{n+1}, I)p(x_{n+1}|y_n, I)}{p(y_{n+1}|y_n, I)}. \tag{3.6}$$

Due to the assumption of Gaussian process and measurement noise, the posterior is a Gaussian distribution and it is fully described by its mean $\hat{x}_{n+1|n+1}$ and its associated covariance $P_{n+1|n+1}$. The notation $\hat{x}_{n+1|n+1}$ represents the estimation of x at time $n+1$, given observations $Y = \{y_1, y_2, ..., y_{n+1}\}$.

Using a similar derivation as described in [143], the maximum *a posteriori* (MAP) estimate of the PLI $\hat{x}_{n+1|n+1}$ and its covariance $P_{n+1|n+1}$ can sequentially be updated according to the KF equations, given by:

$$\hat{x}_{n+1|n+1} = A\hat{x}_{n|n} + K_n(y_{n+1} - h^{\mathsf{T}}A\hat{x}_{n|n}) \tag{3.7}$$

$$P_{n+1|n+1} = AP_{n|n}A^{\mathsf{T}} + q_n bb^{\mathsf{T}} - K_n h^{\mathsf{T}}(AP_{n|n}A^{\mathsf{T}} + q_n bb^{\mathsf{T}}) \tag{3.8}$$

and K_n the Kalman gain [144]:

$$K_n = \frac{(AP_{n|n}A^{\mathsf{T}} + q_n bb^{\mathsf{T}})h}{h^{\mathsf{T}}(AP_{n|n}A^{\mathsf{T}} + q_n bb^{\mathsf{T}})h + r_{n+1}}. \tag{3.9}$$

After estimating the PLI, the ECG signal is obtained by the innovation signal of the KF:

$$\hat{v}_{n+1} = y_{n+1} - \hat{x}_{n+1|n+1}, \tag{3.10}$$

where $\hat{x}_{n+1|n+1}$ is the first element of $\hat{x}_{n+1|n+1}$.

3.2.2 Fixed-lag Kalman Smoother

The KF update equations described by Eqs. 3.7-3.9 provide causal estimations of the PLI, which means that at time $n+1$ they yield estimates given all past observations and the current observation (Y). While for real-time applications causality is required, for most applications a small delay of τ samples is often acceptable to improve the estimation accuracy. When appropriately designed, the combination of a causal filter and a backward filter that uses future information results in smaller estimation errors compared to the causal filter alone [140, 141].

Our goal is to estimate $\hat{x}_{n-\tau|n+1}$ for some fixed time-lag τ. In other words, we want to estimate the state at time $n-\tau$, given past observations $\{y_1, ..., y_{n-\tau}\}$ and future observations $\{y_{n-\tau+1}, ..., y_{n+1}\}$. The key concept is to define an augmented state vector $x^a \in \mathbb{R}^{2(\tau+1)}$ [142]

$$x_{n+1}^a = \begin{bmatrix} x_{n+1}^{(0)} \\ x_{n+1}^{(1)} \\ \vdots \\ x_{n+1}^{(\tau+1)} \end{bmatrix} = \begin{bmatrix} A & 0 & \cdots & 0 \\ I_2 & 0 & \cdots & 0 \\ 0 & I_2 & \cdots & 0 \\ \vdots & \vdots & \cdots & \vdots \\ 0 & \cdots & I_2 & 0 \end{bmatrix} \begin{bmatrix} x_n^{(0)} \\ x_n^{(1)} \\ \vdots \\ x_n^{(\tau+1)} \end{bmatrix} + \begin{bmatrix} b \\ 0 \\ \vdots \\ 0 \end{bmatrix} w_n, \tag{3.11}$$

with I_2 is the [2×2] identity matrix and element $x_{n+1}^{(i)}$ is the ith time lag of x_{n+1}.

From Eq. 3.11, we can see that, except for the first component, the components of the augmented vector x_{n+1}^a are sequentially delayed versions of the previous augmented vector x_n^a. Moreover, if we initialize $x_n^{(0)}$ as the state at time n of the original system described by Eq. 4.6, we observe that the first row of the augmented system describes the original system, while the remaining rows give successive time delays. The last component of the estimate $\hat{x}_{n+1|n+1}^a$ is $\hat{x}_{n-\tau|n+1}$, which is the estimate we are looking for.

Based on the augmented state vector, we can obtain an augmented state-space model

$$\begin{aligned} x_{n+1}^a &= A^a x_n^a + b^a w_n \\ y_{n+1} &= h^{a^T} x_{n+1}^a + v_{n+1}, \end{aligned} \tag{3.12}$$

with model parameters defined as

$$A^a = \begin{bmatrix} A & 0 & \cdots & 0 \\ I_2 & 0 & \cdots & 0 \\ 0 & I_2 & \cdots & 0 \\ \vdots & \vdots & \cdots & \vdots \\ 0 & \cdots & I_2 & 0 \end{bmatrix}, \; b^a = \begin{bmatrix} b \\ 0 \\ \vdots \\ 0 \end{bmatrix}, \text{ and } h^a = \begin{bmatrix} h \\ 0 \\ \vdots \\ 0 \end{bmatrix}. \tag{3.13}$$

Since the augmented state-space model in Eq. 3.12 again describes a linear dynamic system, we can use the same reasoning as used in section 3.2.1 to obtain an MAP solution for the augmented system:

$$\hat{x}_{n+1|n+1}^a = A^a \hat{x}_{n|n}^a + K_n^a (y_{n+1} - h^{a^T} A^a \hat{x}_{n|n}^a) \tag{3.14}$$

$$\begin{aligned} P_{n+1|n+1}^a =& A^a P_{n|n}^a A^{a^T} + q_n b^a b^{a^T} \\ &- K_n^a h^{a^T} (A^a P_{n|n}^a A^{a^T} + q_n b^a b^{a^T}) \end{aligned} \tag{3.15}$$

and the augmented Kalman gain

$$K_n^a = \frac{(A^a P_{n|n}^a A^{a^T} + q_n b^a b^{a^T}) h^a}{h^{a^T} (A^a P_{n|n}^a A^{a^T} + q_n b^a b^{a^T}) h^a + r_{n+1}}. \tag{3.16}$$

A drawback of using update equations Eqs. 3.14-3.16 is that it requires computation of a $[2(\tau + 1) \times 2(\tau + 1)]$ covariance matrix $P_{n|n}^a$ at each time instant n. This can become computationally expensive for increasing time delay or for high sampling rates. However, it is possible to show by expansion of the matrix products in Eqs. 3.14-3.16 that only the first column of the covariance matrix is required to calculate the smoothed estimate $\hat{x}_{n-\tau|n+1}$ and Kalman Gain K_n^a, greatly decreasing computational complexity [142].

3.2.3 Pre-processing

For optimal performance of the KS, the observation noise should be white [142]. In our model the observation noise represents all non-PLI signals and thus also contains correlated physiological noise, most importantly the ECG. Ideally, a whitening filter should be implemented that ensures that the innovation signal is white. However, for ECG recordings it is difficult to design such a whitening filter due to the non-stationary frequency content of the ECG (i.e. P-wave, QRS complex, and T-wave have different frequency contents).

Because the ECG has a low-frequency nature (in particular the P- and T-wave), we used a high-pass filter that serves to crudely whiten the innovation signal [112]. To this end, observations y are first pre-processed with the high-pass filter to obtain $\tilde{y}$. Since the frequency content of the P- and T-wave is generally low compared to the PLI frequency [145], the high-pass filter can be designed to suppress the P- and T-wave, while leaving the PLI undisturbed. As a result, the new innovation signal of the KS $\hat{v}_{n+1} = \tilde{y}_{n+1} - \hat{x}_{n+1|n+1}$ no longer contains the P- and T-wave.

We used a linear phase finite impulse response (FIR) filter with 40 coefficients and a cutoff frequency of 30 Hz. The FIR filter has unit gain at the PLI frequency and a group delay of half of the length of the filter. To correct for the group delay, the first 20 samples of the PLI estimation are discarded.

3.2.4 Noise estimation

Sameni showed that under assumption of stationary observation and process noise ($r_n = r$ and $q_n = q$), the KF described in section 3.2.1 converges to a second order notch filter [135]. When the amplitude or phase of the PLI varies, or in case of non-stationary observation noise this assumption is incorrect and the KF performs sub-optimally.

Observation noise

In contrast to the frequency content of the P- and T-wave, the frequency content of the QRS complex overlaps with the PLI frequency. Therefore, a high-pass filter is not able to fully suppress the QRS complex with respect to the PLI and $\tilde{y}$ still contains remainders of the QRS complex. Due to the remainders of the QRS complex, the variance in the observation noise is time-varying and increases during a QRS complex. Moreover, remainders of the QRS complex also cause a temporal increase in the correlation of $\tilde{y}$. Hence, the innovation signal $\hat{v}$ will be less white during a QRS complex, reducing the performance of the parameter estimation by the KS.

From Eq. 3.9 we can see that an increase in r_{n+1} will lead to a decrease in K_n. In turn, from Eq. 3.7 we can observe that for low K_n, a new estimation of the PLI ($\hat{x}_{n+1|n+1}$) will mostly depend on the a priori estimate ($A\hat{x}_{n|n}$) and less on observation $\tilde{y}_{n+1}$. Therefore, to reduce the influence of the remainders of the QRS complex on the parameter estimation, it is important to include in our method a time-varying estimation of r_{n+1}.

Since r_{n+1} represents the variance of the signal without PLI, it can be estimated based on the signal that remains after passing $\tilde{y}$ through a forward coarse fixed-bandwidth notch filter ($\tilde{y}^f$). However, after a sudden change in PLI (e.g. a step increase in amplitude), $\tilde{y}^f$ will be contaminated by some remaining PLI due to the response time of the fixed-bandwidth notch filter, as shown in Fig. 3.2a. As a consequence, if r_{n+1} is estimated based on $\tilde{y}^f$, the value of r_{n+1} will increase after a sudden change in PLI. In turn, the increase in r_{n+1} leads to a decrease in K_n, while actually an increase in K_n is required for fast adaptation of the KS model parameters to the changes in PLI.

Instead of estimating r_{n+1} only based on $\tilde{y}^f$, we estimate r_{n+1} based on a combination of $\tilde{y}^f$ and a backward fixed-bandwidth notch filter (denoted as $\tilde{y}^b$). If a sudden change in PLI occurs at time t, $\tilde{y}^f$ has no remaining PLI before time t, while $\tilde{y}^b$ has no remaining PLI after time t, as shown in Fig. 3.2a. Combining information from $\tilde{y}^f$ and $\tilde{y}^b$ leads to an accurate estimation of r_{n+1}, except at time t.

By taking the sum of absolute values for $\tilde{y}^f$ and $\tilde{y}^b$ over a time window M that corresponds to the length of a QRS complex, the amplitudes of the resulting
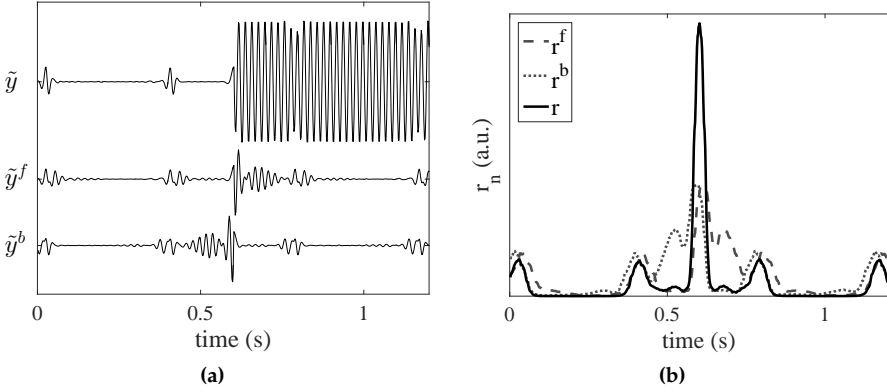
Figure 3.2: Estimation of the observation noise r_n.

signals are expected to be higher during a QRS complex with respect to other parts of the signals. We thus estimate the observation noise as:

$$\hat{r}_n = \frac{1}{M} \sum_{j=n-M/2}^{n+M/2} |\tilde{y}_j^f| \cdot \frac{1}{M} \sum_{j=n-M/2}^{n+M/2} |\tilde{y}_j^b|. \tag{3.17}$$

As fixed-bandwidth notch filter we use a second-order Butterworth notch filter, with cutoff frequencies of 45 Hz and 55 Hz. Note that the approach described above requires a delay τ^{fb} to compute $\tilde{y}^b$. Because $\hat{r}_{n+1}$ needs to be calculated in order to obtain the smoothed estimate of the PLI at time $n - \tau$, the delay τ^{fb} is in addition to the delay τ of the fixed-lag KS.

Process noise

As noted by Sameni, the ratio between the observation and process noise ($\gamma_n = q_n/r_n$) is related to the quality factor (Q-factor) of the KF described in section 3.2.1 [135]. Low γ_n is related to a high Q-factor and a narrow bandwidth notch filter. High γ_n is related to a low Q-factor and a broad bandwidth notch filter.

Similar to [135], an average value $\bar{\gamma}$ is chosen and $\bar{\gamma}$ is then adjusted to variations in SNR. Variations around $\bar{\gamma}$ are based on the ratio between the variance of the innovation signal and the estimated variance of the innovation signal by the KS [135]. The value of γ_n is estimated as

$$\hat{\gamma}_n = \bar{\gamma} \cdot \frac{\hat{v}_n^2}{h^\mathsf{T}(A P_{n-1|n-1} A^\mathsf{T} + q_{n-1} b b^\mathsf{T})h + r_n}. \tag{3.18}$$

The process covariance q_n can then be estimated as the product of $\hat{\gamma}_n$ and $\hat{r}_n$. However, as discussed in section 3.2.4 both $\hat{r}_n$ and $\hat{v}_n$ increase during a QRS complex, due to remainders of the QRS complex in $\tilde{y}$. This means that the process noise also increases during a QRS complex, leading to a faster adaptation of

parameters. To prevent this unwanted effect, we used a moving average window with length L to calculate the process noise as:

$$\hat{q}_n = \frac{1}{L} \sum_{j=n-L+1}^{n} \hat{r}_j \cdot \frac{1}{L} \sum_{j=n-L+1}^{n} \hat{\gamma}_j. \tag{3.19}$$

The value of L should be chosen longer than an inter-beat-interval, so that $\hat{r}_n$ and $\hat{\gamma}_n$ are averaged over multiple heartbeats. Values of $\bar{\gamma}$ and L were empirically determined and set to $\bar{\gamma} = 1 \cdot 10^{-3}$ and $L = 1$ s.

3.2.5 Harmonics

The fixed-lag KS can easily be extended to also suppress the harmonics of the PLI. Since the harmonics are well separated in the frequency domain, it is possible to design a separate KS for each harmonic. Each KS will only affect its corresponding notch frequency and will not interfere with the estimation of a different harmonic.

3.2.6 Other methods for PLI suppression

For comparison, several other methods from the literature for removal of PLI have been implemented. We selected representative methods that use a different approach for suppression of the PLI. To this end, we implemented a fixed notch filter, an LMS based filter, and the KF described in section 3.2.1. These methods are only briefly discussed in this section. Settings for the algorithms were empirically determined and optimized for the current study.

For the fixed notch filter we used a second order IIR Butterworth filter [137]. Fixed notch filters suppress a predetermined frequency range. For the selection of the cutoff values of the stopband, one should account for the distortion of the filter on the ECG and the ability of the filter to suppress a time varying PLI. Selecting a narrow stop band generally causes less distortion of the ECG, however this leads to problems whenever the PLI is unstable. We used a stop band with cutoff values of $f_0 \pm 2$ Hz.

The performance of the fixed notch filter can be improved by filtering the signal in the backwards direction after filtering the signal in the forward direction. Since the fixed notch filter used in this paper is a linear time-invariant filter, any phase distortion of the ECG caused by the forward filter will be canceled out by the backward filtering [146]. Moreover, the amplitude response is squared, meaning that the attenuation in dB is doubled in the stop band. Although forward-backward filtering is generally used for off-line applications, it is possible to implement it with some time delay for semi real-time applications. We set the delay similar to the delay τ^{fb} of the backward filter used to estimate r_n in section 3.2.4.

Besides the fixed notch filter, we also implemented the LMS based Improved Adaptive Canceller (IAC), that was developed by Martens et al. [112]. The IAC

algorithm is able to track amplitude, phase, and frequency changes of the PLI, with frequency deviations up to 4 Hz. Moreover, the method accounts for the interference of the QRS complex in the parameter estimation. Martens showed that performance of IAC was superior to other adaptive algorithms for PLI suppression and this algorithm is thus used to represent adaptive filters. In the study of Martens, separate learning rates were derived for the amplitude (K_a), phase (K_ϕ), and frequency (K_ω) of the PLI. We used similar values for K_ϕ and K_ω as suggested in the paper. However, we noticed that K_a was too low and often parameter estimation of the PLI did not converge. Therefore, the value of K_a was empirically determined and increased from 8 s^{-1} to 100 s^{-1}.

Finally, we also compared our results to the results of the linear KF that was developed by Sameni [135]. Since this algorithm is described in section 3.2.1, we do not further discuss it here. In contrast to the KS, the KF suggested in [135] does not use a time-varying estimation of the observation noise to account for the ECG. Instead, the observation noise is estimated as the variance of the signal that remains after filtering y with a fixed-bandwidth notch filter. We used the same settings for the KF as for the fixed-lag KS ($\bar{\gamma} = 1e^{-3}$ and $L = 1$ s).

3.3 Data acquisition

3.3.1 Simulated PLI

To validate our method a dataset of ten neonatal ECG recordings was used. Signals were acquired at the Máxima Medical Center (Veldhoven, The Netherlands) and were recorded with a sample rate of 500 Hz. From each recording, a segment of one minute was selected. Because the signals were recorded with adhesive electrodes in a controlled environment, we were able to select segments with clean neonatal ECG that did not show any PLI.

The clean ECGs were then corrupted by simulated PLI. Depending on the country, f_0 can be either 50 Hz or 60 Hz. We used 50 Hz for the simulations since this is used in European countries, but methods work similarly for 60 Hz. Algorithms were evaluated for several conditions of PLI: a PLI with a step increase and decrease in amplitude, a constant PLI, and a PLI with sinusoidal modulated amplitude at a frequency of 0.2 Hz to represent respiratory coupled changes.

In order to simulate similar SNR conditions of the clean ECG signals (s_n) with respect to the PLI (x_n) for all recordings, we normalized the ECG signals to unit power. The amplitude of the PLI was then determined based on the SNR as

$$S_{in} = 10 \log_{10} \left(\frac{P_s}{P_x} \right), \tag{3.20}$$

where P_s is the power of the ECG signal and P_x is the power of the PLI. PLI was simulated for different S_{in}, ranging from -20 dB to 20 dB. A step increase in PLI amplitude was simulated by decreasing the SNR from ∞ (0 V PLI amplitude)

to S_{in}. A step decrease in PLI amplitude was simulated by increasing the SNR from S_{in} to ∞ (0 V PLI amplitude). Similarly, PLI with sinusoidal amplitude was simulated by modulating the SNR from ∞ (PLI amplitude of 0 V) to S_{in}.

Besides varying S_{in}, we also considered the influence of frequency deviations from the theoretical PLI frequency. For this purpose, we simulated PLI with frequency deviations up to $\Delta f = \pm 0.1$ Hz, at a S_{in} of -20 dB. We did not separately simulate a phase shift in the PLI, since simulating a frequency deviation from the PLI frequency is equivalent to a phase shift that increases linearly over time by $\Delta f \cdot n$.

3.3.2 Real PLI

Besides simulated PLI, we evaluated the performance of our method for recordings that are contaminated by real PLI. To show that the developed method is not limited to neonatal ECG applications, we used an adult and a fetal ECG recording as examples. Both recordings were obtained from abdominal ECG recordings, acquired at the Máxima Medical Center (Veldhoven, The Netherlands). For the fetal ECG, the abdominal signal was first pre-processed to suppress the maternal ECG using a dynamic template subtraction method [120].

3.3.3 Evaluation criteria

To evaluate the performance of the algorithms, several evaluation criteria were used.

Settling time

To quantify the step response of the algorithms, we used the settling time [147]. The settling time is defined as the time required for the error of the estimation of the PLI to settle within 5% of the step increase or decrease in amplitude. The first of 100 samples for which the error was under 5% for the full 100 samples was selected as the settling time.

For causal filters such as IAC and KF, once parameter estimation has converged before the step increase or decrease, only an error is seen in the parameter estimation after the step. In contrast, KS and the forward-backward filtering of IIR will also show an error before the step increase or decrease. Therefore, we used the sum of the settling time before and after the step as the total settling time.

Output SNR

To evaluate the performance of the algorithms for ECGs that were corrupted with constant PLI and PLI with sinusoidal amplitude modulation, we used the

SNR at the output of the filters. Similar to the definition of S_{in}, the SNR at the output was defined as

$$S_{out} = 10 \log \left(\frac{P_s}{P_z} \right), \qquad (3.21)$$

with $z = x - \hat{x}$, which represents the remaining PLI. To calculate P_z, the first and final second of z were excluded. Otherwise, results might be influenced by initialization effects that are unrelated to the type of simulated PLI (i.e. constant amplitude or PLI with sinusoidal amplitude modulation).

Computational complexity

To measure the computational complexity, we used the number of multiplications per sample (MPS) after the initialization phase of the algorithms. Because for most digital signal processors (DSPs) the complexity of additions and subtractions is negligible compared to multiplications, additions and subtractions were not considered.

3.4 Results

The fixed-lag KS and the methods described in section 3.2.6 were implemented in Matlab. The time delays of the KS and forward-backward IIR were determined empirically and both were set to 0.2 s (100 samples). The total delay of KS therefore is $\tau^{fb} + \tau = 0.4$s. The computational complexity of KS depends on its time delays. Based on our implementation of KS, we empirically determined that the computational complexity is equal to $10 + 10\tau^{fb} + 16\tau$, which is in the order of 10^3 MPS.

Fig. 3.3 shows examples of the output of the PLI filters for a neonatal ECG recording that is corrupted by simulated PLI with a step increase and decrease in amplitude, a constant PLI, and a PLI with sinusoidal amplitude modulation. In each example, PLI was simulated at $S_{in} = -20$ dB and $\Delta f = 0$ Hz. Fig. 3.4 shows examples of the output of the PLI filters for an adult and a fetal ECG recording that are corrupted by real PLI.

Table 3.1 shows the average settling time for a step increase and decrease in PLI amplitude. Tables 3.2-3.4 shows the average performance for different segments of the ECG (P-wave, QRS complex, and T-wave) under different PLI conditions. We defined the QRS complex as a segment of size M surrounding the R-peak (i.e. 80 ms for adult and 40 ms for fetal ECG [138]). The P-wave was defined as the segment before the start of the QRS complex and the T-wave as the segment after the end of the QRS complex. Table 3.2 shows average S_{out} if there is no PLI, Table 3.3 for PLI with constant amplitude, and Table 3.4 for PLI with sinusoidal amplitude modulation. All values are expressed as mean $\pm$ standard-deviation.

(a) Step increase.

(b) Step decrease.

(c) Constant amplitude.

(d) Sinusoidal amplitude.
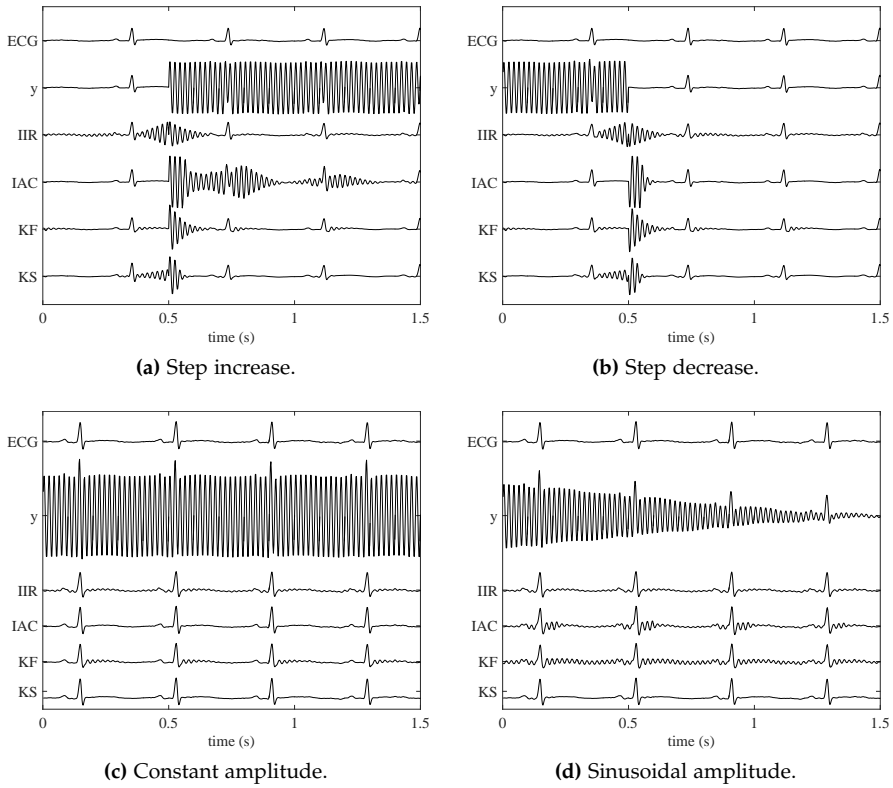
Figure 3.3: Examples for a neonatal ECG recording corrupted with simulated PLI. The following signals are depicted: ECG is the original recording, y is the recording corrupted by simulated PLI, and IIR to KS are the results of the filters.

(a) Adult ECG (with $M = 80$ ms).

(b) Fetal ECG (with $M = 40$ ms).
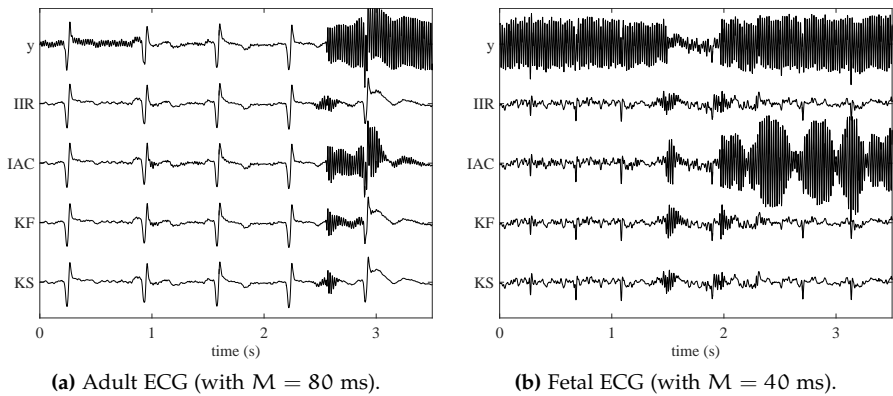
Figure 3.4: Examples for an adult and a fetal ECG recording with real PLI.

Table 3.1: Settling time for a step increase and decrease in PLI amplitude ($S_{in} = -20$ dB and $\Delta f = 0$ Hz).

Algorithm	amplitude increase (s)	amplitude decrease (s)
IIR	0.26 ± 0.01	0.27 ± 0.06
IAC	1.15 ± 0.23	**0.14 ± 0.06**
KF	0.22 ± 0.10	0.22 ± 0.10
KS	**0.16 ± 0.07**	**0.14 ± 0.03**

Table 3.2: S_{out} in absence of PLI ($S_{in} = \infty$).

Algorithm	overall	P-wave	QRS complex	T-wave
IIR	20 ± 3	20 ± 3	16 ± 4	21 ± 4
IAC	**38 ± 5**	**40 ± 6**	**42 ± 6**	**40 ± 5**
KF	17 ± 3	35 ± 4	11 ± 3	18 ± 4
KS	37 ± 5	36 ± 4	36 ± 5	39 ± 5

Table 3.3: S_{out} for constant PLI amplitude ($S_{in} = -20$ dB and $\Delta f = 0$ Hz).

Algorithm	overall	P-wave	QRS complex	T-wave
IIR	20 ± 3	20 ± 3	16 ± 4	21 ± 4
IAC	34 ± 4	**36 ± 5**	35 ± 5	36 ± 4
KF	17 ± 3	35 ± 4	11 ± 3	18 ± 4
KS	**37 ± 5**	**36 ± 4**	**36 ± 5**	**41 ± 6**

Table 3.4: S_{out} for sinusoidal PLI amplitude ($S_{in} = -20$ dB and $\Delta f = 0$ Hz).

Algorithm	overall	P-wave	QRS complex	T-wave
IIR	20 ± 3	20 ± 3	16 ± 4	21 ± 4
IAC	7 ± 2	15 ± 1	7 ± 1	10 ± 1
KF	9 ± 1	12 ± 0	7 ± 1	11 ± 1
KS	**30 ± 2**	**32 ± 3**	**26 ± 2**	**35 ± 4**

The effect of varying S_{in} on the S_{out} is shown in Fig. 3.5 and the effect of varying the frequency deviation from the theoretical PLI frequency is shown in Fig. 3.6.

(a) Constant amplitude.

(b) Sinusoidal modulated amplitude.
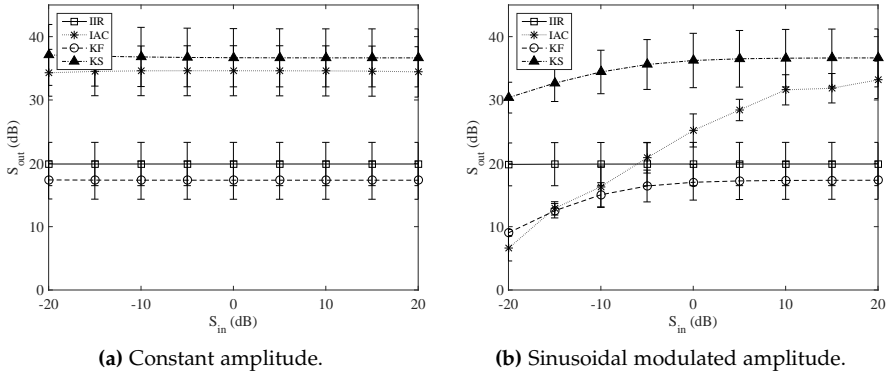
Figure 3.5: Influence of PLI amplitude on S_{out}. PLI was simulated with $\Delta f = 0$ Hz.

(a) Constant amplitude.

(b) Sinusoidal modulated amplitude.
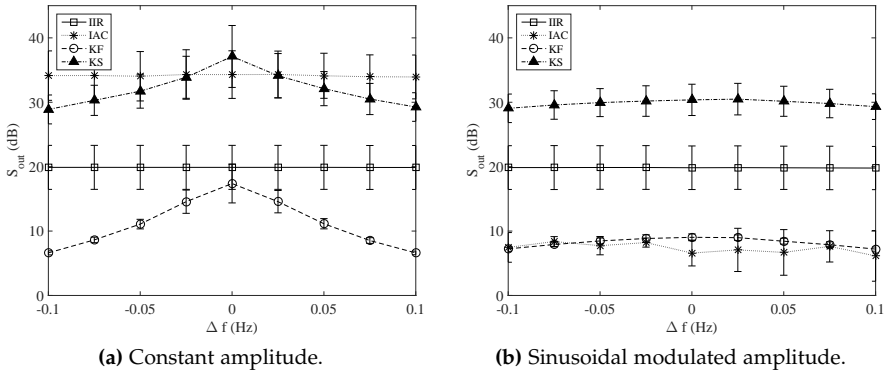
Figure 3.6: Influence of frequency deviation from the PLI frequency on S_{out}. PLI was simulated for $S_{in} = -20$ dB.

3.5 Discussion

Filtering PLI from ECG recordings can lead to significant distortions of the ECG waveform. Traditional fixed-bandwidth notch filters distort the ECG by ringing due to the overlap of the frequency content of the QRS complex with the PLI frequency. As an alternative to suppress PLI, adaptive filtering techniques can be used. However, the ECG often interferes with the parameter estimation of the adaptive filters, also leading to distortion of the ECG waveform. In this study, the problem of interference of the ECG with parameter estimation was solved by implementation of a fixed-lag KS in combination with an adaptive noise estimation. The examples in Fig. 3.3 and 3.4 show that the proposed method can be used for filtering PLI from adult, neonatal, and fetal ECG recordings.

3.5.1 Step response

We quantified the step response of the filters based on the settling time. From the examples in Fig. 3.3a and Fig. 3.3b it can be observed that the output of the forward-backward IIR filter and KS are also affected by the step increase and decrease in the period before the step occurs.

Overall, KS has the shortest settling time for both a step increase and decrease in PLI amplitude (0.16 s and 0.14, respectively), as shown in Table 3.1. Although the settling time of IAC was similar for a step decrease (0.14 s), the settling time for a step increase was much longer (1.15 s). Slower convergence of IAC for a step increase was also observed by Martens [112]. This is partially due to the fact that IAC requires separate estimation of the amplitude and phase of the PLI. Since both are unknown before the step increase, a longer period is required for the filter to converge. The KF and KS do not have this problem, because amplitude and phase variations are combined into a single parameter.

Although KS uses a fixed-bandwidth notch filter to estimate observation noise r_n, the settling time of KS is shorter than the settling time of IIR (0.27 s and 0.29 s for step increase and decrease, respectively). From Fig. 3.3a and 3.3b it can be seen that a fixed-bandwidth notch filter performs suboptimal during a step in PLI amplitude, which would in turn result in a poor estimation of the observation noise. By combining information from a forward and backward fixed-bandwidth notch filter, we were able to give a more accurate estimate of the observation noise during a step. The settling time of KS is thus minimally affected by the poor performance of the fixed-band notch filter.

3.5.2 Influence PLI amplitude

Results in Tables 3.2, 3.3, and Fig. 3.5a show that under stationary PLI conditions, IAC and KS perform similarly well. In the absence of PLI the performance of IAC is slightly better (S_{out} is 38 dB for IAC and 37 dB for KS), while for a constant PLI amplitude the performance of KS is slightly better (S_{out} is 34 dB for IAC and 37 dB for KS). Regardless of S_{in}, performance of both IAC and KS is substantially better compared to the performance of IIR and KF (S_{out} is 20 dB and 17 dB, respectively).

Since the attenuation of IIR is -70 dB at the PLI frequency, the performance of IIR does not depend on S_{in} and the lower performance of IIR is due to ringing caused by the QRS complexes. The lower performance of the KF is because the model parameters are adapted to the QRS complexes, leading to distortion of the ECG waveform. Since KF is a causal filter, in particular the QRS complex and T-wave are distorted, as is seen from Tables 3.2 and 3.3. Unlike KF, in IAC and KS the learning rate is reduced during a QRS complex to prevent QRS complexes from interfering with the parameter estimation. As a result, under stationary PLI conditions the QRS complex and T-wave are hardly distorted after filtering with IAC and KS.

For a PLI with sinusoidal modulated amplitude the performance of all adaptive filters (IAC, KF, and KS) depends on S_{in}, as shown in Fig. 3.5b. In this case, the PLI amplitude changes continuously and thus PLI parameters also need to be adapted continuously. As S_{in} decreases, the amplitude of the sinusoidal modulation increases and hence the PLI amplitude changes more rapidly. In particular IAC and KF shows poor performance for low S_{in} (respectively 7 dB and 9 dB at $S_{in} = -20$ dB).

As a consequence of the continuous variation in PLI amplitude, reducing the learning rate during a QRS complex results in an error in the estimation of the PLI amplitude. As S_{in} decreases this error increases, leading to a decrease in S_{out}. Although both IAC and KS reduce parameter adaptation during a QRS complex, for KS the error in the estimation of the amplitude after each QRS complex is corrected for by the backward smoothing. This effect is reflected by the relatively high S_{out} of the P-wave and T-wave with respect to S_{out} of the QRS complex, as shown in Table 3.4. As a result, KS performs well ($S_{out} = 30$ dB) even in case of $S_{in} = -20$ dB and performance is significantly better compared other filters.

3.5.3 Influence PLI frequency deviation

In Fig. 3.6 the influence of deviating the frequency from the theoretical PLI frequency is shown on the S_{out}. Although according to the power system quality standards frequency deviations are typically limited to ± 0.01 Hz [139], we simulated frequency deviations up to ± 0.1 Hz.

From Fig. 3.6 it is observed that frequency deviations have little effect on the performance of IIR and IAC. Since for IIR the stopband was set to 48 to 52 Hz, no effect was expected. Besides, IAC was developed to track changes in frequency deviations and also no effect was expected for IAC.

In contrast to IIR and IAC, performance of KF and KS is affected by varying the PLI frequency from the frequency that is assumed by the model of KF and KS. Since for KS parameter adaptation is reduced during a QRS complex, the estimated PLI during a QRS complex is mostly determined by previous estimates and less by observations of the PLI. This means that, if the frequency of the model differs from the frequency of the observed PLI, the phase of the estimated PLI differs from the phase of the observed PLI after each QRS complex. As the frequency deviation increases, this phase difference increases and S_{out} decreases.

Instead of assuming a fixed PLI frequency, for future work it might be interesting to develop a KS for a model that includes the PLI frequency as a separate model parameter. Note, however, that in this case the expression in Eq. 3.2 would no longer be valid and the model becomes non-linear [136].

Despite the dependency of the performance of KS on the frequency deviation, our simulations show that KS outperforms other algorithms, even up to frequency deviations of ± 0.1 Hz. Although for a PLI with constant amplitude

and frequency deviation of ± 0.1 Hz IAC has a better S_{out} (S_{out} is 35 dB for IAC and 29 dB for KS), the S_{out} for a PLI with sinusoidal modulated amplitude is much worse (S_{out} is 7 dB for IAC and 29 dB for KS).

3.5.4 Computational complexity

The computational complexity of KS depends on the time delay used for the filter (τ^{fb} and τ). Since for each new sample the smoothing needs to be performed over the entire delay, increasing the delay substantially contributes to the complexity. For the selected time delays in this study, the computation complexity was in the order of 10^3 MPS. In contrast, IAC and KF are causal filters and their MPS is much smaller (39 MPS and 50 MPS, respectively).

Despite the relatively high computational complexity with respect to the causal filters, at a sampling rate of 500 Hz KS still only requires about 10^6 multiplications per second. Assuming that the clock frequency of a modern DSP is in the order of GHz (e.g. C6000™ series by Texas Instruments, Dallas, TX), KS only requires 0.1% of the entire capacity of the DSP. Therefore, real time implementation of KS should not be a problem.

For off-line applications it is possible to use a fixed-interval KS as an alternative to a fixed-lag KS [140]. Instead of calculating smoothed estimates for a fixed time lag τ, the fixed-interval KS gives smoothed estimates based on all observations in the signal. The fixed-interval KS first runs the forward KF over the entire signal, after which smoothed estimates are obtained by a backward KS. Since this approach only requires a single forward and backward run, the computational complexity reduces to 129 MPS.

3.6 Conclusion

In this study, a linear fixed-lag KS was developed to suppress PLI in ECG recordings. The developed KS outperforms other methods that have been proposed in the literature in terms of step response settling time and output SNR. The proposed method can be used for semi real-time applications with a time delay of 0.4 s.

4

HIERARCHICAL BAYESIAN FRAMEWORK FOR FETAL R-PEAK DETECTION, USING ECG WAVEFORM AND HEART RATE INFORMATION

Abstract - *The abdominal fetal electrocardiogram (ECG) can provide valuable information about fetal well-being. However, fetal R-peak detection in abdominal fetal ECG recordings is challenging due to the low signal-to-noise ratio (SNR) and the non-stationary nature of the fetal ECG waveform in the abdominal recordings. In this paper, we propose a multichannel hierarchical Bayesian framework for fetal R-peak detection, that combines predictive models of the ECG waveform and the heart rate. The performance of our method was evaluated on set-A of the 2013 Physionet/Computing in Cardiology Challenge and compared to the performance of several methods that have been proposed in the literature.The hierarchical Baysian framework presented in this study outperforms other methods for fetal R-peak detection with a mean overall detection accuracy for set-A of 99.6%. Even for recordings with low SNR our method enables reliable fetal R-peak detection (accuracy of 99.4%).*[1]

4.1 Introduction

Since the 1960s, the most widely used technique for fetal monitoring is cardiotocography (CTG) [5]. CTG provides simultaneous information on the fetal heart rate (FHR) and uterine activity. However, interpretation of CTG suffers from a low specificity, resulting in unnecessary operative deliveries [9].

To obtain additional information on fetal well-being in case of an abnormal CTG, the fetal electrocardiogram (ECG) could be used [19]. From the fetal ECG it is possible to extract beat-to-beat FHR information that is required for reliable analysis of fetal heart rate variability (HRV) [42]. Moreover, analysis of the fetal ECG waveform could provide information on fetal oxygen deficiency [1]. Both for HRV analysis and fetal ECG waveform analysis accurate R-peak detection is required.

Generally, the fetal ECG is obtained invasively using an electrode attached to the fetal scalp [1]. Although the signal quality of invasive fetal ECG is good, it can only be used during delivery after the fetal membranes have ruptured. An alternative that can also be used earlier in the pregnancy is to measure the fetal ECG non-invasively by electrodes placed on the maternal abdomen [118].

The low invasiveness of the abdominal fetal ECG comes at a cost of a reduction in signal-to-noise ratio (SNR) [148]. The abdominal fetal ECG is contaminated by electrical interferences such as the maternal ECG, muscle activity, power line interference, and measurement noise. Moreover, in the period between 28 to 32 weeks of gestation, an isolating layer (the vernix caseosa) surrounds the fetus and reduces the amplitude and affects the shape of the abdominal fetal ECG [106].

In recent years, abdominal fetal ECG recordings have been extensively studied, most studies focusing on suppression of the maternal ECG, which is the dominant interference [44, 118–123]. In 2013, the aim of the PhysioNet/Computing in Cardiology Challenge (further referred to as Challenge) was to extract the FHR from abdominal recordings [149]. A variety of algorithms was presented for maternal ECG suppression, such as template subtraction [118–120], adaptive filtering [44, 121], blind source separation (BSS) [122, 123, 125], or a combination of different algorithms [126–128]. For an extensive review see [148] or [46]. To compare different algorithms, a database of abdominal fetal ECG recordings was made publicly available.

After maternal ECG suppression, fetal R-peak detection is often performed by adapting existing algorithms for adult R-peak detection [127, 128, 150]. However, even after maternal ECG suppression, the SNR of the abdominal fetal ECG is generally still much lower than the SNR for adult ECG recordings. Since algorithms for adult R-peak detection are optimized for relatively high SNR, this can lead to numerous mis-detections for the low-SNR abdominal fetal ECG.

Besides low SNR, the position and orientation of the fetus within the abdomen are a priori unknown and can change during a recording. Therefore, the abdominal fetal ECG is typically recorded using multiple electrodes spread across

Figure 4.1: Block diagram of fetal heart rate detection. M is the number of channels and T is the total time of the recording.

the abdomen [114]. The SNR and waveform of the fetal ECG in each channel depends on the fetal position and orientation. Hence, fetal movement with respect to the abdominal electrodes can cause variations in the SNR and fetal ECG waveform of a certain channel [48]. Despite this fact, several studies performed R-peak detection on each individual channel after which a post-processing step was used to select the channel with the best RR-series [125–127]. Although in [128] a multi-channel matched filter approach was used for fetal R-peak detection, changes in fetal ECG waveform were not considered for the matched filter. Both approaches can lead to reduced performance in case of fetal movement.

In short, the low SNR and the non-stationary nature of the abdominal fetal ECG make fetal R-peak detection challenging. In this study, we propose an adaptive multi-channel R-peak detection method that combines ECG waveform and FHR information. A schematic overview of the detection algorithm is shown in Fig. 4.1. The paper is structured as follows: first, pre-processing and maternal ECG suppression are discussed in section 4.2.1. Then, the fetal ECG and FHR model are explained in section 4.2.2, and a hierarchical Bayesian framework for R-peak detection is discussed in sections 4.2.3 to 4.2.8. Extension to multiple channels is explained in section 4.2.9. Finally, results and discussion are presented in sections 6.3 and 6.4.

4.2 Methods

4.2.1 Pre-processing and maternal ECG suppression

Analysis of the results of the Challenge showed that the best performing algorithms used a similar approach to suppress the maternal ECG [126–128]. In this approach, a matrix of maternal ECG complexes is created, with each row corresponding to one maternal ECG complex. Then, a Principal Component Analysis based approach is used to extract the most significant eigenvectors of this matrix. These eigenvectors contain information about the average maternal ECG complex and morphological variations in the maternal ECG complexes (e.g. due to respiration). The largest eigenvectors are used to estimate the maternal ECG and subtract it from the original signal.

In this study, we used the algorithm of Varanini et al. [126] for maternal ECG suppression, that is online available [149]. Note that in this algorithm the data is pre-processed to suppress baseline wandering, high frequency noise, and power

(a) Raw signals (maternal and fetal ECG).

(b) Fetal ECG.

(c) Fetal ECG after ICA (**Y**).
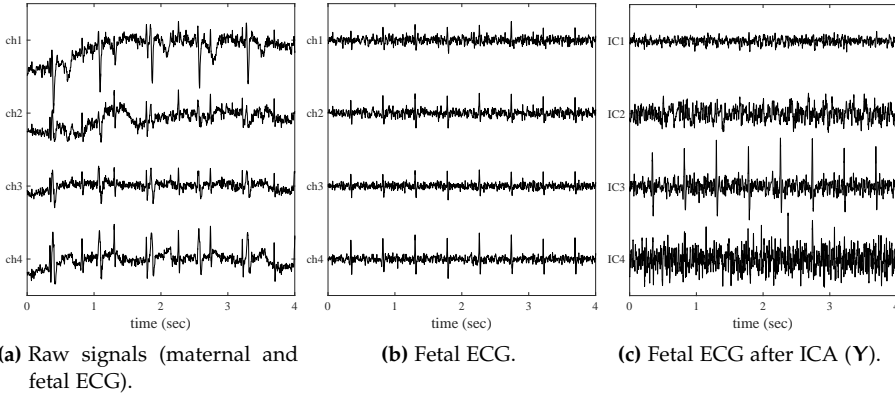
Figure 4.2: Signals before and after pre-processing, maternal ECG suppression, and ICA.

line interference. After pre-processing and maternal ECG suppression, Independent Component Analysis (ICA) is used to further enhance the fetal ECG. Since our study focuses on fetal R-peak detection, the method of Varanini is not discussed in detail and we will use the signals after maternal ECG suppression and ICA (**Y**) as starting point for our fetal R-peak detection method. An example of the original signals, the fetal ECG after pre-processing and maternal ECG suppression, and **Y** are shown in Fig. 4.2.

4.2.2 Fetal ECG model

We now proceed with a single channel approach (sections 4.2.2-4.2.8) and then extend our model to multiple channels in section 4.2.9. A single ECG signal after pre-processing, maternal ECG suppression, and ICA is denoted as $y(t)$, where t is a time index. The location of the k-th fetal R-peak is denoted as μ_k, and the k-th RR-interval as $w_k = \mu_k - \mu_{k-1}$.

Gaussian QRS model

In abdominal fetal ECG recordings, the amplitude of the fetal QRS complex is generally large compared to other segments of the fetal ECG (the P-, and T-wave). Therefore, our model for R-peak detection is limited to describing the fetal QRS complex. It is important that the QRS model is flexible, because it is a priori unknown what the fetal orientation and location is with respect to the abdominal electrodes.

Our QRS model is inspired by a model that was proposed by McSharry et al., which uses Gaussian kernels to describe the fetal ECG [151, 152]. A disadvantage of the model of McSharry is that a relatively large number of parameters is
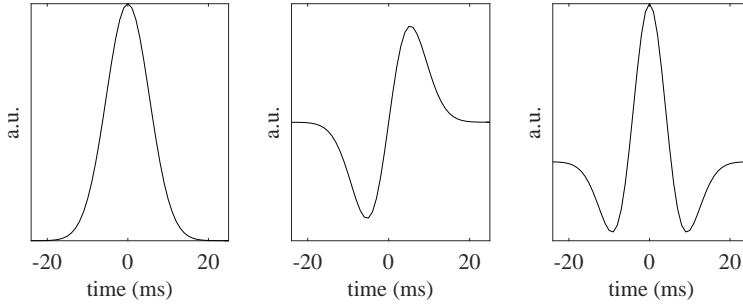
Figure 4.3: Example QRS model. From left to right: Gaussian, first derivative, and second derivative.

required to described the QRS complex (nine parameters in total). Moreover, the locations of the Q- and S-peak need to be determined with respect to the R-peak.

As noted by Biglari et al., the abdominal fetal ECG is recorded at far-field and the morphology of the QRS complex is not as diverse and complex as for the adult ECG [50]. In our approach, the QRS complex is modeled by the sum of a Gaussian (mainly modeling the R-wave), its first derivative (mainly modeling the Q- and S-wave), and its second derivative (modeling the Q-, R-, and S-wave). Examples of these functions are shown in Fig. 4.3. The combination of these functions can be used to describe the QRS complex for most abdominal fetal ECG recordings [50].

Assuming that the Gaussian, its first, and second derivative are centered around time μ_k, our QRS model is written as

$$G(t, \mu_k, z) = \left(a_1 + a_2(t - \mu_k) + a_3\left(1 - \frac{(t - \mu_k)^2}{b^2}\right) \right) e^{\frac{-(t - \mu_k)^2}{2b^2}}, \tag{4.1}$$

where $z = [a_1, a_2, a_3, b]$, and $a_{1,2,3}$ are the amplitudes of the Gaussian, its first and its second derivative. Note that for the first and second derivative a factor $1/b^2$ is included in terms a_2 and a_3, respectively. The QRS model in Eq. 4.1 depends on four parameters and does not require knowledge on the location of the Q- and S-peak.

Besides containing the fetal QRS complex, $y(t)$ will be contaminated by electrical interferences, such as muscle artifacts, remainders of the maternal ECG, and measurement noise. These inferences are represented by an additive noise term ξ_t, which will be referred to as the observation noise of the QRS model. Because ξ_t is a combination of several signals, including measurement noise, we will assume ξ_t to have a zero-mean Gaussian distribution with variance λ_t. Given the location of the $k+1$-th R-peak, μ_{k+1}, we can write $y(t)$ during the $k+1$-th QRS complex as:

$$y(t) = G(t, \mu_{k+1}, z) + \xi_t \qquad \xi_t \sim \mathcal{N}(0, \lambda_t). \tag{4.2}$$

Since for each (regular) heartbeat the electrical activity of the fetal heart propagates in a similar way through the heart, the electrical activity will be similar across heartbeats. However, the electrical activity measured by the abdominal electrodes can vary over time due to fetal movement with respect to the electrodes. Assuming that during a ventricular contraction the fetal orientation remains constant, we can express the model parameters of the $k+1$-th QRS complex as

$$z_{k+1} = z_k + \eta_k \qquad \eta_k \sim \mathcal{N}(0, \Sigma_k). \tag{4.3}$$

Here, variations in z_k are assumed to be described by a zero-mean Gaussian random walk process η_k, with $[4 \times 4]$ covariance matrix Σ_k. We refer to η_k as the process noise of the QRS model.

Time-varying autoregressive FHR model

To describe the fetal HR, we use a p-th order time-varying autoregressive (TVAR) model [153, 154]. In the TVAR model the $k+1$-th RR-interval w_{k+1} is described as a linear combination of p previously detected RR-intervals $\mathbf{w}_k = [w_k, w_{k-1}, ..., w_{k-p+1}]^T$. Since $w_{k+1} = \mu_{k+1} - \mu_k$, we can use this model to predict the location of μ_{k+1}, given previous RR-intervals and μ_k. The order of the TVAR model was empirically determined and set to $p = 6$. The TVAR model is written as

$$w_{k+1} = \mathbf{w}_k^T \theta + v_{k+1} \qquad v_{k+1} \sim \mathcal{N}(0, R_{k+1}), \tag{4.4}$$

with $\theta = [\theta_1, ..., \theta_p]^T$ the TVAR model parameters. In Eq. 4.4, any variation in the FHR that cannot be captured by the linear TVAR model is represented by v_{k+1}. We refer to v_{k+1} as the observation noise of the FHR model and it is assumed to be zero-mean Gaussian with variance R_{k+1}.

Because variations in the FHR are regulated by the autonomic nervous system and the autonomic regulation varies over time (e.g. due to changes in fetal behavioral states [87]), parameters θ are also time-varying. We will assume that variations in θ can be modeled by a zero mean Gaussian $\mathbf{d}_k$, with $[p \times p]$ covariance $\mathbf{Q}_k$:

$$\theta_{k+1} = \theta_k + \mathbf{d}_k \qquad \mathbf{d}_k \sim \mathcal{N}(0, \mathbf{Q}_k). \tag{4.5}$$

The noise term $\mathbf{d}_k$ is referred to as the process noise of the FHR model.

4.2.3 Hierarchical Bayesian framework

Given μ_k and the estimated $k+1$-th RR-interval $\hat{w}_{k+1}$, we will look for the next R-peak μ_{k+1} within a predefined search window. The search window is limited to the interval $\mathbf{t} = \mu_k + \hat{w}_{k+1} \pm \frac{T}{2}$, with T the width of the search window (set to 400 ms). The search window is further limited by a minimum and maximum RR-interval (RR_{min} and RR_{max}, respectively), that are defined based on a range of
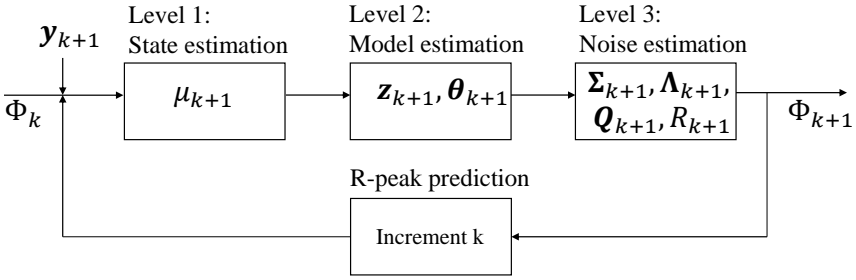
Figure 4.4: Schematic overview of the hierarchical model.

the FHR between 50 and 210 beats per minute (bpm) [1]. The observation noise in y_{k+1} is described by ξ_{k+1}, with covariance Λ_{k+1}. Notice that with respect to Eq. 4.2, we have changed from scalar to vector notation.

Based on this description of y_{k+1} and 4.4 we can define a state-space model for the $k+1$-th QRS complex:

$$
\begin{aligned}
\mu_{k+1} &= \mu_k + w_k^\mathsf{T}\theta_{k+1} + \nu_{k+1} & \nu_{k+1} &\sim \mathcal{N}(0, R_{k+1}) \\
y_{k+1} &= G(t, \mu_{k+1}, z_{k+1}) + \xi_{k+1} & \xi_{k+1} &\sim \mathcal{N}(0, \Lambda_{k+1}),
\end{aligned}
\tag{4.6}
$$

Given y_{k+1}, we are interested in estimating the new R-peak location μ_{k+1}. The uncertainties in the state-space model in Eq. 4.6 suggest that a probabilistic approach can be used to solve the estimation problem for μ_{k+1}. To find a tractable solution for inferring μ_{k+1}, we propose a hierarchical probabilistic framework that consists of three inference levels:

Level 1: State estimation. In this level, we estimate μ, while assuming that θ, z, and covariances Q, R, Σ, and Λ are known.

Level 2: QRS and FHR model estimation. In this level, we estimate θ and z, while assuming μ, Q, R, Σ, and Λ to be known.

Level 3: Noise estimation. In this level, we estimate Q, R, Σ, and Λ, while assuming μ, θ, and z to be known.

A schematic overview of the inference is presented in Fig. 4.4. Note that we used different inference strategies to estimate the model parameters (as summarized in Table 4.1), hence our hierarchical model is not fully Bayesian.

4.2.4 Level 1: State estimation

Given the estimated model parameters after observing the k-th QRS complex and new observation y_{k+1}, we want to predict the location of the $k+1$-th QRS complex. Using Bayes' rule we can describe the *posterior* probability density function for μ_{k+1} as

$$
p(\mu_{k+1}|y_{k+1}, \Phi_k) = \frac{p(y_{k+1}|\mu_{k+1}, \Phi_k)p(\mu_{k+1}|y_k, \Phi_k)}{p(y_{k+1}|y_k, \Phi_k)},
\tag{4.7}
$$

Table 4.1: Model parameters (Φ) and inference strategy.

Parameter	Estimation strategy
μ	MAP
z	EKF
θ	KF
Σ	empirically determined
Λ	from signal
Q	maximum likelihood
R	empirically determined

with $\Phi_k = \{\mu_k, z_k, \theta_k, w_k, \Sigma_k, \Lambda_k, Q_k, R_k\}$ our prior information about the model parameters from the previous iteration.

Because $p(y_{k+1}|y_k, \Phi_k)$ is a normalization factor that is independent of μ_{k+1}, the maximum *a posteriori* (MAP) estimate for μ_{k+1} can be written as:

$$\hat{\mu}_{k+1} = \underset{\mu_{k+1}}{\text{argmax}} \left(\ln p(y_{k+1}|\mu_{k+1}, \Phi_k) + \ln p(\mu_{k+1}|y_k, \Phi_k) \right), \qquad (4.8)$$

where the use of the log-posterior is justified by the monotonic behavior of the logarithm, which will not influence the MAP solution. In the next levels $\hat{\mu}_{k+1}$ is used to estimate the model parameters and noise covariances.

4.2.5 Level 2: QRS and FHR model estimation

Given observation y_{k+1} and the location of the $k+1$-th R-peak at $\hat{\mu}_{k+1}$, we want to update our model parameters θ and z. We will assume that the FHR does not influence the QRS waveform, and consider θ and z to be independent.

Extended Kalman filter to estimate QRS model

Using the QRS model that is explained in section 4.2.2, we can describe the waveform of the $k+1$-th QRS complex by the following state-space equations:

$$\begin{aligned}
z_{k+1} &= z_k + \eta_k & \eta_k &\sim \mathcal{N}(0, \Sigma_k) \\
y_{k+1} &= G(t, \hat{\mu}_{k+1}, z_{k+1}) + \xi_{k+1} & \xi_{k+1} &\sim \mathcal{N}(0, \Lambda_{k+1}).
\end{aligned} \qquad (4.9)$$

A tractable approximation for the MAP estimate $\hat{z}_{k+1}$ for z_{k+1} of this non-linear state-space model can be calculated using an Extended Kalman Filter (EKF) [140]. In the EKF formalism, a first order approximation is used to describe the non-linear function $G(t, \hat{\mu}_{k+1}, z_k)$. Note that the EKF provides the minimum mean

square error estimate, which is not necessarily identical to the MAP estimate in case of a non-linear model. The EKF update equations are given by [140]:

$$\hat{z}_{k+1} = \hat{z}_k + K_{k+1}^{QRS}(y_{k+1} - G(t, \hat{\mu}_{k+1}, \hat{z}_k)) \tag{4.10}$$

$$P_{k+1} = P_k + \Sigma_k - K_{k+1}^{QRS}J_{k+1}^T(P_k + \Sigma_k) \tag{4.11}$$

$$K_{k+1}^{QRS} = (P_k + \Sigma_k)J_{k+1}(J_{k+1}^T(P_k + \Sigma_k)J_{k+1} + \Lambda_{k+1})^{-1}, \tag{4.12}$$

with P_k the $[4 \times 4]$ covariance in z_k, K_{k+1}^{QRS} the $[4 \times T]$ Kalman gain of the QRS model, and J_{k+1} the $[4 \times T]$ Jacobian matrix $J_{k+1} = \frac{\partial G}{\partial z}\big|_{(z=\hat{z}_k)}$.

Kalman filter to estimate FHR model

Using the FHR model that is explained in section 4.2.2, the $k + 1$-th RR-interval can be described by the following state-space equations:

$$\begin{aligned} \theta_{k+1} &= \theta_k + d_k & d_k &\sim \mathcal{N}(0, Q_k) \\ w_{k+1} &= w_k^T\theta_{k+1} + v_{k+1} & v_{k+1} &\sim \mathcal{N}(0, R_{k+1}). \end{aligned} \tag{4.13}$$

Following a similar derivation as in [143], it is possible to show that the MAP estimate $\hat{\theta}_{k+1}$ for θ_{k+1} can be calculated using the linear Kalman filter update equations:

$$\hat{\theta}_{k+1} = \hat{\theta}_k + K_{k+1}^{HR}(w_{k+1} - w_k^T\hat{\theta}_k) \tag{4.14}$$

$$V_{k+1} = V_k + Q_k - K_{k+1}^{HR}w_k^T(V_k + Q_k) \tag{4.15}$$

$$K_{k+1}^{HR} = \frac{(V_k + Q_k)w_k}{w_k^T(V_k + Q_k)w_k + R_{k+1}}, \tag{4.16}$$

where V_k is the $[p \times p]$ covariance of θ_k and K_{k+1}^{HR} is the $[p \times 1]$ Kalman gain for the FHR model.

4.2.6 Level 3: Noise estimation

Process noise Σ_{k+1} of QRS model

Variations in the QRS waveform due to e.g. fetal movement are described by the process noise Σ_{k+1}. We assume identical and uncorrelated process noise for all QRS model parameters $a = [a_1, ..., a_3]^T$. The process noise variance σ_a^2 is assumed constant, and is defined as a fraction of the maximum of the squared average QRS complex in the initialization phase (see section 4.2.8): $\sigma_a^2 = c_a \max |QRS|^2$, where fraction c_a is empirically determined. Furthermore, although the width of the fetal QRS complex can vary during pregnancy, fetal movement will have little effect on the width. Hence the width is assumed to remain constant throughout a recording. Therefore, we assume zero process noise

for parameter b, which means that b is estimated recursively. The process noise Σ_{k+1} for z_{k+1} is thus described as

$$\Sigma_{k+1} = \Sigma = \begin{bmatrix} \sigma_a^2 & & & O \\ & \sigma_a^2 & & \\ & & \sigma_a^2 & \\ O & & & 0 \end{bmatrix}. \tag{4.17}$$

Observation noise Λ_{k+1} of QRS model

To estimate the covariance Λ_{k+1}, we will assume that the observation noise is uncorrelated and constant for observation y_{k+1}. Note that since ξ_{k+1} also describes correlated physiological noise (i.e. muscle activity) this assumption is only approximately true. The covariance matrix can then be written as $\Lambda_{k+1} = \lambda_{k+1}I_T$. with I_T the $[T \times T]$ identity matrix.

The estimation of λ_{k+1} is based on the variance in y_{k+1}. Typically, the duration of the fetal QRS complex is about $L = 40$ ms [138], which is about 10% of a fetal ECG complex (assuming a heart rate of 150 bpm). In the state estimation in level 1 (where the location of μ_{k+1} is estimated), the contribution of the QRS complex to the variance of y_{k+1} is accounted for by omitting the top 10% of the values of y_{k+1}. For the estimation of z_{k+1} in level 2 we update our estimate of λ_{k+1} by omitting samples of y_{k+1} within the region $\hat{\mu}_{k+1} \pm \frac{L}{2}$. The value of λ_{k+1} is determined as the variance in y_{k+1} over the remaining samples.

Process noise Q_{k+1} of FHR model

In a hierarchical Bayesian model, the likelihood function at a particular level is equal to the evidence at the next higher level [143]. This means that by maximizing the evidence of the FHR model in level 2 we can obtain the maximum likelihood solution for Q.

The evidence of the FHR model is given by:

$$p(w_{k+1}|y_{k+1}, \Phi_k) = \mathcal{N}(w_{k+1}|w_k^T\hat{\theta}_k, w_k^T(Q_k + V_k)w_k + R_{k+1}). \tag{4.18}$$

The value of $\hat{Q}_{k+1}$ can be calculated by differentiating Eq. 4.18 with respect to Q and equating it to zero. If we assume that $Q_{k+1} = q_{k+1}I_p$ and define the residual error of the FHR model as $r_{k+1} = w_{k+1} - w_k^T\hat{\theta}_k$, it can be shown that the maximum likelihood estimate for q_{k+1} is [143]:

$$\hat{q}_{k+1} = \begin{cases} \dfrac{r_{k+1}^2 - \mathbb{E}[r_{k+1}^2|q_{k+1}=0]}{w_k^T w_k} & \text{if } q_{k+1} \geqslant 0 \\ 0 & \text{otherwise} \end{cases} \tag{4.19}$$

Here $\mathbb{E}[r_{k+1}^2|q_{k+1} = 0] = w_k^T V_k w_k + R_{k+1}$, is the covariance of r_{k+1} if we assume that $q_{k+1} = 0$. Eq. 4.19 implies that, if r_{k+1} is larger than the predicted variance, the value of q_{k+1} increases. If q_{k+1} increases, the Kalman gain K^{HR} also increases and a new estimate of θ will depend more on incoming data.

Observation noise R_{k+1} of FHR model

Following discussions on HRV, we know that variations in the heart rate often cannot be fully described by a linear model [95]. This means that even in case we have optimally inferred θ, we can only approximate a new RR-interval up to a certain degree. Any stochastic or non-linear variation in the FHR is described by R_{k+1}.

Since the value of R_{k+1} defines how well we expect our linear model to describe the FHR, we will assume that $R_{k+1} = R_0$ is constant. A low value of R_0 leads to relatively high values of $\mathbf{Q}$ through Eq. 4.19. This means that θ will be adapted even for a small residual error. A large value of R_0 leads to relatively low values of $\mathbf{Q}$. In this case adaptation of θ is reduced, which allows for larger discrepancies between the predicted FHR and the observed FHR. The value for R_0 was empirically determined.

4.2.7 R-peak prediction

We can use our estimates for z_k and θ_k at the k-th iteration to predict the R-peak location at the $k+1$-th iteration. Accounting for the covariances in our estimation of z_k and θ_k (denoted by $\mathbf{P}_k$ and $\mathbf{V}_k$, respectively), and making use of the state space model in Eq. 4.6, we can write:

$$p(\mu_{k+1}|\mathbf{y}_k, \Phi_k) = \mathcal{N}(\mu_{k+1}|\hat{\mu}_k + \hat{w}_{k+1}, \Gamma^{HR}), \text{ and} \tag{4.20}$$

$$p(\mathbf{y}_{k+1}|\mu_{k+1}, \Phi_k) = \mathcal{N}(\mathbf{y}_{k+1}|\hat{\mathbf{y}}_{k+1}, \Gamma^{QRS}), \tag{4.21}$$

with

$$\hat{w}_{k+1} = \mathbf{w}_k^T \hat{\theta}_k, \tag{4.22}$$

$$\Gamma^{HR} = \mathbf{w}_k^T(\mathbf{V}_k + \mathbf{Q}_k)\mathbf{w}_k + R_{k+1}, \tag{4.23}$$

$$\hat{\mathbf{y}}_{k+1} = G(\mathbf{t}, \mu_{k+1}, \hat{z}_k), \text{ and} \tag{4.24}$$

$$\Gamma^{QRS} = \mathbf{J}_{k+1}^T(\mathbf{P}_k + \Sigma_k)\mathbf{J}_{k+1} + \Lambda_{k+1}. \tag{4.25}$$

Hence, the log-posterior for μ_{k+1} in Eq. 4.8 can be written as:

$$\mathcal{L} = \text{const.} - \frac{(\mu_{k+1} - \hat{\mu}_k - \hat{w}_{k+1})^2}{\Gamma^{HR}}$$

$$- (\mathbf{y}_{k+1} - \hat{\mathbf{y}}_{k+1})^T \Gamma^{QRS^{-1}} (\mathbf{y}_{k+1} - \hat{\mathbf{y}}_{k+1}). \tag{4.26}$$

Notice that $\hat{\mathbf{y}}_{k+1}$ depends on μ_{k+1} through the function $G(\mathbf{t}, \mu_{k+1}, \hat{z}_k)$. Furthermore, $\mathcal{L}$ can be multimodal and is necessarily not Gaussian.

Regardless of the signal quality, it is always possible to find a $\hat{\mu}_{k+1}$ that maximizes $\mathcal{L}$. However, in case of poor signal quality $\hat{\mu}_{k+1}$ might be inaccurate, leading to mis-detections of the R-peak. To prevent mis-detection, a sanity check is performed during which we compare the probability that $\hat{\mu}_{k+1}$ is the location of an R-peak to the probability that $\hat{\mu}_{k+1}$ is not the location of an R-peak.

Focusing on the samples during a QRS complex $i = \hat{\mu}_{k+1} \pm \frac{L}{2}$, we can compare the likelihood for $y_i = y(i)$ in case $\hat{\mu}_{k+1}$ is an R-peak to the likelihood for y_i in case $\hat{\mu}_{k+1}$ is not an R-peak. If $\hat{\mu}_{k+1}$ is an R-peak, the likelihood for y_i is $p(y_i|\hat{\mu}_{k+1} = \text{R-peak}) = \mathcal{N}(y_i|\hat{y}_i, \Gamma^{QRS})$. If $\hat{\mu}_{k+1}$ is not the location of an R-peak, the likelihood for y_i is $p(y_i|\hat{\mu}_{k+1} \neq \text{R-peak}) = \mathcal{N}(y_i|0, \Lambda_{k+1})$. This means that:

$$\hat{\mu}_{k+1} \begin{cases} = \text{R-peak, if } (y_i - \hat{y}_i)^T \Gamma_{k+1}^{QRS^{-1}} (y_i - \hat{y}_i) < y_i^T \Lambda_{k+1}^{-1} y_i \\ \neq \text{R-peak, otherwise} \end{cases} \quad (4.27)$$

If according to Eq. 4.27 $\hat{\mu}_{k+1}$ is the location of an R-peak, we use $\hat{\mu}_{k+1}$ in levels 2 and 3 to estimate the model parameters and noise covariances. In case $\hat{\mu}_{k+1}$ is not the location of an R-peak according to Eq. 4.27, the model parameters and noise covariances are not updated. Instead, we extrapolate an R-peak location based on the FHR model and continue to predict μ_{k+2} given the prior information Φ_k (i.e. predict $p(\mu_{k+2}|y_{k+2}, \Phi_k)$). In case more than five consecutive detected peaks were no R-peaks according to Eq. 4.27, the entire algorithm is re-initialized (see section 4.2.8).

4.2.8 Parameter initialization

In the (re-)initialization phase, a segment of 10 seconds is used to obtain estimates for $\Phi_0 = \{\mu_0, z_0, \theta_0, w_0, \Lambda_0, \Sigma, Q_0, R\}$. During initialization, the QRS model described by Eq. 4.1 is used as a frequency bandpass filter with a peak frequency of 42 Hz[150]. After filtering, a simple local maximum search is used for peak detection, where each search window is defined based on a previous maximum.

The detected peaks within the segment are used to calculate an average QRS complex, from which initial estimates z_0 are obtained using a least-squares approach. Furthermore, RR-intervals are calculated from the detected peaks and RR-intervals outside a range of RR_{min} to RR_{max} are removed. On the remaining RR-intervals a Yule-Walker method is used to obtain initial estimates θ_0. The first R-peak is used as μ_0 and the first p RR-intervals were used as w_0.

Initial covariances of the QRS model Σ and Λ_0 are calculated as described in Section 4.2.6 and 4.2.6, and we initialized $P_0 = 3\Sigma$. Initial covariances of the FHR model were set to $Q_0 = 10^{-4} \max|\theta_0|^2$, $R = R_0$, and $V_0 = Q_0$.

If forward prediction fails (i.e. more than five consecutive detected peaks were no R-peaks according to Eq. 4.27) and new parameters were found in re-initialization, we can use future information to obtain smoothed estimates of any missed (or mis-detected) R-peaks in the period before the start of the re-initialization. In essence, backwards prediction is similar to forward prediction, with the difference that the FHR and QRS model are trained in the backwards

direction. By combining the information of our forwards prediction and backwards prediction we obtain smoothed estimates for μ_{k+1}:

$$p(\mu_{k+1}|y_{k+1}, y_{k+2}, \Phi_k, \Phi_{k+2}) \propto p(\mu_{k+1}|y_{k+1}, \Phi_k)$$
$$\cdot p(\mu_{k+1}|y_{k+2}, \Phi_{k+2}). \quad (4.28)$$

4.2.9 Multichannel extension

As described before, the abdominal ECG is commonly recorded from multiple channels. Because the ECG signals are correlated, recording the ECG on multiple channels can be exploited to improve the signal to noise conditions.

The model in Eq. 4.9 can be extended to M electrodes by training a QRS model to each channel. Assuming that the noise in each channel is uncorrelated, we can write

$$y_{k+1}^{(1)} = G(t, \hat{\mu}_{k+1}, z_{k+1}^{(1)}) + \xi_{k+1}^{(1)} \qquad \xi_{k+1}^{(1)} \sim \mathcal{N}(0, \Lambda_{k+1}^{(1)})$$

$$\vdots$$

$$y_{k+1}^{(M)} = G(t, \hat{\mu}_{k+1}, z_{k+1}^{(M)}) + \xi_{k+1}^{(M)} \qquad \xi_{k+1}^{(M)} \sim \mathcal{N}(0, \Lambda_{k+1}^{(M)}), \quad (4.29)$$

with $z_{k+1}^{(m)} = [a_{k+1}^{(m)}, b^{(m)}]$. Since the width of the QRS complex is similar for all channels, we only need to estimate one width parameter $b = b^{(1)}, ..., b^{(M)}$.

We can write a similar state-space model as the single channel ECG in Eq. 4.9 for the multichannel ECG:

$$z_{k+1}^a = z_k^a + \eta_k^a \qquad\qquad \eta_k^a \sim \mathcal{N}(0, \Sigma_k^a)$$
$$y_{k+1}^a = G(t, \hat{\mu}_{k+1}, z_{k+1}^a) + \xi_{k+1}^a \quad \xi_{k+1}^a \sim \mathcal{N}(0, \Lambda_{k+1}^a). \quad (4.30)$$

Here, we defined the multichannel state and observation vectors as:

$$z_k^a = [a_k^{(1)}, ..., a_k^{(M)}, b]^\top \text{ and} \quad (4.31)$$
$$y_{k+1}^a = [y_{k+1}^{(1)}, ..., y_{k+1}^{(M)}]^\top, \quad (4.32)$$

and the multichannel noise covariances as:

$$\Sigma_k^a = \begin{bmatrix} \sigma_a^2 I_3 & & & O \\ & \ddots & & \\ & & \sigma_a^2 I_3 & \\ O & & & 0 \end{bmatrix} \text{ and} \quad (4.33)$$

$$\Lambda_k^a = \begin{bmatrix} \Lambda_k^{(1)} & & O \\ & \ddots & \\ O & & \Lambda_k^{(M)} \end{bmatrix}. \quad (4.34)$$

A similar approach can be used as the one discussed in section 4.2.5 to calculate the MAP estimate $\hat{z}_{k+1}^a$ for z_{k+1}^a.

4.2.10   Algorithms from the literature

The performance of our algorithm is compared to the performance of the algorithms of Varanini et al. [126] and Behar et al. [127], both scored high in the Challenge and have source codes that were online available. Besides algorithms from the Challenge, we also implemented the algorithm of Biglari et al. [50], because they used similar (fixed) templates for peak detection as our QRS model presented in Eq. 4.1.

Our pre-processing for maternal ECG suppression is equal to the one used by Varanini. After maternal ECG suppression and ICA, Varanini performs fetal R-peak detection on all individual channels and the channel with the best fetal RR-series is selected. Varanini uses a two step fetal R-peak detection. In the first step, potential fetal R-peaks are detected using a derivative filter. In the second step a forward and backward TVAR model is trained on the RR-series from the first step, starting from an RR-interval that is closest to the mode RR-interval. The forward and backward TVAR model are then used in combination with the derivative signal to detect the fetal R-peaks. After R-peak detection, the channel with the best RR-series is selected based on some statistical features of the RR-series.

For the algorithm of Biglari we used the same maternal ECG suppression as the one proposed by Varanini. After maternal ECG suppression, Biglari uses predefined templates for fetal R-peak detection that are based on most common fetal QRS morphologies. Fetal R-peaks are detected in each channel separately. First, each channel is passed through the matched filters using normalized cross-correlation. From the cross-correlated signals, the vectorcardiogram amplitude (VA) [44] is calculated per channel, which is then used to detect the fetal R-peaks with a local search algorithm over a sliding window [44]. Finally, channels were ranked according to the robust weighted average [155] and the R-peaks from the channel with the highest rank were stored.

The algorithm of Behar uses a combination of template subtraction techniques and BSS techniques to suppress the maternal ECG and enhance the fetal ECG after maternal ECG suppression [127]. Then, fetal R-peak detection is performed on all generated signals using an adapted version of the Pan and Tomkins algorithm [156] and a quality index is used to select the best RR-series. Finally, a smoothing step is performed to remove extra detected fetal R-peaks and fix missed fetal R-peaks. Note that we unchecked the *cinc-match* option, since this reduced the performance of the algorithm of Behar.

4.3   Data acquisition and evaluation

We used simulations to evaluate the flexibility of our algorithm for changing conditions of the fetal ECG morphology due to fetal movement. We assumed that the maternal ECG was already suppressed and used the model presented in [44] to simulate the fetal ECG. This model assumes that the electrical activity

of the heart (at far-field) can be approximated by a single dipole field vector. The three-dimensional path that is described by this vector over time is called the vectorcardiogram (VCG). The ECG is a projection of the field vector onto electrode leads. We simulated a full rotation of the fetus within the abdomen by changing the position and orientation of the VCG with respect to a vertical and horizontal electrode lead (as shown in Fig. 4.5a). Similar to [44], non-stationary noise was generated based on real noise signals (muscle artifacts and electrode movements) that can be obtained in the MIT-BIH non-stress test database [157]. Note that we did not consider baseline wander, because this would be removed by high-pass frequency filtering in maternal ECG suppression [126].

To evaluate our method we used the set-A of the 2013 Physionet/Computing in Cardiology Challenge [149]. The database consists of 75 abdominal ECG recordings, measured with four channels at a sampling rate of 1000 Hz. For set-A, the reference fetal R-peaks are provided. Recordings a33, a38, a52, a54, a71, and a74 were excluded due to partially missing annotations [126, 127], leaving 69 recordings for evaluation.

The performance of the R-peak detection is evaluated by comparing the detected fetal R-peaks to the annotated peaks. As evaluation metrics we used the accuracy (Ac):

$$Ac = \frac{TP}{TP + FN + FP}. \tag{4.35}$$

Here, TP is the number of correctly detected fetal R-peaks, FN is the number of missed R-peaks, and FP is the number of falsely detected R-peaks. A detected R-peak is considered a TP if it falls within a window of 50 ms from an annotated peak [125, 127].

To determine the performance for different SNR conditions, we calculated an average SNR for each recording and split the data-set into three groups: recordings with low SNR (lowest 10%), median SNR (middle group), and high SNR (highest 10%). We calculated the SNR in the signals after maternal ECG suppression and ICA, because these are the signals that were used for fetal R-peak detection. For each annotated R-peak in each IC, the SNR was calculated as:

$$S = 10 \log_{10} \left(\frac{P_s}{P_n} \right), \tag{4.36}$$

with P_s the power of the QRS complex and P_n the power of the noise. P_s was calculated as the variance in a window of ± 20 ms surrounding the annotated R-peak and P_n as the variance in a window of [-150:-20 20:150] ms surrounding the annotated R-peak. The average SNR was calculated for each IC and the SNR of a recording was defined as the maximum average SNR.

Note that we did not consider evaluation metrics for heart rate estimation (e.g. mean-squared-error (MSE) between detected and annotated heat rate). Post-processing techniques such as those proposed in [125] or [127] could be used to improve the FHR estimation, but this is outside the scope of this study. For the

Table 4.2: Performance (Ac) for varying c_a and R_0.

		R_0 (ms^2)				
		1	4	25	100	400
	10^{-1}	39.8	64.9	82.8	92.9	96.4
	10^{-3}	49.1	82.5	88.1	94.7	97.6
c_a (a.u.)	10^{-5}	94.8	98.8	99.2	**99.6**	99.1
	10^{-7}	96.0	98.7	99.3	**99.6**	99.4
	10^{-9}	96.1	98.0	99.1	99.4	99.2

other sets of the Challenge (B and C), no evaluation of peak detection is possible, only on heart rate estimation.

4.4 Results

The process noise of the QRS model (Σ, determined by c_a) and the observation noise of the FHR model (R, determined by R_0) were empirically determined. Table 4.2 are shown for varying the value of c_a between 10^{-1} to 10^{-9} and R_0 between 1 to 400 ms^2. Based on these results, we set $c_a = 10^{-5}$ and $R_0 = 100$ ms.

The simulated fetal ECG signals of a verticale and horizontal lead for a full rotation of the fetus are shown in Fig. 4.5. The fetal ECG with and without noise are shown in Fig. 4.5b and 4.5c, respectively. The QRS complexes that were estimated by our algorithm ($\hat{y}$) are shown for both leads in Fig. 4.5d.

In Fig. 4.6, examples for the log-posterior $\mathcal{L}$ are shown of a signal with good and a signal with poor quality. Note that the Independent Components (IC's) after maternal ECG suppression and ICA are presented. In Fig. 4.7, an example is shown with fetal ECG visible in multip IC's and with SNR that varies over time. The detected fetal R-peaks are indicated by the vertical lines.

The detection performance for the set-A of the Physionet/Computing in Cardiology 2013 Challenge is shown in Table 4.3. Mean Ac is presented for different SNR regions. The mean Ac of the total dataset was 99.6% for our algorithm, and 98.6%, 92.9%, and 54.5% for the algorithms of Varanini, Behar, and Biglari, respectively.

4.5 Discussion

Fetal R-peak detection in abdominal fetal ECG recordings is challenging due to the low SNR and the non-stationary nature of the fetal ECG waveform in the abdominal recordings. Although important processing steps have been developed for suppression of the maternal ECG, less attention has been paid to fetal R-peak

(a) Simulation setup.

(b) Simulated ECG without noise.

(c) Simulated ECG with noise (y).

(d) Estimated QRS complexes ($\hat{y}$).
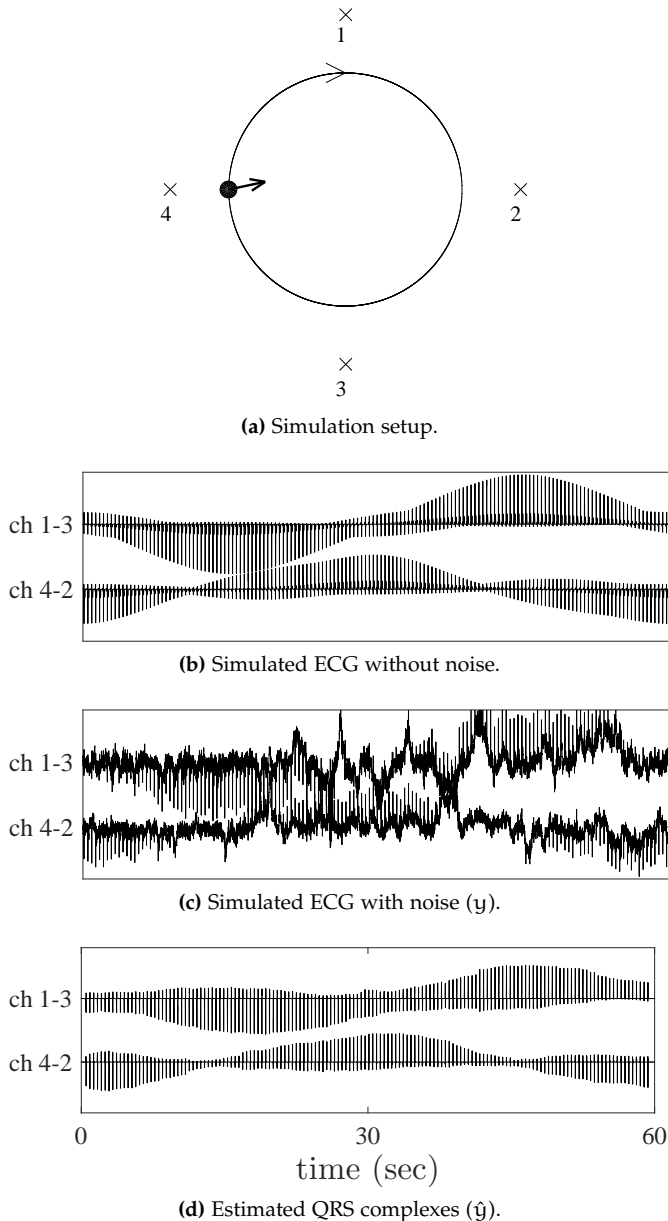
Figure 4.5: Simulation of a full fetal rotation. In (a), 'x' indicates electrodes and the black dot indicates the location of the fetal heart at the start of the simulation. The vector that originates from the fetal heart represents the direction of the main electrical activity at that position (third dimension is not displayed). The circle shows the path over which the fetal heart rotates.
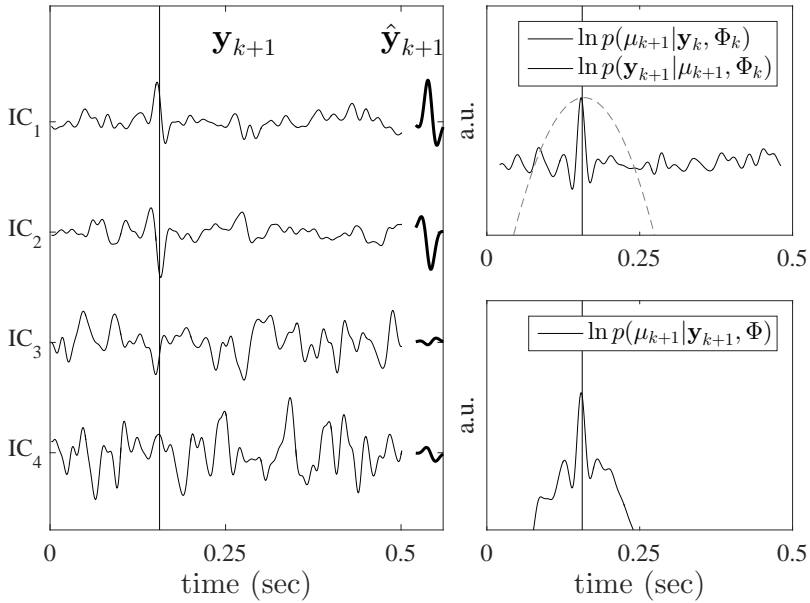
(a) Good signal quality.
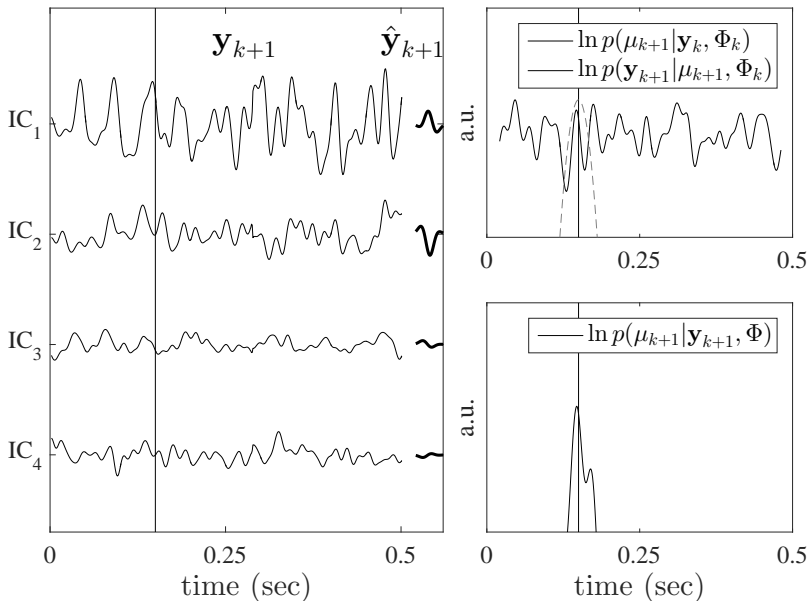
(b) Poor signal quality.

Figure 4.6: Example of good (a) and poor (b) quality signal. The verticale line show the location of the annotated R-peak. In case of good quality, the QRS model dominates the posterior, while in case of poor quality the FHR model dominates the posterior.

(a) Single channel.

(b) Multiple channels.
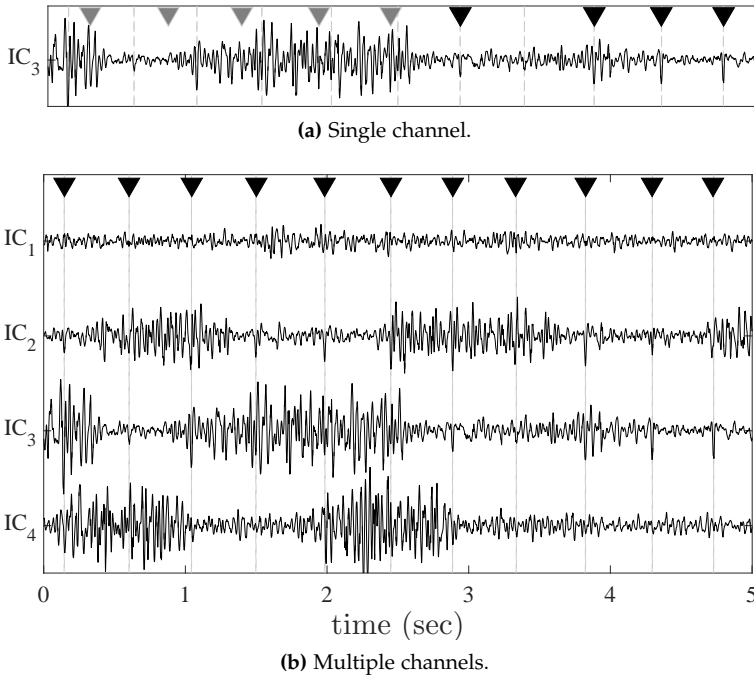
Figure 4.7: Example of a signal with varying SNR in the IC's. The fetal ECG is visible in IC_2 and IC_3. The annotated R-peaks are indicated by the verticale lines, and the detected peaks by the downward triangles. Correctly detected R-peaks are indicated by the black triangles and mis-detections by gray triangles. Detected peaks using a single IC are shown in (a) and detected peaks using all IC's are shown in (b).

detection. In this paper we present a hierarchical Bayesian framework for fetal R-peak detection that combines predictive models of the ECG waveform and FHR.

4.5.1 QRS and FHR model

For the QRS model we made the assumption that the fetal orientation remains constant throughout the period of a QRS complex. In reality, fetal movement also occurs during the period of a QRS complex, but since the period of the QRS complex is relatively short (approximately 40 ms), we expect the effect on the QRS waveform to be limited. This assumption allows us to estimate the model parameters z over L samples instead of only one sample, making the estimation more robust against noise.

Although our QRS model requires a relatively small number of parameters, we expect that the model is able to describe the QRS complex for most normal abdominal fetal ECG recordings [50]. The simulation in Fig. 4.5 confirm that the

Table 4.3: Average Ac for set-A.

algorithm	All SNR (%)	Low SNR (%)	Median SNR (%)	High SNR (%)
this work	**99.6**	**99.4**	**99.6**	**99.9**
Varanini et al. [126]	98.6	93.5	99.1	99.8
Behar et al. [127]	92.9	59.7	96.3	99.8
Biglari et al. [50]	54.5	41.5	53.7	74.2

QRS model is flexible and that changes in fetal ECG morphology due to fetal movement can be described by our model. However, if our model is unable to describe the QRS complex (e.g. in case of a congenital defect) the performance might be reduced due to the sanity check in Eq. 4.27. Moreover, since the model is limited to describing the QRS complex, it cannot be used for ECG waveform analysis.

For the FHR model we used a linear autoregressive model. A more complete description of the FHR could be obtained by a point-process model [158]. Besides, a linear model might be insufficient to fully describe the heart rate, as several studies in the literature have identified non-linear dynamics in the heart rate [95]. However, as noted in [158], a stochastic parameter estimation of a linear model can still lead to an accurate description of the heart rate under normal conditions. During labor it could be interesting to extend the FHR model to a non-linear model (e.g. such as the one proposed in [159]) to describe complicated accelerations or decelerations.

In the presence of cardiac arrhythmias we expect the performance of our algorithm to decrease. This can either be due to abnormal variations in the ECG waveform, abnormal variations in the FHR or both. Since our model is developed to detect normal sinus rhythms, for future work it could be interesting to extend our model for arrythmia detection and classification at periods where R-peak detection fails.

4.5.2 Noise models

To allow for an analytically tractable solution, we have made assumptions that the observation and process noise in the QRS and FHR model have a zero-mean Gaussian distribution.

The process noise covariance of the QRS model (Σ) is assumed constant, meaning that the QRS waveform is allowed to vary similarly throughout a recording. In reality, variations in the QRS waveform are mainly caused by fetal movements or arrhythmias, which do not occur continuously over time. Hence, adaptive estimation of Σ seems more appropriate. For adaptive estimation of Σ, the residual error between the estimated QRS waveform and the observed signal could be

used (similar to the method used for estimating the process noise of the FHR model). However, because the estimated QRS waveform is also used to identify mis-detections through Eq. 4.27, this approach reduces the performance. Despite having a fixed process noise covariance, the QRS model is still capable to adapt in case of fetal movement, as shown in Fig. 4.5.

For the estimation of the observation noise covariance of the QRS model (Λ), we assumed the observation noise to be uncorrelated. However, also correlated physiological noise (e.g. muscle activity) is described by the observation noise of the QRS model. Although a whitening filter could be implemented as a pre-processing step, it is not straightforward to develop such a whitening filter for ECG recordings since the correlation in the signal varies over time. In [142], it was shown that even in case the observation noise is not white the Kalman filter provides the optimal mean squared error solution.

For estimation of the process noise of the FHR model ($\mathbf{Q}$), the observation noise R plays an important role. If the value of R is overestimated, the process noise will be underestimated and the FHR model becomes less capable at adapting its model parameters to dynamical FHR variations that are caused by changes in autonomic regulation. On the other hand, underestimating R leads to overestimation of the process noise and overfitting of the parameter estimation. For future work it might be interesting to estimate R dynamically.

4.5.3 R-peak detection

New R-peaks are detected as the MAP estimate for the state-space model in Eq. 4.6. The log-posterior is the sum of the estimation of the QRS and FHR model, weighted by the uncertainties in the respective models. If the quality of the recorded signal is high, the QRS model dominates the posterior distribution, as is shown in Fig. 4.6a. Conversely, if the signal quality is poor, the FHR model dominates the posterior distribution, as is shown in Fig. 4.6b.

An MAP solution for R-peak detection was also proposed in [160]. However, the model that is used in [160] is designed for fiber-optic signals, from which it is not possible to detect the actual R-peaks locations due to differences in timing between audible and electrical activity of the heart. In [160], different detection methods are combined in an MAP estimate of the (ECG) R-peak location, that accounts for the delays and uncertainties in each of the methods with respect to true R-peak locations. This multimethod approach is not required in our case, because we measure the ECG and can detect actual R-peak locations.

In Fig. 4.7 an example is shown where ICA is unable to separate the fetal ECG information in a single IC. In this example the SNR of the IC's varies over time, which reduces performance for algorithms that detect R-peaks on individual channels, as demonstrated in Fig. 4.7a. In the multichannel extension of our model all channels are used for R-peak detection, which improves the performance in case of varying SNR conditions (Fig. 4.7b).

The performance of our algorithm has been evaluated for set-A of the Challenge. We compared performance of our algorithm to the performance of the algorithms of Varanini et al. [126], Behar et al. [127], and Biglari et al. [50]. Varanini and Behar obtained the best scores for the Challenge. It should be noted that for set-B of the Challenge Andreotti et al. [125] and Lipponen et al. [128] achieved slightly better scores compared to Varanini and Behar in terms of FHR estimation. Since these algorithms were not publicly available we did not include them in our comparison.

Highest overall Ac was achieved by our algorithm (99.6%). The lowest performance was obtained by the algorithm of Biglari (54.5% overall Ac). Reasons for the relatively low performance of the algorithm of Biglari could be that Biglari uses fixed templates for R-peak detection and that R-peaks are detected on the individual channels. The algorithms of both Varanini and Behar achieved good overall Ac (98.6% and 92.9%, respectively). However, from Tabel 4.3 it becomes clear that the performance of these algorithms is reduced for low SNR conditions (93.5% for Varanini and 59.7% for Behar). In contrast, our algorithm achieved 99.4% for the recordings with low SNR, indicating that our algorithm works well even for low SNR conditions.

4.6 Conclusion

In this study, a hierarchical Bayesian framework was developed for fetal R-peak detection. The developed method combines predictive models of the ECG waveform and heart rate, and can be used for multichannel recordings. The developed method outperforms other methods that have been proposed in the literature in terms of detection accuracy.

PART II

Interpretation of fetal heart rate variability
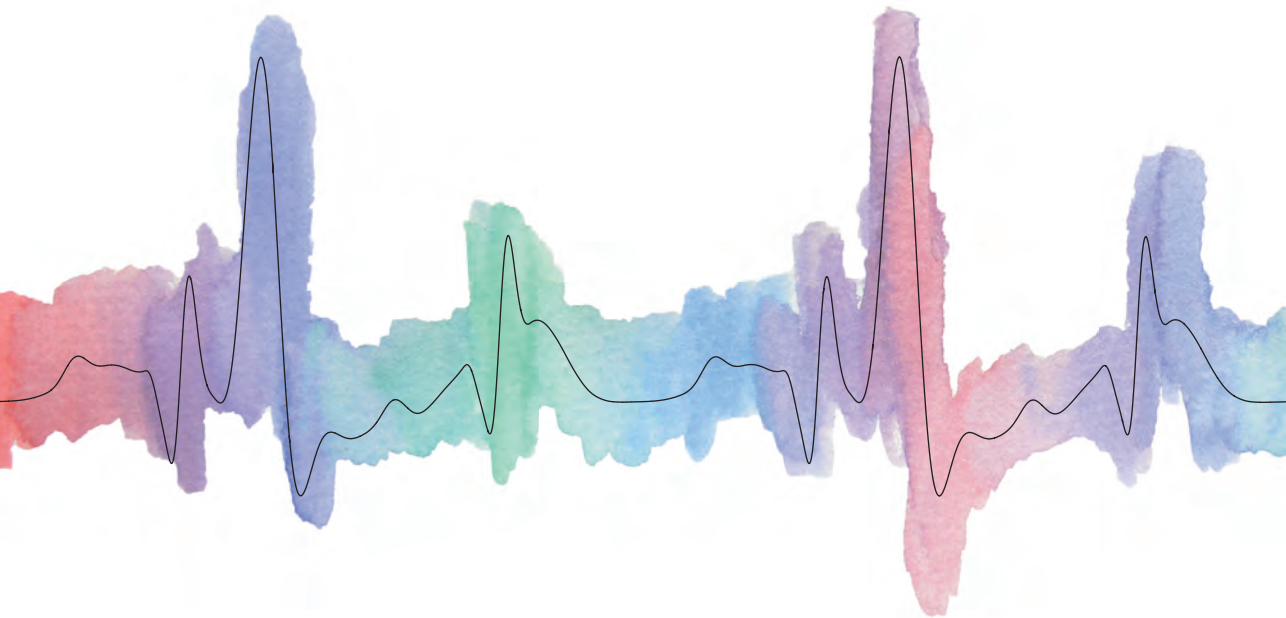
5

USING UTERINE ACTIVITY TO IMPROVE FETAL HRV ANALYSIS FOR DETECTION OF ASPHYXIA DURING LABOR

Abstract - *During labor, uterine contractions can cause temporary oxygen deficiency for the fetus. In case of severe and prolonged oxygen deficiency this can lead to asphyxia. The currently used technique for detection of asphyxia, cardiotocography (CTG), suffers from a low specificity. Recent studies suggest that analysis of fetal heart rate variability (HRV) in addition to CTG can provide information on fetal distress. However, interpretation of fetal HRV during labor is difficult due to the influence of uterine contractions on fetal HRV. The aim of this study is therefore to investigate whether HRV features differ during contraction and rest periods, and whether these differences can improve the detection of asphyxia. To this end, a case-control study was performed, using 14 cases with asphyxia that were matched with 14 healthy fetuses. We did not find significant differences for individual HRV features when calculated over the fetal heart rate without separating contractions and rest periods ($p > 0.30$ for all HRV features). Separating contractions from rest periods did result in a significant difference. In particular the ratio between HRV features calculated during and outside contractions can improve discrimination between fetuses with and without asphyxia ($p < 0.04$ for three out of four ratio HRV features that were studied in this paper).*[1]

5.1 Introduction

During labor, uterine contractions can cause temporary oxygen deficiency for the fetus. Although a fetus is generally well-equipped to handle brief periods of oxygen deficiency, if oxygen deficiency is severe and prolonged it can result in asphyxia which is associated with neonatal morbidity and mortality [2]. It is therefore important that clinicians can timely intervene before asphyxia develops.

Currently, cardiotocography (CTG) is the most often used method for detection of asphyxia. CTG simultaneously records the fetal heart rate (FHR) and uterine activity (UA). The CTG is interpreted visually, based on standardized guidelines [161]. Despite these guidelines, CTG interpretation has a high inter- and intra-observer variability [10]. Furthermore, the specificity of CTG is low, leading to a high false alarm rate [9]. To reduce the number of unnecessary operative deliveries, additional information is required when the CTG is abnormal.

Recent studies have shown interest in analysis of fetal heart rate variability (HRV) to aid in the detection of asphyxia [31, 32, 36–39]. Because variations in the heart rate are regulated by the autonomic nervous system (ANS), various HRV features have been developed that attempt to quantify different aspects of the cardiac autonomic regulation [30]. Most of these features have been developed for adults, but they might also provide diagnostic information about fetal distress. Note that HRV features are usually defined for the analysis of inter-beat interval (R-R interval) signals and HRV features should thus not be applied directly to the FHR signal in beats per minute (BPM). Instead FHR should be recalculated to R-R intervals first.

Reviews of HRV features can be found in [33, 37, 94, 95]. Features describing the statistical properties of a FHR signal have been used in [34] and [36] for detection of fetal asphyxia. In [31], spectral analysis was used to examine the effect of fetal asphyxia on the regulation of the sympathetic and parasympathetic branch of the ANS. Since the sympathetic and parasympathetic nervous system control the heart rate in different frequency bands, spectral analysis is able to separate regulation by these two branches [29]. In [31] it was shown that for fetuses with asphyxia normalized low frequency power increased while normalized high frequency power decreased, indicating a predominance of sympathetic regulation.

Spectral analysis is based on a linear model to describe the relation between ANS regulation and variations in the heart rate. Besides spectral analysis, other HRV features have been developed that quantify variations that cannot be explained by this linear model. FHR signals were analyzed using HRV features that quantify the complexity in a time series in [36, 162–164]. Furthermore, fractal analysis has also been employed to describe the FHR signal during labor [38, 165].

To improve the predictive capacity of HRV features, several studies have combined multiple HRV features by using classifiers such as support vector machines [35, 37] or neural networks [39].

Despite these efforts, it remains difficult to interpret HRV features calculated from a FHR signal during labor, since most HRV features have been developed for adults. Unlike for adults, changes in the fetal cardiovascular system during labor cannot be controlled and they are strongly influenced by uterine contractions. There are several ways by which contractions can influence the fetal cardiovascular system [1]. The rise in external pressure can directly change the fetal blood pressure, which activates a baroreceptor reflex. Contractions can also indirectly influence the fetal cardiovascular system, by blocking the oxygen supply to the fetus (e.g. due to umbilical cord occlusion or reduced maternal blood flow to the placenta), activating a chemoreceptor reflex. After a contraction, some time is needed for the fetal blood gases to recover. In addition, labor can be divided into different stages and the influence of contractions on the fetus changes over time. The first stage is a period of progressive cervical dilation, followed by the second stage of active pushing where the fetal head descends into the birth canal. As a result of this uncontrolled environment, HRV features are often calculated over highly non-stationary FHR signals.

This is also indicated by [52] and [51], who showed that for healthy fetuses spectral power is significantly higher during contractions as compared to rest periods (i.e. the periods in between contractions). The increase in spectral power indicates a capability of the ANS to react to uterine contractions. Calculating HRV features over the entire FHR signal, without consideration of contractions, averages this effect over the rest periods.

The aim of this study was therefore to examine whether separating contractions from rest periods can improve HRV analysis for the detection of asphyxia during labor. To this end, a case-control study was used to examine the value of several conventional HRV features in discriminating between fetuses with and without asphyxia.

5.2 Methods

5.2.1 Data acquisition

Data for this study was obtained at the Máxima Medical Center in Veldhoven and the University Medical Center in Utrecht over the period 2001 to 2008. All registrations were recorded on a Neoventa STAN® system. We used beat-to-beat FHR signals that were recorded using a scalp electrode. The UA was measured either via a tocodynamometer or via an intra-uterine pressure catheter (IUPC).

Registrations were included from healthy mothers who had an uncomplicated pregnancy of at least 36 weeks of gestation and did not use any medication. Pregnancies complicated by intra-uterine growth restriction or fetal congenital anomalies were excluded. Furthermore, we only included registrations with at least 15 minutes of FHR signal during the second stage of labor. Contractions were annotated by a clinical expert based on the UA trace, who was blinded to the FHR signal and any other patient or medical information, including the fetal

Table 5.1: Clinical characteristics of included fetuses.

Clinical features	fetuses without asphyxia (cases n=14)	fetuses with asphyxia (cases n=14)
Gestational age (days)	284 ± 10	284 ± 9
Birth weight (g)	3773 ± 587	3601 ± 442
1-minute Apgar score	9 ± 1	7 ± 2
5-minute Apgar score	10 ± 0	8 ± 2
Cord arterial pH	7.26 ± 0.06	6.99 ± 0.06
Cord arterial base excess (mmol/l)	-5 ± 2	-17 ± 3
Length second stage of labor (min)	58 ± 27	71 ± 49
Start before birth (min)	17 ± 3	25 ± 11

[a] Values are expressed as mean and standard deviation.

outcome. Only registrations with good quality UA trace were used, defined as registrations where the expert was able to distinguish the contractions.

Fetal outcome was based on the umbilical arterial acid-base status; a pH above 7.20 was defined as healthy, and a pH below 7.05 and base excess below -12 as asphyxia [1, 22]. Out of the 1232 registrations, 14 cases of fetuses with asphyxia remained for analysis, that were matched with the registration of 14 healthy fetuses that were randomly selected from the available data. Besides the inclusion criteria mentioned in the previous paragraph, no further criteria were used to match the two populations. The main clinical characteristics of the included fetuses is shown in Table 6.1.

5.2.2 Signal processing

HRV features were calculated on R-R interval signals that were extracted from Neoventa STAN® recordings. Since beat-to-beat R-R intervals can only be determined when a heartbeat occurs, the R-R intervals are not equidistantly sampled. To obtain an equidistantly sampled signal, a sample and hold technique was used [166]. To obtain a smooth function, the resulting signal was convoluted with a square function of width 0.5 s and sampled at a rate of 4 Hz.

When the difference between two successive R-R intervals was more than 25 BPM or more than 200ms, both R-R intervals were considered as artifacts. The reason we also used 200 ms as criterion is that, in case of very low heart rate, it can occur that the difference between successive beats is more than 200 ms but less than 25 BPM. Artifacts were corrected by linear interpolation from the previous correct R-R interval to a new segment of 5 consecutive R-R intervals with less than 10 BPM difference between them [35]. For each registration, we

analyzed the 15 minutes closest to birth, where there was no loss of UA signal and less than 20% interpolation of the FHR signal.

5.2.3 HRV features

For each 15 minute FHR signal, conventional HRV features were calculated that describe different properties of the heart rate. Since there are several reviews on HRV features in the literature (e.g. [37, 94, 95]), this section only briefly discusses the underlying physiological model and implementation of the HRV features used in this study.

Statistical features

The standard deviation (SD) and the root mean square of successive differences (RMSSD) were calculated as statistical features. SD is a measure for the overall variability in the heart rate and it reflects both sympathetic and parasympathetic regulation. Since RMSSD is sensitive to beat-to-beat variations, it mainly reflects parasympathetic regulation [97].

Let $x[n]$ be the resampled FHR signal for $n = 1, ...N$, with N the length of the signal. Then SD and RMSSD are defined as

$$SD = \sqrt{\frac{1}{N-1} \sum_{n=1}^{N} (x[n] - \bar{x})^2} \tag{5.1}$$

$$RMSSD = \sqrt{\frac{1}{N-1} \sum_{n=2}^{N} (x[n] - x[n-1])^2}, \tag{5.2}$$

with $\bar{x}$ the mean heart rate.

Frequency domain features

Spectral analysis accounts for correlation in a signal. The use of spectral analysis to analyze the heart rate is based on the observation of periodic variations in the heart rate that can be related to different regulatory mechanisms of cardiovascular control [29]. Since regulation of the sympathetic nervous system is slow compared to regulation of the parasympathetic nervous system, low frequency oscillations are related to both sympathetic and parasympathetic regulation, and high frequency oscillations are only related to parasympathetic regulation.

Spectral analysis was performed by the Continuous Wavelet Transform (CWT) with a fifth order symlet wavelet [166]. In contrast to the traditional Fourier Transform, CWT enables a simultaneous time and frequency analysis, making CWT suitable for analysis of the non-stationary frequency content of a FHR signal. Since in this study we are only interested in the average spectral power, results of the CWT are comparable to other approaches for spectral analysis

that account for non-stationarity in a signal, such as the Short Term Fourier Transform (STFT) used in [31] or the Welch method used in [36]. However, unlike STFT and Welch method, CWT allows for a multi-resolution time frequency analysis. Since artefact correction in the FHR signal mainly affects the higher frequencies, having a higher time resolution for these frequencies will reduce the influence of artefact correction [166].

The CWT compares the FHR signal ($x[n]$) to an analyzing wavelet function ψ. A wavelet is defined as a *mother* wavelet function $\psi[n]$, with a family of scaled and time-shifted *daughter* wavelets $\psi[\frac{n-\tau}{s}]$. The CWT coefficients $W[s, \tau]$ can be obtained by continuously varying the scale parameter s and the position parameter τ. For real discrete signals, as is the case for the FHR signal, $W[s, \tau]$ can be calculated according to

$$W[s, \tau] = \frac{1}{\sqrt{s}} \sum_{n=1}^{N} x[n]\psi[\frac{n-\tau}{s}].$$ (5.3)

To correct for the convolution of the beat-to-beat FHR signal with a square function that was used for smoothing (as explained in section 5.2.2), $W[s, \tau]$ is first divided by the coefficients of the wavelet transform of this square function. From the corrected wavelet coefficients ($\tilde{W}[s, \tau]$) the power at each time instant at a certain scale is calculated as

$$P[s, \tau] = \frac{1}{C_g} \left(\frac{\tilde{W}[s, \tau]}{s} \right)^2,$$ (5.4)

where C_g is the admissibility constant. Since each daughter wavelet is related to a certain frequency, the total power in a frequency band is then calculated by integrating $P[s, \tau]$ over the scales within that frequency band and by averaging over time. Note that unlike the discrete wavelet transform, the CWT is not limited to a dyadic decomposition of a signal in the time-frequency plane [167]. The scale is a continuous parameter and can be selected such that it corresponds to a frequency within a certain frequency band.

The low frequency band was set to 0.04-0.15 Hz and the high frequency band to 0.4-1.5 Hz [31, 32]. Scales corresponding to the frequencies between these bands (0.15-0.4 Hz) were discarded. Besides absolute low frequency power (LF) and high frequency power (HF), also normalized LF (LF_n) and normalized HF (HF_n) power are calculated by dividing LF and HF by the total power (TP, 0.04-1.5 Hz) [31].

The minimum length of FHR signal that is required to calculate LF (and TP) is determined by the largest wavelet of the LF band. Therefore, a segment of at least 50 seconds is required to reliably calculate LF [168]. Similarly, calculation of normalized frequency powers (LF_n and HF_n) also requires 50 seconds.

Complexity features

Although spectral analysis provides information about regulation mechanisms of the cardiovascular system, variations in the heart rate often cannot be explained by spectral analysis alone. Since many factors can cause blood pressure changes (e.g. changes in external pressure or through chemoreceptor reflex), blood pressure often shows complicated and irregular fluctuations. Because adjusting the heart rate is one of the main tools of the ANS to stabilize these blood pressure fluctuations, also the heart rate can show complicated and irregular fluctuations. The occurrence of irregularities in the heart rate is therefore indicative of healthy blood pressure control by the ANS.

A measure that is often used to quantify the complexity of very short signals in terms of randomness is Sample Entropy ($SampEn$) [99]. $SampEn$ estimates the conditional probability that when patterns are similar for length $m-1$, they will also be similar for length m. This probability is small in case the heart rate is complex and large in case the heart rate is not complex.

To calculate $SampEn$, the FHR signal is divided vectors $\mathbf{u}$ of length m

$$\mathbf{u}[i] = \{x[i], x[i+1], ..., x[i+m-1]\}. \tag{5.5}$$

Two vectors $\mathbf{u}[i]$ and $\mathbf{u}[j]$ are similar if the maximum distance between the elements of $\mathbf{u}[i]$ and $\mathbf{u}[j]$ is less than tolerance parameter r. Let us define $C_i^m[r]$ as the number of vectors $\mathbf{u}[j]$ that are similar to $\mathbf{u}[i]$ (for $j \neq i$), normalized by the total number vectors of length m. The probability (Φ^m) of finding similar vectors of length m is then calculated as the average of $C_i^m[r]$

$$\Phi^m[r] = (N-m+1)^{-1} \sum_{i=1}^{N-m+1} C_i^m[r]. \tag{5.6}$$

$SampEn$ is the natural logarithm of the conditional probability in the limit $N \to \infty$

$$SampEn[m,r] = \lim_{N\to\infty} -\ln \frac{\Phi^{m+1}[r]}{\Phi^m[r]}. \tag{5.7}$$

The *embedding dimension* m was set to $m=2$ and the tolerance to $r=0.2SD$, similar to [36, 37, 163]. For finite time series, $SampEn$ can be approximated reliably with $N > 100$ samples [99].

Fractal features

Besides examining how the heart rate is controlled at certain specific time scales (e.g. LF and HF band for spectral analysis), for adults, fluctuations in the heart rate show self-similarity on different time scales [\cite]Goldberger2002. In this context, self-similarity means that structure of the heart rate on long time scales

is resembled at shorter time scales. Fractal analysis describes the scaling proper-ties of the heart rate. In [38], fractal analysis was used to investigate the scaling properties of the FHR during labor.

In our study, the variability at different time scales is described by the scaling exponent α, which is obtained by Detrended Fluctuation Analysis (DFA) [169, 170]. To calculate α, first an integrated version of the original time series is obtained:

$$y[k] = \sum_{n=1}^{k} (x[n] - \bar{x}). \qquad (5.8)$$

Next, $y[k]$ is divided into equally spaced segments of length a and the linear trend of each segment ($y_a[k]$) is determined. The characteristic fluctuation F at each scale a is computed as the root mean square (RMS) deviation between $y[k]$ and its trend:

$$F[a] = \sqrt{\frac{1}{N} \sum_{k=1}^{N} (y[k] - y_a[k])^2}. \qquad (5.9)$$

If a linear relation exists between $\log(F[a])$ and $\log(a)$, the heart rate is said to show self-similarity, such that variability at long time scales is related to variabil-ity at shorter time scales in a power-law fashion ($F[a] \sim a^{\alpha}$). The slope α of the relation between $\log(F[a])$ and $\log(a)$ characterizes the type of the time series (e.g. $\alpha = 0.5$ for white noise and $\alpha = 1.5$ for Brownian noise). Also note that α is related to the Hurst exponent used in [38] as $H = \alpha - 1$ [171].

Similar to [38], α was computed over the scales ranging from 1 to 60 seconds, which corresponds to the physiological range of the baroreflex.

5.2.4 HRV analysis during contractions and rest periods

For calculation of HRV features during contractions and rest periods separately, the expert annotations of the contractions were used. To calculate HRV features during contractions, values based on R-R intervals measured during rest pe-riods were excluded. Similarly, to calculate HRV features during rest periods, values based on R-R intervals measured during contractions were excluded. In our study, we also considered the ratio between HRV features calculated during contractions and rest periods.

It is important to note that in the second stage of labor the duration of con-tractions and rest periods is often less than one minute. Since computation of LF, LF_n, HF_n, and α requires approximately one minute of consecutive FHR signal, we could not extract these HRV features during contractions and rest periods separately.

Our study of HRV features during contractions and rest periods was thus limited to SD, $RMSSD$, HF, and $SampEn$. Besides calculating these HRV features
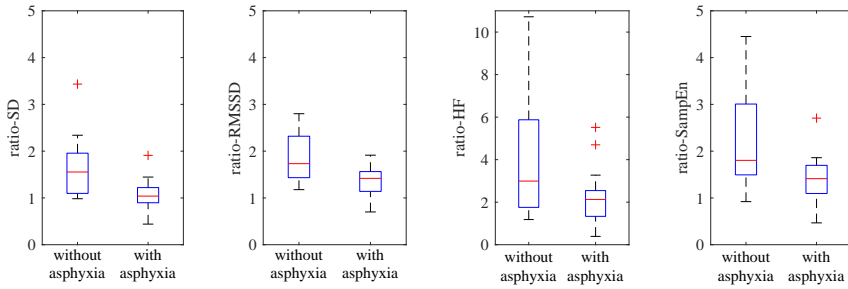
Figure 5.1: Boxplots of the ratio between HRV features calculated during contractions and rest periods. The central mark and the edges of the box indicate the median and inter quartile range. The whiskers correspond to the most extreme values that are not considered outliers (where outliers are defined as $\pm 2.7\sigma$, with σ the standard deviation).

during contractions and during rest periods, we also examined the ratio between HRV features calculated during contractions and rest periods.

5.2.5 Statistical methods

A Wilcoxon ranksum test was used to determine for each HRV feature whether the median of the distribution of the healthy group was significantly different from the median of the distribution of the group with asphyxia [172]. Statistical significance was set at a p value of less than 0.05.

5.3 Results

The HRV features discussed in the previous section were calculated from the 15 minute FHR signals. Results are shown in tables 5.2-5.5 as median and inter quartile range. An example of a CTG registration of a healthy fetus and that of a fetus with asphyxia is displayed in Fig. 6.2.

Table 5.2 shows the results for HRV features that were calculated over the entire FHR signal. No significant difference in median was found between the group with and without asphyxia for any of the individual HRV features. HRV features calculated during contractions are compared for fetuses with and without asphyxia in Table 5.3, and HRV features calculated during rest are compared for fetuses with and without asphyxia in Table 5.4. No significant difference was found between fetuses with and without asphyxia either during contractions or during rest periods. Finally, Table 5.5 shows the results of the ratio of HRV features calculated during contractions and HRV features calculated during rest periods. For SD ($p = 0.01$), RMSSD ($p = 0.02$), and SampEn ($p = 0.03$) the ratio was significantly lower for the group with asphyxia compared with the healthy

Table 5.2: HRV analysis over the entire FHR signal.

HRV features	fetuses without asphyxia	fetuses with asphyxia	Significance (p-value)
SD	78 [56-116]	96 [52-122]	0.80
RMSSD	7.7 [4.0-8.9]	6.7 [4.8-7.8]	0.37
LF	817 [202-1147]	478 [201-1290]	0.45
HF	24 [11-54]	20 [12-31]	0.60
LF_n	0.78 [0.73-0.83]	0.80 [0.73-0.85]	0.32
HF_n	0.06 [0.05-0.10]	0.06 [0.03-0.08]	0.48
SampEn	0.17 [0.09-0.24]	0.16 [0.11-0.22]	0.98
α	1.40 [1.21-1.55]	1.43 [1.37-1.56]	0.37

Table 5.3: HRV analysis during contractions.

HRV features	fetuses without asphyxia	fetuses with asphyxia	Significance (p-value)
SD	78 [55-123]	72 [49-121]	0.54
RMSSD	9.5 [4.6-11.6]	7.2 [3.9-8.7]	0.16
HF	38 [13-72]	27 [9-47]	0.30
SampEn	0.22 [0.16-0.30]	0.20 [0.13-0.26]	0.30

Table 5.4: HRV analysis during rest periods.

HRV features	fetuses without asphyxia	fetuses with asphyxia	Significance (p-value)
SD	54 [39-80]	83 [50-117]	0.22
RMSSD	4.3 [3.0-7.4]	5.7 [4.3-6.3]	0.60
HF	11 [4-29]	17 [8-21]	0.66
SampEn	0.11 [0.07-0.18]	0.11 [0.08-0.16]	0.57

Table 5.5: HRV analysis: ratio between contractions and rest periods.

HRV features	fetuses without asphyxia	fetuses with asphyxia	Significance (p-value)
SD	**1.6 [1.1-2.0]**	**1.0 [0.9-1.2]**	**0.01**
RMSSD	**1.7 [1.4-2.3]**	**1.4 [1.1-1.6]**	**0.02**
HF	3.0 [1.8-5.9]	2.1 [1.3-2.6]	0.16
SampEn	**1.8 [1.5-3.0]**	**1.4 [1.1-1.7]**	**0.03**

[a] Values in Tables 5.2-5.5 are expressed as median [inter quartile range].
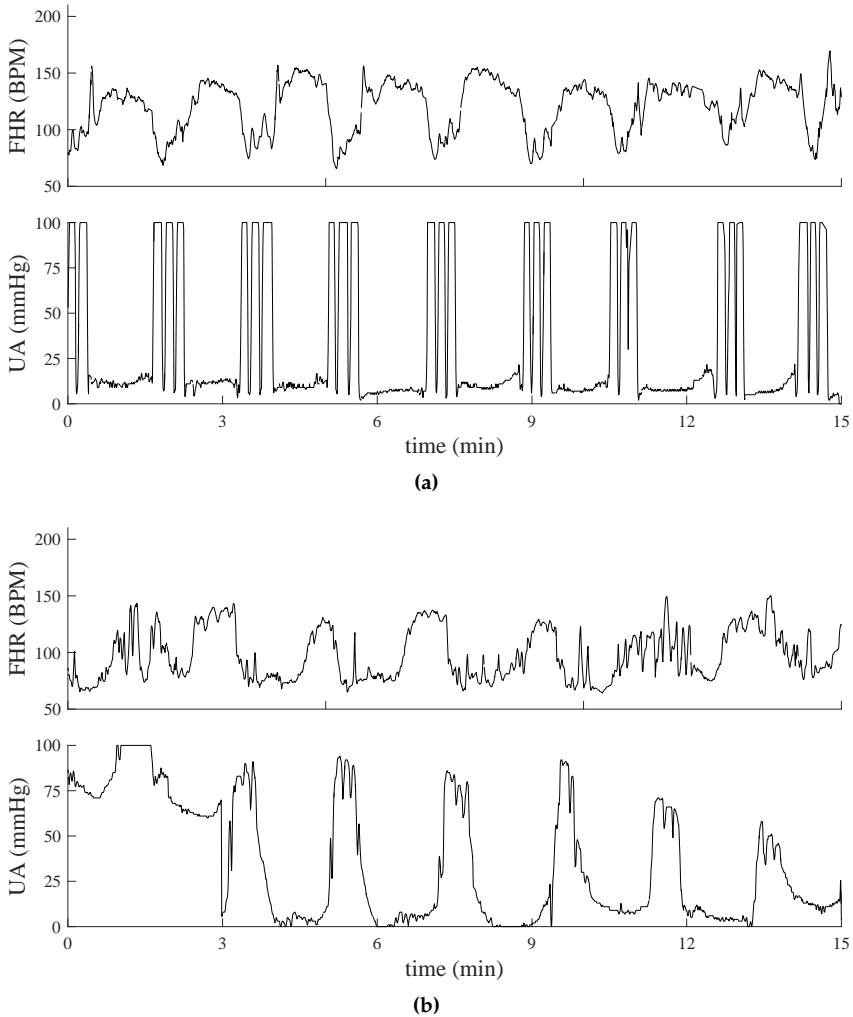
Figure 5.2: Example of a FHR signal of a healthy fetus (a) and a fetus with asphyxia (b). For the healthy fetus, the ratios between HRV features during contractions and rest periods are: SD = 3.4, RMSSD = 2.8, HF = 10.5, and SampEn = 4.5. For the fetus with asphyxia, the ratios are: SD = 1.0, RMSSD = 1.6, HF = 2.1, and SampEn = 1.7.

group. Although the median ratio for HF was also lower for the group with asphyxia, this difference was not significant. Complementary to results in Table 5.5, the distributions of the ratio of HRV features are shown as boxplots in Fig. 5.1.

5.4   Discussion

There are many factors that determine the response of the fetus to a temporal loss of oxygen caused by uterine contractions. Therefore, CTG registrations often display a large variety of complicated patterns, making it difficult to interpret them. Automated analysis of fetal HRV attempts to support clinicians in their interpretation by providing additional quantitative information on the cardiovascular system. However, existing HRV features have been mainly developed for adults and do not account for the strong influence of uterine contractions on the cardiovascular control. When calculating these HRV features over the entire FHR signal, the effect of contractions is averaged with rest periods. The goal of this study was to show that separating contractions from rest periods improves HRV analysis for the detection of fetal asphyxia.

Despite the relatively large number of available registrations, only 14 cases with pH below 7.05 could be included for the analysis. This is partly due to the low incidence of asphyxia (between 0.6% [173] and 3.5% [174]), but also because of the strict inclusion criteria we used. We required a good quality UA trace, so that the expert could clearly identify contractions. In clinical practice, however, it frequently occurs that the UA trace is of poor quality [175]. A potential solution might be the use of electrohysterography for the registration of UA [176]. Note that in our dataset the number of registrations that measured UA with tocodynamometer or with IUPC was the same for both the healthy group and the group with asphyxia (10 with tocodynamometer and 4 with IUPC). Since we only included registrations with good quality UA trace, we expect that the use of tocodynamometer or IUPC did not influence our results.

For some recordings we were unable to analyze the final minutes before birth, either due to loss of FHR signal or insufficient quality of UA trace (Table 6.1). As a result, segments for the healthy group were selected closer to birth than for the group with asphyxia. Because it has been reported that, in absence of sudden catastrophic events, asphyxia in term fetuses develops within a period of at least 90 minutes [177], we can assume that fetuses in the group with asphyxia were already under more stressful conditions than fetuses in the healthy group. We expect the effect of asphyxia to increase as labor progresses and differences between healthy fetuses and fetuses with asphyxia to be even more pronounced during the final minutes before birth.

5.4.1   HRV features over the entire FHR signal

We did not find a significant difference between the healthy group and the group with asphyxia for individual HRV features when calculated over the entire FHR signal (Table 5.2). This could partly be explained by the small number of recordings and large inter-patient variability of the HRV features.

For absolute LF and HF, our results are similar to the findings in [36] and [31], despite the different method they used for spectral analysis (Welch method

and STFT respectively, versus CWT used in this study). Although in our study normalized LF was higher for the group with asphyxia, in line with [31], this difference was not significant. Furthermore, in contrast to the findings in [36], $SampEn$ was not statistically different. These differences in results obtained in our study and [36] and [31], might be because [36] and [31] calculated the HRV features over short segments of FHR signal (5 minutes). As discussed in [36], HRV analysis could be more efficient when performed on shorter segments. However, we used longer segments because in shorter segments a bias could be introduced due to an unbalance in the presence of contractions and rest periods within the segment. The use of shorter segments can therefore lead to large intra-patient variability of HRV features over time.

In our study also no difference was found between healthy fetuses and fetuses with asphyxia for the scaling exponent α. Recently [165] showed promising results calculating the scaling exponent using a wavelet based scattering transform. This might improve the fractal analysis.

5.4.2 HRV features during contractions and rest periods

Similar to [51] and [52], we found that for healthy fetuses HF was significantly increased during contractions with respect to rest periods (p = 0.01). This result has not been shown explicitly, but can be seen by comparing the left columns of tables 5.3 and 5.4. The increase in HRV features during contractions relative to the HRV features during rest periods indicates that a stronger cardiovascular control is required to stabilize the blood pressure during contractions. The rise in external pressure due to contractions can activate a combination of baroreceptor and chemoreceptor reflexes, leading to relatively high HRV during contractions. This finding was confirmed by the observed increase in RMSSD (p < 0.01) and $SampEn$ (p < 0.01). In contrast to the results of the healthy group, for the group with asphyxia HRV features were not significantly different during contractions with respect to rest periods (all p > 0.12, obtained by comparing the right columns of Table 5.3 and 5.4).

Despite this increase in HRV features during contractions for the healthy group, no significant difference was found when comparing HRV features of the healthy group to the group without asphyxia either during contractions or during rest periods, as shown in tables 5.3 and 5.4 respectively. A possible reason why no significant difference was observed between the two groups (either during contractions or during rest periods) might be the large inter-patient variability in obtained values for the HRV features and the relatively small dataset.

5.4.3 HRV features: ratio between contractions and rest periods

When considering the ratio between HRV features calculated during contractions and rest periods, SD, RMSSD, and $SampEn$ were all significantly lower for the group with asphyxia than for the healthy group (Table 5.5). Also the ratio for

HF was lower (as can be seen in Fig. 5.1), but this was not significant due to the large spread in the distribution.

For healthy fetuses, a high ratio of HRV features during contractions and rest periods might indicate a response of the fetal ANS to stabilize the cardiovascular system. On the one hand, during contractions HRV features are high because the fetus needs to adapt its cardiovascular system to changes in external pressure [51, 52]. On the other hand, during rest periods little cardiovascular control is required because in the second stage of labor fetal movement is reduced [178]. Furthermore, after a contraction has ended, a healthy fetus has not suffered much from indirect effect of contractions on the cardiovascular system (i.e. umbilical cord occlusion or reduced maternal blood flow). Therefore, healthy fetuses quickly recover from contractions and HRV features will be low during rest periods. As a result, a high ratio is observed for HRV features during contractions and rest periods. Note that if a fetus is not compromised by contractions, HRV features will be similar during contractions and rest periods, leading to a low ratio rather than a high ratio. However, the case where a fetus does not suffer at all is relatively simple to recognize by a clinician based on the FHR signal (e.g. when there are no decelerations in the FHR trace).

Unlike healthy fetuses, a fetus with asphyxia is not able to adequately adapt its cardiovascular system during contractions. Therefore, HRV features during contractions are relatively low for fetuses with asphyxia compared to healthy fetuses (although not significant, as shown in Table 5.3). Even after a contraction has ended, the oxygen concentration of the fetal blood is still low due to aforementioned indirect effects of contractions on the fetal cardiovascular system. The fetus thus also needs to adapt its cardiovascular system during rest periods, which can lead to decelerations that last until after contractions or even start after contractions have ended [1]. HRV features during rest are thus higher for fetuses with asphyxia compared to healthy fetuses (although not significant, as shown in Table 5.4). As a result, the ratio of HRV features during contractions and rest periods is lower for fetuses with asphyxia than for healthy fetuses.

An example of a registration of a fetus with and without asphyxia is shown in Fig. 6.2. For the healthy fetus, decelerations occur on top of contractions and a stable heart rate is observed during rest periods. The ratios of HRV features during contractions and rest periods are therefore high (SD = 3.4, RMSSD = 2.8, HF = 10.5, and SampEn = 4.5). For the fetus with asphyxia, decelerations are prolonged and last until after the contractions have ended. The ratios of HRV features during contractions and rest periods are therefore low (SD = 1.0, RMSSD = 1.6, HF = 2.1, and SampEn = 1.7).

5.4.4 Future perspective

Our results are promising and show that distinguishing contractions from rest periods improves HRV analysis for detection of asphyxia. However, we only

used a small dataset. To determine the diagnostic value for clinical practice, further study is required using a larger dataset. Besides, we only examined the effect on individual HRV features. In [35, 37, 39, 179], it was shown that combinations of multiple HRV features using classifiers can improve the detection rate of fetal asphyxia. It is therefore interesting to combine multiple HRV features calculated over the entire fetal heart signal with HRV features calculated during contractions and rest periods. Furthermore, it might also be interesting to monitor changes in HRV features over the course of labor as was done in [31, 165, 180].

5.5 Conclusion

Analysis of fetal HRV provides information on fetal asphyxia. Results in our study suggest that separating contractions and rest periods improves HRV analysis for the detection of asphyxia during labor. In particular, using the ratio between HRV features calculated from contractions and rest periods improves the ability of the HRV features to discriminate between healthy fetuses and fetuses with asphyxia. Further studies are required to determine the diagnostic value in clinical practice.

6

DETECTION RATE OF FETAL DISTRESS USING CONTRACTION-DEPENDENT FETAL HEART RATE VARIABILITY ANALYSIS

Abstract - Objective*: Monitoring of the fetal condition during labor is currently performed by cardiotocography (CTG). Despite the use of CTG in clinical practice, CTG interpretation suffers from a high inter- and intra-observer variability and a low specificity. In addition to CTG, analysis of fetal heart rate variability (HRV) has been shown to provide information on fetal distress. However, fetal HRV can be strongly influenced by uterine contractions, particularly during the second stage of labor. Therefore, the aim of this study is to examine if distinguishing contractions from rest periods can improve the detection rate of HRV features for fetal distress during the second stage of labor.* Methods*: We used a dataset of 100 recordings, containing 20 cases of fetuses with adverse outcome. The most informative HRV features were selected by a Genetic Algorithm and classification performance was evaluated using Support Vector Machines.* Results*: Classification performance of fetal heart rate segments closest to birth improved from a geometric mean of 70% to 79%. If the classifier was used to indicate fetal distress over time, the geometric mean at 15 minutes before birth improved from 60% to 72%.* Conclusion and significance*: Our results show that combining contraction-dependent HRV features with HRV features calculated over the entire fetal heart rate signal improves the detection rate of fetal distress.*[1]

6.1 Introduction

The introduction of cardiotocography (CTG) in the 1960s, has enabled continuous monitoring of the fetal heart rate (FHR) and uterine contractions. In current obstetric units, CTG has become the worldwide standard for detection of fetal distress during labor. However, the CTG is interpreted visually and the inter- and intra-observer variability is high [10]. Furthermore, despite a high sensitivity of CTG interpretation, the specificity is poor [7]. As a result of the low specificity, the rate of unnecessary operative interventions has increased since the introduction of CTG in the clinic [9]. To detect if the fetus is in distress, additional information is therefore often required when the CTG is abnormal.

In recent studies, analysis of fetal heart rate variability (HRV) has been shown to provide information on fetal distress [31, 32, 36–39, 179, 181]. Since the autonomic nervous system (ANS) regulates the heart rate, variations in the heart rate reveal autonomic regulation and might indirectly provide information on fetal distress. To quantify changes in HRV, several features have been developed in the literature that describe different aspects of HRV. For overviews of the most commonly used HRV features the reader is referred to [95] or [94].

Most HRV features have been developed and validated for adults in controlled experiments. However, unlike for adults, changes in the exterior of the fetus cannot be controlled during labor. Uterine contractions can lead to a temporary reduction of oxygen supply to the fetus (e.g. due to umbilical cord occlusion or reduced maternal placental blood flow). Besides, uterine contractions can cause large fluctuations in the intrauterine pressure, directly influencing the fetal cardiovascular system. As labor progresses into a stage of active pushing, the strength and influence of contractions increases.

In [51] and [52], it was shown for healthy fetuses that HRV was significantly higher during contractions as compared to rest periods (i.e. the period in between contractions). Moreover, [180] used an input-output model to describe the relation between the uterine activity (UA) and FHR signal, and showed that features extracted from this model provided information about fetal distress. The change in FHR during contractions could indicate a healthy response of the fetal ANS to stabilize the cardiovascular system. In a recent study we showed that the differences between HRV features during contractions and rest might be used to improve the detection of fetal distress [181].

In [35, 37, 39, 179] it was shown that the detection of fetal distress can be improved by classifying combinations of multiple HRV features. Therefore, in this paper we examine whether the detection of fetal distress can be improved by combining HRV features that were calculated over the entire heart rate with HRV features that were calculated separately during contractions and during rest periods. To determine the most informative subset of HRV features, both with and without the additional contraction-dependent HRV features, we used a Genetic Algorithm (GA) [182]. Furthermore, the classification performance of
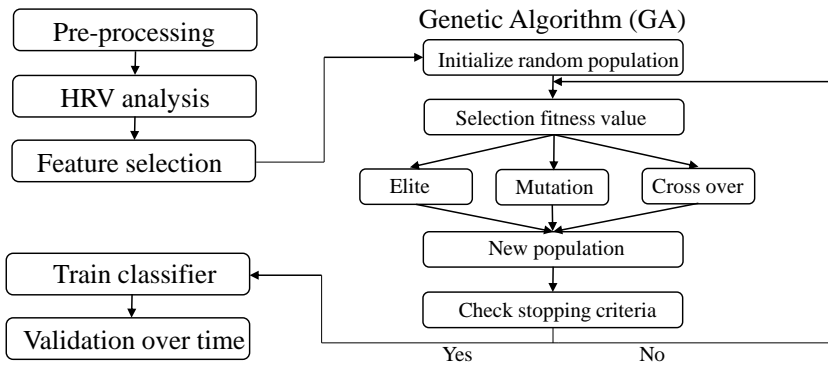
Figure 6.1: Flowchart of signal processing.

these subsets for detection of fetal distress was evaluated over time, using Support Vector Machines (DSPs) [183].

The rest of this paper is organized as follows; Section 6.2.1 discusses the data acquisition and pre-processing. In Sections 6.2.2 and 6.2.3 we summarize the implementation of the used HRV features. Feature selection, classification, and validation are explained in Sections 6.2.4-6.2.6. Results and discussion are presented in Sections 6.3 and 6.4.

6.2 Methods

This section describes the different HRV features, feature selection, and the classification that was used in this paper. The overall classification procedure is presented in Fig. 6.1.

6.2.1 Data acquisition and pre-processing

We used FHR and UA signals that were recorded on a Neoventa STAN® (Mölndal, Sweden) in the Máxima Medical Center in Veldhoven, the University Medical Center in Utrecht, and registrations collected in Sweden in the context of STAN evaluation over the period 2001-2008. Registrations of at least 36 weeks of gestation were included. Pregnancies complicated by intra-uterine growth restriction, fever, fetal congenital anomalies, or use of ritodrine were excluded. We used beat-to-beat FHR signals that were recorded by a scalp electrode. UA was recorded with either a tocodynamometer or intra-uterine pressure catheter. Contractions were annotated by a clinical expert that had no knowledge of the FHR signal or fetal outcome.

Because the beat-to-beat R-R intervals are determined when a heartbeat occurs, the R-R intervals are not equidistantly sampled. We used linear interpolation to obtain an equidistantly sampled FHR signal, sampled at a rate of 4 Hz. If an R-R

Table 6.1: Clinical characteristics of included fetuses.

Clinical features	healthy fetuses (cases n=80)	fetuses with adverse outcome (cases n=20)
Gestational age (days)	280 ± 10	283 ± 8
Birth weight (g)	3551 ± 471	3560 ± 467
1-minute Apgar score	8.6 ± 1.1	6.3 ± 2.0
5-minute Apgar score	9.5 ± 0.5	7.8 ± 2.0
Cord arterial pH	7.25 ± 0.03	7.00 ± 0.04
Cord arterial base excess (mmol/l)	-5.8 ± 2.3	-16.0 ± 2.2
Length second stage of labor (min)	58 ± 24	62 ± 24

[a] Values are expressed as mean and standard deviation.

interval changed by more than 25 BPM or more than 200 ms with respect to the adjacent R-R interval, the R-R interval was considered an artifact. Artifacts were corrected by linear interpolation.

Each registration was divided into segments of 10 minutes, with five minute overlap. If a segment contained less than 20% loss of FHR signal and at least annotation of two contractions and two rest periods, the segment was used for further analysis. We only included FHR signal during the second stage of labor (stage of active pushing), since during this stage contractions have a strong effect on the fetus. Besides, because we expect that the effects of oxygen deficiency increase as labor progresses, we only considered FHR segments up to maximally 45 minutes before birth. Since we are also interested in the classification performance over time, only registrations were included with at least 3 usable 10 minute segments within the final 45 minutes before birth.

The fetal outcome was based on the umbilical arterial acid-base state. Adverse outcome was defined as a pH below 7.05 and base excess below -12 mmol/l, and healthy as a pH above 7.20 [1]. Out of 1232 registrations, our dataset contained 44 cases with adverse outcome. Of these 44 cases, 6 cases were excluded due to either intra-uterine growth restriction, fever, fetal congenital anomalies, or used of ritodrine. Another 6 had to be excluded because no information was available on the onset of the second stage of labor. Of the remaining 32 cases, 20 cases had sufficient quality FHR and UA signal, and were used for further analysis. The 20 cases with adverse outcome were matched with 80 healthy cases (1-to-4 ratio between the size of both groups). We have attempted to match the prevalence of certain medications that can cross the placenta and influence fetal HRV (e.g. anti-hypertensives or pain killers) in accordance with the difference in size of the two groups. The main clinical characteristics of the included fetuses is shown in Table 6.1.

<div align="center">**Table 6.2:** HRV features.</div>

HRV features	Abbreviation
Standard deviation	SD
Root mean square of successive differences	RMSSD
Low frequency power	LF
High frequency power	HF
Total power	TP
Normalized low frequency power	LF_n
Normalized high frequency power	HF_n
Sample entropy	SampEn
Scaling exponent	α
Deceleration capacity	DC

6.2.2 HRV analysis

For each 10 minute FHR segment, conventional HRV features were calculated over the resampled FHR signal. The HRV features used in this paper have been described in detail in our previous study [181] and only the implementation is discussed here. The used HRV features are listed in Table 6.2. In the rest of this paper we will denote the resampled FHR signal by $x[n]$, for samples $n = 1, ..., N$, with N the length of the signal.

As shown by [166], artifact correction by interpolation influences the HRV analysis. Excluding these periods for the computation of HRV features reduces the error made in the HRV analysis [166]. This section also describes how we reduced the influence of artifacts for each HRV feature.

Statistical features   The standard deviation (SD) and the root mean square of successive differences (RMSSD) were calculated as statistical features. For the calculation of SD and RMSSD all artifact corrected samples were excluded.

Frequency domain features   Spectral analysis was performed to examine the heart rate at specific frequency bands that are related to sympathetic and parasympathetic activity [30]. Frequency bands for analysis of fetal HRV differ from frequency bands for analysis of adult HRV [184]. Power in the low frequency band (LF, 0.04-0.15 Hz) is related to both sympathetic and parasympathetic activity, and power in the high frequency band (HF, 0.4-1.5 Hz) is related to parasympathetic activity only. Besides absolute LF and HF, also normalized frequency powers were calculated (LF_n and HF_n), by dividing LF and HF by the total power (TP, 0.04-1.5 Hz).

Spectral analysis was performed by the Continuous Wavelet Transform (CWT) with a fifth order symlet wavelet [166, 181]. In this study, we used the complex CWT [167]. Because the complex CWT also provides phase information, it is

possible to calculate the spectral power at each sample, leading to more reliable calculation of LF_n and HF_n. Note that resampling of the beat-to-beat FHR signal to an equidistant signal may cause some distortion of the spectral analysis [185]. Yet, we expect that the influence of this distortion on the outcome is limited since resampling was performed for all registrations.

CWT compares $x[n]$ to a family of analyzing wavelet functions $\psi[\frac{n-\tau}{s}]$, where s is a scaling parameter and τ the position parameter of the wavelet. The CWT coefficients $W[s, \tau]$ can be obtained by varying the scale parameter s and the position parameter τ. The power at each time instant and scale is proportional to the square of the CWT coefficients. The total power in a frequency band is then calculated by integrating the power over the scales within the frequency band of interest and averaging over time.

Each wavelet $\psi[\frac{n-\tau}{s}]$ has a support width that is related to the scaling parameter s. Similar to [166], we considered one-third of support width of $\psi[\frac{n-\tau}{s}]$ as the effective support width. A CWT coefficient was excluded for the calculation of HF if one or more samples within the effective support width was artifact corrected. To calculate LF, we excluded CWT coefficients when more than five seconds of consecutive FHR signal was artifact corrected within the effective support width.

Complexity features   The presence of irregularities in the heart rate is seen as healthy blood pressure control by the ANS. Complexity in short time signals can be quantified by Sample Entropy (SampEn) [99]. To calculate SampEn, the FHR is divided into vectors $\mathbf{u}[i] = \{x[i], x[i+1], ..., x[i+m-1]\}$. SampEn estimates the conditional probability that if patterns are similar for length $m-1$, they will also be similar for length m. A tolerance parameter r is used to define a threshold for similarity between two patterns. We excluded vectors $\mathbf{u}[i]$ from the calculation of SampEn if any of the samples $\{i, i+1, ..., i+m-1\}$ was artifact corrected. Similar to [36], [37] and [181], the length of the vectors was set to $m = 2$ and the tolerance to $r = 0.2SD$.

Fractal features   To describe the scaling properties of HRV over different time scales, we used scaling exponent α, which is obtained from Detrended Fluctuation Analysis (DFA) [170]. To calculate α, first the cumulative sum $y[n]$ of the FHR signal is obtained. Next, $y[n]$ is divided into equally spaced segments of length a and the linear trend of each segment ($y_a[n]$) is determined. The characteristic fluctuation F at each scale a is computed as the root mean square (RMS) deviation between $y[n]$ and its trend $y_a[n]$.

The scaling exponent α is given by the slope of the relation between $\log(F[a])$ and $\log(a)$. Similar to [38], α was computed over the scales ranging from 1 to 60 seconds, which corresponds to the physiological range of the baroreflex.

Artifact corrected samples are excluded from the calculation of the linear trend $y_a[n]$ and the characteristic fluctuation F. Moreover, if the percentage of artifact correction within a segment of length a is more than 20%, it is excluded entirely.

Phase rectified signal averaging   In addition to the HRV features that were included in our previous study [181] and have been described above, we also used Phase Rectified Signal Averaging (PRSA). PRSA has shown promising results for the detection of fetal distress [186] and [179]. The basic idea of PRSA is to account for non-stationarities in the heart rate by aligning heart rate segments based on predefined events, called anchor points (v). For analysis of the heart rate, anchor points are typically defined as decelerations and accelerations in the heart rate, and PRSA quantifies the average response to a deceleration (the deceleration capacity, DC) or acceleration (the acceleration capacity, AC). It was shown by [186] that DC and AC are highly correlated and that their performance for detection of fetal distress is similar. Therefore, we only included DC in our analysis.

PRSA depends on two parameters: a filter parameter T and a window parameter L [187]. Similar to [186] we used $T = 5$ and $L = 45$. Artifact corrected samples were not used as anchor points. Moreover, when there was more than 20% artifact correction within a window $v \pm L$, the anchor point v was also excluded.

6.2.3   Contraction-dependent HRV features

In addition to calculating HRV features over the entire FHR signal, we also calculated HRV features separately during contractions and rest periods. Using the expert annotations, the rest period was defined as the period in between two contractions. No contraction or rest period was defined if the length of a contraction or the time between contractions was less than 20 seconds. Note that the fetus typically requires some recovery time directly after a contraction, but has enough time to recover before a new contraction. Therefore, if the time between two contractions was more than one minute, we only considered the final minute preceding the second contraction as rest period. In Fig. 6.2 an example is shown of an FHR signal that is recorded during contractions and during rest periods.

HRV features during contractions were based on R-R intervals that were recorded during contractions (denoted as $feature_{uc}$). Similarly, HRV features during rest periods were based on R-R intervals that were recorded during rest periods (denoted as $feature_{rest}$). Also the ratio between HRV features calculated during contractions and during rest was included (denoted as $feature_{ratio} = feature_{uc}/feature_{rest}$), as the ratios have shown promising results in our previous studies [181]. Because the time between contractions or the length of the contractions was often less than one minute, we could not calculate LF, LF_n, HF_n, α and DC separately during contractions and during rest periods. Our analysis of contraction-dependent HRV features was therefore limited to SD, $RMSSD$, HF, and $SampEn$.

In total, 22 HRV features were used: 10 calculated over the entire FHR, 4 during rest, 4 during contractions, and 4 ratio features, as presented in Table 6.3.
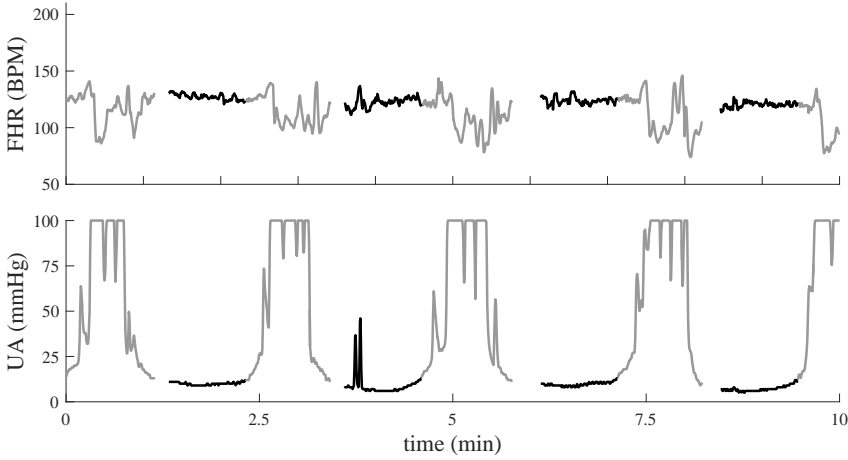
Figure 6.2: Example of an FHR (upper graph) and UA signal (bottom graph) of healthy fetus. Black lines are rest periods and gray lines contractions.

Table 6.3: HRV feature sets.

Feature set	HRV features
$S_1 \in \mathbb{R}^{10}$	SD, RMSSD, LF, HF, TP, LF_n, HF_n, SampEn, α, DC
$S_2 \in \mathbb{R}^{12}$	SD_{uc}, $RMSSD_{uc}$, HF_{uc}, $SampEn_{uc}$ SD_{rest}, $RMSSD_{rest}$, HF_{rest}, $SampEn_{rest}$ SD_{ratio}, $RMSSD_{ratio}$, HF_{ratio}, $SampEn_{ratio}$
$S_3 \in \mathbb{R}^{22}$	$S_1 \cup S_2$

We defined HRV feature set $S_1 \in \mathbb{R}^{10}$ as the set of HRV features that are calculated over the entire FHR, without distinguishing contractions and rest periods. The set of HRV features that contain the contraction-dependent HRV features is defined as $S_2 \in \mathbb{R}^{12}$. The set of HRV features that contains both HRV features that are calculated over the entire FHR signal and contraction-dependent HRV features is defined as $S_3 = S_1 \cup S_2$.

6.2.4 Feature selection

In [188] it was shown that many HRV features that are described in Section 6.2.2 are correlated and might therefore contain redundant information. Besides, our dataset is relatively small, with only 20 cases of fetuses with adverse outcome. As a consequence, there is a risk of overfitting when too many HRV features are used for classification. Therefore, we used a GA to select the best combination of HRV features. GA has the advantage that it can effectively explore the entire

Table 6.4: GA settings.

Parameter	Value
Population size	100
Number of elite children	2
Crossover fraction	80%
Mutation function	single point
fitness value	SVM performance
fitness function	rank
Genotype selection	roulette system
Maximum number of features in genotype	5
Maximum iterations with same fitness value	10
Maximum iterations	200

feature space, without running through all possible combinations of features and it has successfully been used for detection of fetal distress by [179].

A schematic overview of GA is presented on the right side of Fig. 6.1. GA iteratively creates populations of candidate feature subsets (genotypes) by randomly combining and mutating genotypes of the population in a previous iteration, until certain convergence criteria are reached. In each iteration, the genotypes of the current population are scored by a fitness function. Genotypes are then selected at random to generate a new population with a probability that is proportional to their fitness value. Each new population consists of elite children (best performing genotypes that are guaranteed to survive to the next iteration), children that are produced by random mutations of a single genotype, and children that are produced by random crossover between pairs of genotypes.

For the implementation of GA, we used *ga* from the standard Global Optimization Toolbox of Matlab® (The Mathworks, Inc. Natick, MA). As fitness function, we used the performance of an SVM classifier, which is explained in Section 6.2.5. Based on the ranking in fitness value, genotypes are selected using a roulette system [182]. Genotypes with equal scores were given equal rank and only the best 50% was used to generate the next population. Similar to [179], the population size was set to 100, two elite children were used, and the crossover fraction was set to 80%. The remaining 20% for the new population was obtained by single point mutation. If two equal genotypes were selected for crossover, single point mutation is used instead to generate the child. To prevent GA from reaching a local minimum with a relatively large number of selected features, the number of selected features of a genotype was restricted to a maximum of five features. The GA was terminated if the best fitness value of the population did not improve for 10 iterations or in case 200 iterations were done. The settings for GA are summarized in Table 6.4.

Table 6.5: SVM settings.

Parameter	Value
Kernel function	rbf
Kernel width (σ)	1
Penalty factor (C)	1
Optimization metric	g
Misclassification cost majority class	0.25
Misclassification cost minority class	1

6.2.5 Classification

We used SVMs to classify healthy fetuses and fetuses with adverse outcome. SVMs are supervised learning models that construct a set of hyperplanes that minimize the classification error while maximizing the distance between the hyperplanes and its nearest data points [183]. We used a Gaussian radial base function (rbf) to allow for non-linear decision boundaries. To implement the SVMs, we used the standard implementation *fitcsvm* in the Statistics and machine learning toolbox of Matlab®. We used the default settings of the SVM for the width of the Gaussian kernel function (σ = 1) and the penalty parameter for misclassification (C = 1).

The imbalance in the distribution of the two classes in our dataset causes the SVM to be accurate for classification of the majority class (healthy fetuses) but to perform poorly for classification of the minority class (fetuses with adverse outcome) [189]. To prevent poor classification of the minority class, we defined a cost function based on the imbalance in the class distribution: the cost for misclassification of the minority class was thus four times higher than misclassification for the majority class. The SVM settings are summarized in Table 6.5.

6.2.6 Validation

In case of an imbalanced dataset, the accuracy (Acc) is not the best metric to evaluate the classification performance [189] and [35]. Instead, we used the geometric mean (g) as metric to train the classifier and as fitness function for the feature selection in GA. The metric g provides a balance between the classification accuracy of the majority class (specificity, Sp) and the classification accuracy of the minority class (sensitivity, Se), and is defined as $g = \sqrt{Sp \cdot Se}$ [189]. The SVM rbf is a soft-type classifier, meaning that the output of the classifier can be a continuous value. Changing the threshold settings of the classifier will vary Se and Sp. Receiver operating characteristic (ROC) curves can be used to evaluate how the classifier performs for various classification threshold settings. The area

under the ROC curve (AUC) can be used as a metric to evaluate the classification performance for various classification threshold settings.

For feature selection, the FHR segments of all registrations were used that were closest to birth. We used the 10-fold cross validation performance of the SVM as fitness value in GA. Note that for feature selection we only used the 10 minute FHR segment of each fetus that was closest to birth, meaning that from each fetus only a single FHR segment was used. The 10 minute FHR segment was either included in the training or in the test partition, but never in both. Using 10-fold cross validation ensures that the fitness value for genotypes is not overestimated. Due to our relatively small dataset, containing only 20 cases of fetuses with adverse outcome, feature selection and classification could be influenced by the location where the dataset was split into ten fold. To obtain a more objective result, feature selection was repeated 50 times, starting from different data splits. Hence, we generated 50 subsets of HRV features with 50 outcome measures for sets S_1, S_2, and S_3.

Besides classification performance for the FHR segments closest to birth, we are also interested in the classification performance over time. To this end, a classifier was trained for each generated feature subset on the FHR segments closest to birth. Then, the trained classifiers were used to classify if a fetus was in distress or not for all FHR segments within a registration, starting from 45 minutes before birth up to the time of birth. Since the purpose of the classifier would be to initiate an intervention in case an FHR segment is classified as fetal distress, all remaining FHR segments of that registration up to the time of birth were also indicated as fetal distress.

At each time instant the g, Se, and Sp for a classifier were calculated. Note that since not all registrations have 45 minutes of active pushing, the outcome measures were calculated with respect to the total number of registrations with at least one FHR segment up to that time (as shown in Fig. 6.3). Furthermore, for some recordings we were unable to analyze the final minutes before birth, either due to loss of FHR signal or insufficient quality UA signal. For these recordings, we retained the classification value of the final available segment up to the time of birth.

6.3 Results

Figure 6.4 show boxplots of the HRV features that were calculated separately during contractions and rest periods (SD, RMSSD, HF, and SampleEn) for the entire dataset. The correlation matrix of the HRV features used in this study is presented in Figure 6.5. Figure 6.6 shows the HRV features that were selected in the 50 runs by GA. From S_1 (only HRV features that are calculated over the entire FHR segments), TP, LF_n, HF_n, and DC were most frequently selected. In case of S_2 (only contraction-dependent HRV features) SD_{ratio} and $RMSSD_{uc}$ were most frequently selection. In case of S_3 (combined set of HRV features in
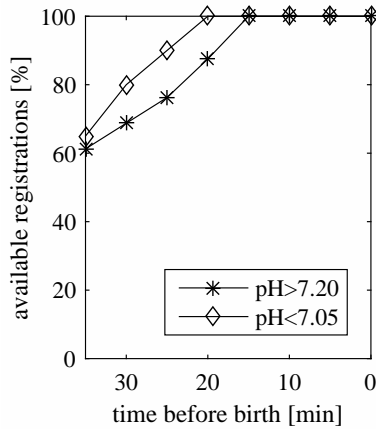
Figure 6.3: Percentage of registrations with at least one FHR segment up to that time.

Table 6.6: Average 10-fold cross validation performance for classification of the FHR segments closest to birth.

Feature set	g (%)	Se (%)	Sp (%)	Ac (%)	AUC
S_1	70	66	76	74	69
S_2	76	75	76	76	78
S_3	**79**	**81**	77	**78**	**80**

S_1 and S_2), SD_{ratio} and HF were most frequently selected. The average size of selected subsets from S_1 was 3.0, from S_2 2.6, and from S_2 3.5 HRV features.

The average cross validation performance for classification of the FHR segments closest to birth is shown in Table 6.6. The average g for S_1, S_2, and S_2 were g = 70%, g = 76%, and g = 79%, respectively. Finally, Fig. 6.7 shows the classification performance over time.

6.4 Discussion

Analysis of fetal HRV provides information on fetal distress. Most HRV features have been developed and validated for adults in controlled experiments. However, during labor the fetal cardiovascular system is strongly influenced by contractions. As can be seen in Fig. 6.4, HRV features are higher during contractions compared to HRV features during rest periods. In this study we showed that separating contractions from rest periods improves HRV analysis for the detection of fetal distress during labor.
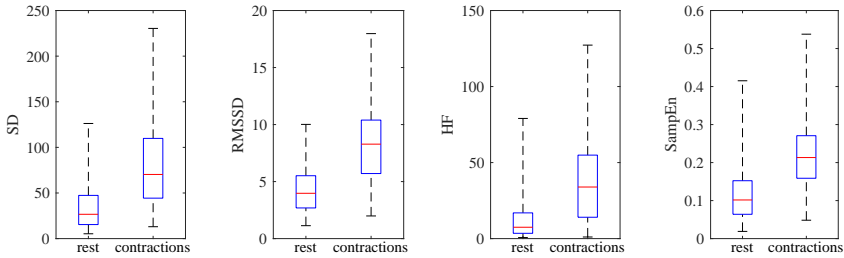
Figure 6.4: Comparison of HRV features measured during rest periods and contractions. Results are shown as boxplots where the central marker indicates the median and the edges of the box the interquartile range. The whiskers correspond to the full range of the data.
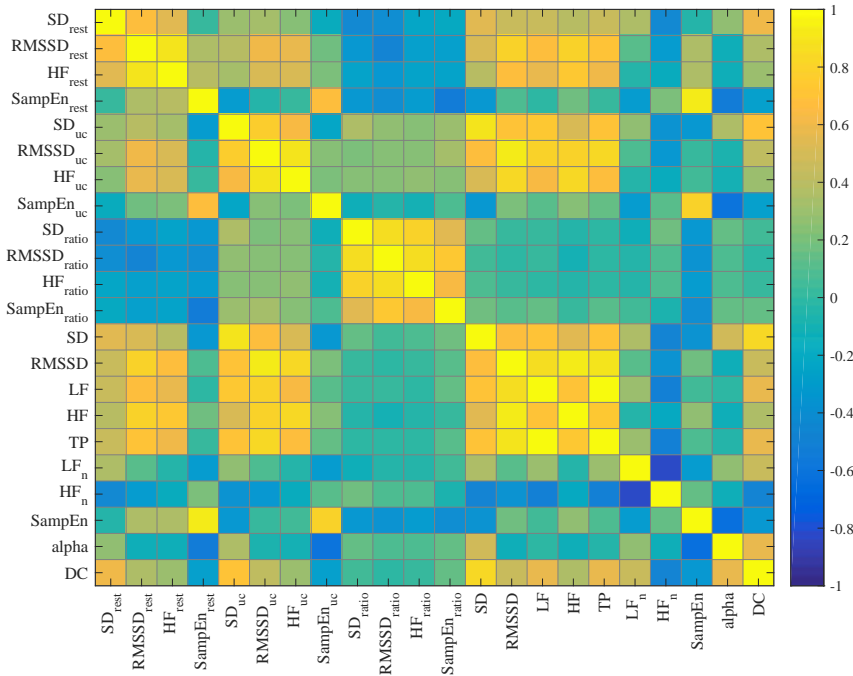
Figure 6.5: Correlation matrix of the HRV features in S_3. The color indicates the strength of the correlation.

6.4.1 Data acquisition

Out of the relatively large number of available registrations, we could only include 20 cases of fetuses with adverse outcome. This is partly due to the low incidence of fetuses with pH below 7.05 and partly due to our strict inclusion criteria. Moreover, we required a good quality UA signal to be able to clearly identify contractions. Because in clinical practice the UA signal is often of poor
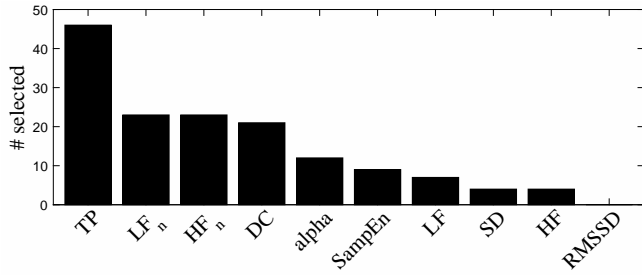
(a) Selected HRV features from S_1.
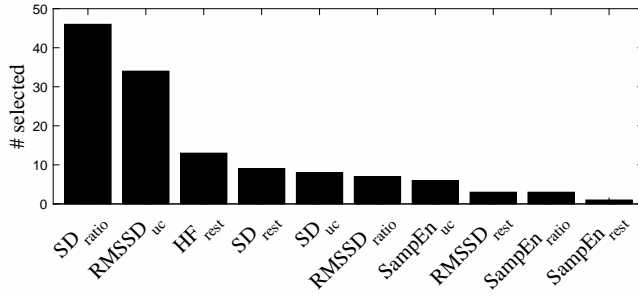
(b) Selected HRV features from S_2.
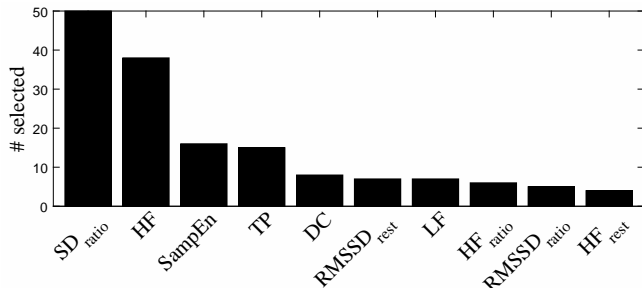
(c) Selected HRV features from S_3.

Figure 6.6: Results feature selection by GA.
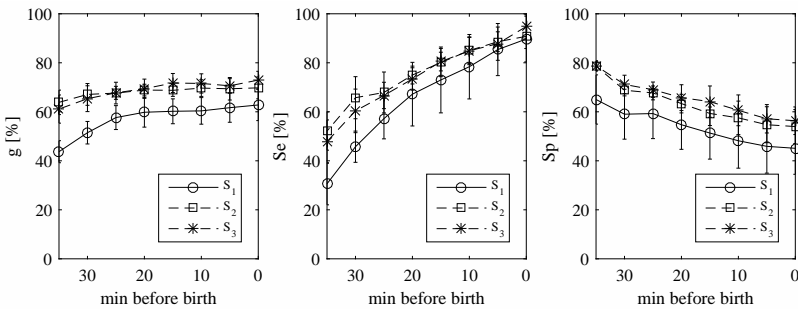
Figure 6.7: Average performance classification over time.

quality, this requirement limits the application of contraction-dependent HRV features. A potential solution to improve the quality of the UA signal might be to use electrohysterography to record the UA instead of a tocodynamometer [176] and [115]. In addition to good quality UA signal, less than 20% loss of FHR signal was allowed. To minimize the influence of artifact correction of the FHR signal, periods with artifact corrected FHR were excluded from the calculation of HRV features.

In this study we only focussed on FHR segments during the second stage of labor. During the second stage, contractions generally have a strong effect on the fetus. In contrast, during the first stage of labor (stage of cervical dilation), the effect of contractions is less pronounced. Therefore, a classifier that is trained on FHR from the second stage of labor might be less predictive during the first stage of labor. For future work it would be interesting to also examine the classification performance during the first stage of labor.

Because the goal of this study was to examine whether separating contractions from rest periods can improve the HRV analysis, we limited our dataset to two groups that are well separated in terms of fetal outcome and did not consider registrations with pH between 7.05 and 7.20. However, this approach simplifies the classification task and does not represent true clinical conditions. Before a classifier can be used in clinical practice, future study should use a dataset that contains registration with all pH values.

6.4.2   Feature selection

Fig. 6.5 shows that several of the HRV features that were used in this study were correlated. In particular, HRV features calculated on the entire FHR signal were correlated to their counterpart that was calculated during contractions or during rest periods (e.g. SD was correlated to SD_{rest} and S_{uc}). To select the best combination of HRV features for detection of fetal distress we used GA. The average size of selected subsets from S_1, S_2, and S_3 (3.0, 2.6, and 3.5, respectively) was smaller than the maximum number of five features that was allowed for GA, indicating that larger feature subsets would not have improved classification.

Because GA uses the classification performance to score candidate subsets, selected HRV features could perform differently for other classifiers. Furthermore, since feature selection could be influenced by splitting the dataset in the 10-fold cross validation, GA was repeated fifty times using different data splits. The influence of splitting the dataset on feature selection can be seen from Fig. 6.6 by the number of HRV features that were selected multiple times.

The most frequently selected HRV feature for S_1 was TP, and the most frequently selected HRV feature for S_2 and S_3 was SD_{ratio}. Although TP was selected most of the time from S_1, TP was only selected a few times for S_3, as shown in Fig. 6.6. Since both TP and SD_{ratio} are related to the presence of decelerations, these HRV features contain similar information. SD_{ratio} also contains information about how well the fetus is able to recover from contractions: a high

SD_{ratio} indicates that the fetus quickly recovers from a contraction and is able to stabilize its cardiovascular system during the rest periods. On the other hand, a low ratio indicates that the variability during contractions and rest periods is similar, meaning that the fetus is unable to recover during the rest periods. In case SD_{ratio} is selected, the information of TP becomes redundant.

Other HRV features that were often selected for S_1 were LF_n, HF_n, and DC. In [31] it was also found that normalized spectral powers were predictive of fetal distress. Since changes in normalized spectral powers are not masked by changes in the total power, normalized spectral powers can give better insight in cardiovascular control than absolute spectral powers.

Interestingly, although HF_n was frequently selected for S_1 it was not often selected for S_3. Instead, for S_3 HF was often selected in combination with SD_{ratio}. Since SD_{ratio} is related to the presence of decelerations and the total power, it could be that the combination of SD_{ratio} and HF also contains the information in HF_n, since SD_{ratio} is related to TP. In line with the selection of HF for S_3 is the selection of $RMSSD_{uc}$ and HF_{rest} for S_2, as the combined information of $RMSSD_{uc}$ and HF_{rest} is similar to the information of HF.

To gain more insight in cardiovascular control, it would be interesting to examine HF_n and LF_n during contractions and rest periods. However, the length of contractions or rest periods was often less than the required length to calculate LF_n and HF_n, and we were unable to calculate HF_n and LF_n separately during contractions and rest periods. Besides LF_n and HF_n, in this study DC was also frequently selected from S_1, similar to findings in [179]. Since DC contains information about decelerations, it contains similar information as SD_{ratio} and was not frequently selected from S_3. In our results, scaling exponent α was selected less often. Recently, [165] obtained promising results for detection of fetal distress by calculating scaling exponents using a wavelet based scattering transform. In [38] it was shown that the influence of decelerations on the scattering transform is limited and using the scattering transform might improve the fractal analysis.

6.4.3 Classification

Many factors can influence the response of the fetus to contractions. There are clinical parameters that can influence the FHR, such as gestational age [190], behavioral states [184], or medication [191]. Furthermore, uterine contractions can directly influence the fetal cardiovascular system through a rise in intrauterine pressure, or indirectly by blocking the oxygen supply to the fetus (e.g. umbilical cord occlusion) [192]. As labor progresses, the effect of contractions on the fetal cardiovascular system increases. As a consequence, in the literature many different FHR patterns have been described with different characteristics, several of which have been related to fetal distress (e.g. late decelerations, bradycardia, sinusoidal patterns, or saltatory patterns) [1]. The relatively low number of cases

with adverse fetal outcome in combination with the large variation in FHR patterns makes training of a classifier challenging.

We did not compare our classification performance to visual CTG interpretation, because the inter- and intra-observer variability of CTG interpretation is generally high [10]. Besides, in the final minutes before birth the CTG is typically abnormal in most registrations. Hence, results obtained from visual CTG interpretation might in this case not be representative.

The average 10-fold cross validation performance for classification of the FHR segments closest to birth improved from $g = 70\%$ for S_1 to $g = 76\%$ for S_2, and $g = 79\%$ for S_3. The difference is less pronounced in terms of Ac (Acc=74% for S_1, Acc=76% for S_3, and Acc=78% for S_3), because Ac is mostly determined by correct classification of the majority class. Note that the classifier was trained to optimize g, which is a balance between Se and Sp. Depending on the use of the classifier in clinical practice, it would be more appropriate to train a classifier that is either more sensitive to misclassification of the minority group (and increase Se) or misclassification of the majority group (and increase Sp). This can be achieved by changing the penalty parameter for misclassification or the SVM threshold settings. As AUC is higher for S_2 and S_3 compared to S_1 (AUC=69% for S_1, AUC=78% for S_2, and AUC=80% for S_3), using S_2 and S_3 will perform better for varying settings for the penalty parameter or classification threshold.

The earlier a prediction, the more useful the information for clinical intervention. For classification over time, the performance of S_2 and S_3 were similar, although performance of S_3 was slightly better. The average g over time for S_3 increased by 12% with respect to the average g of S_1 (57% for S_1, 68% for S_2, and 69% for S_3). At 15 minutes before birth, the classification performance for S_1 was $g = 60\%$, for S_2 $g = 69\%$, and for S_3 $g = 72\%$. For all sets S_1, S_2, and S_3, classification performance over time was lower than the classification performance for the FHR segments closest to birth. It should be noted that fetal distress develops gradually over time [177]. Since it is unclear at which point the fetus is no longer capable of handling the stress, the relatively low Se at 35 minutes before birth (Se=31% for S_1, Se=52% for S_2, and Se=48% for S_3) could be because at that time some of the fetuses with adverse outcome were still relatively healthy. Further study using a larger dataset is required to gain more insight into which combination of HRV features is the most informative and to improve the classification.

6.5 Conclusion

Fetal HRV analysis provides information on fetal distress. Combining HRV features calculated over the entire fetal heart rate with contraction-dependent HRV features improves the classification performance during the second stage of labor. Further studies are required to gain more insight in the which combination of HRV features is most informative.

7 | FETAL HEART RATE VARIABILITY DURING PREGNANCY

Abstract - Objective*: Non-invasive spectral analysis of fetal heart rate variability is a promising new field of fetal monitoring. To validate this method properly, we studied the relationship between gestational age and the influence of fetal rest–activity state on spectral estimates of fetal heart rate variability.* Design*: Prospective longitudinal study.* Setting*: Tertiary care teaching hospital.* Population*: Forty healthy women with an uneventful singleton pregnancy.* Methods*: Non-invasive fetal electrocardiogram measurements via the maternal abdomen were performed at regular intervals between 14 and 40 weeks of gestation (wG) and processed to detect beat-to-beat fetal heart rate. Simultaneous ultrasound recordings were performed to assess fetal rest–activity state.* Main outcome measures*. Absolute and normalized power of fetal heart rate variability in the low (0.04–0.15 Hz) and high (0.4–1.5 Hz) frequency band were obtained, using Fourier Transform.* Results*: 14% of all measurements and 3% of the total amount of abdominal data (330 segments) was usable for spectral analysis. During 21–30 wG, a significant increase in absolute low and high frequency power was observed. During the active state near term, absolute and normalized low frequency power were significantly higher and normalized high frequency power was significantly lower compared with the quiet state.* Conclusions*: The observed increase in absolute spectral estimates in preterm fetuses was probably due to increased sympathetic and parasympathetic modulation and might be a sign of autonomic development. Further improvements in signal processing are needed before this new method of fetal monitoring can be introduced in clinical practice.*[1,2]

---

1 Results in this chapter were obtained with signal processing methods that date back to 2012. With the methods presented in chapters 3 and 4, the percentage of recordings with usable fetal heart increases from 14% to 66%.

2 This chapter is based on the paper published as *Van Laar J.O.E.H., Warmerdam G.J.J., Verdurmen K.M.J., Vullings R., Peters C.H.L., Houterman S., Wijn P.F.F., Andriessen P., Van Pul C., Oei S.G., "Fetal heart rate variability in frequency-domain during pregnancy, obtained from noninvasive electrocardiogram recordings". Acta Obstet Gynecol Scand. 2014, 93: 93-101.*

7.1   Introduction

Cardiotocography (CTG) is the widespread method for fetal monitoring, despite its poor diagnostic value in detecting fetal distress [9]. The poor specificity of this method has resulted in increased rates of operative deliveries without a significant improvement in long-term fetal outcome [9]. Additional ST-waveform analysis of the fetal electrocardiogram (ECG; STAN®, Neoventa Medical, Mölndal, Sweden) and fetal scalp blood sampling, applied in the case of a non-reassuring CTG, have a limited capability of improving neonatal outcome or reducing unnecessary interventions [9, 26, 27]. Besides, these techniques can only be used during labor at term due to their invasiveness. Therefore, there is an urgent need to develop non-invasive methods that provide complementary information on fetal well-being and that can be used intra- and antepartum during the term and preterm period.

The analysis of variations in beat-to-beat heart rate is an established non-invasive technique for investigating the autonomic cardiac control system [30]. In human adults, heart rate variability (HRV) estimated by spectral analysis reflects the modulation of the sympathetic and parasympathetic limbs of the autonomic nervous system [30]. The low frequency cardiovascular fluctuations are ascribed to the baroreceptor reflex and are under sympathetic and parasympathetic control, whereas high frequency fluctuations are associated with respiration and are under parasympathetic control only [29, 30].

As in human adults, quantifying the variations in beat-to-beat fetal heart rate (FHR) by spectral analysis can be used to monitor autonomic nervous system modulation and may provide an early diagnostic tool for detection of fetal distress [193]. Spectral analysis during labor was previously performed on beat-to-beat heart rate, obtained from direct fetal ECG recordings by scalp electrode [31, 32, 184, 193]. Our previous studies during labor showed that spectral estimates are associated with severe metabolic acidosis at birth [31] and might predict fetal distress in an early stage [32]. In addition, spectral estimates are related to fetal behavioral state and weeks of gestation (wG) during labor at term [184].

Before using spectral analysis for fetal monitoring, more insight needs to be gained into normal autonomic development. However, at present, limited research has been done on human fetal HRV in the frequency-domain during the second and third trimester of pregnancy, and thus during the development of autonomic reflex mechanisms [78, 79]. To measure spectral estimates during gestation, beat-to-beat FHR should be obtained non-invasively. Previous studies are limited considering developmental aspects either because no longitudinal follow up was performed during pregnancy or because the studies did not take into account fetal movement during the third trimester. Changes in fetal HRV due to fetal rest–activity state occur after 30 wG [85]. Since spectral estimates of fetal HRV are known to be associated with rest–activity states at term gestation [79, 184], it is difficult to interpret spectral values without classifying fetal movements.

By measuring low frequency power (LF) and high frequency power (HF) at regular time intervals during gestation, the development of the fetal autonomic cardiac control can be examined. We developed a new method to obtain the fetal ECG non-invasively from the maternal abdomen [45]. This method allows for beat-to-beat detection of the fetal R-waves and provides fetal beat-to-beat heart rate and spectral estimates non-invasively.

The first objective of the current study is to present a non-invasive method for fetal ECG and beat-to-beat heart rate detection, and to evaluate its clinical feasibility. The second objective is to study the relationship between wG and spectral estimates of fetal HRV and to study the influence of fetal rest–activity states on spectral estimates after 30 wG.

7.2   Material and methods

A prospective longitudinal study was performed in a tertiary care teaching hospital. The study protocol was approved by the institutional review board at the Máxima Medical Center (reference number 0650). Participants were recruited consecutively from a healthy population, undergoing routine pregnancy follow-up during one of the first outpatient visits. Only healthy women with an uneventful singleton pregnancy, not taking medication other than iron tablets or vitamins, were asked to participate before 12 wG. Excluded were women under the age of 18 years. Participants were included after a written informed consent form was signed. Pregnancy duration was determined from the last menstrual period and confirmed by crown–rump length at 10–12 wG. Only pregnancies which progressed uneventfully, resulting in the delivery of a healthy infant with a birth weight above the 10th percentile corrected for wG, maternal parity and fetal sex [194], were included in the data analysis.

7.2.1   Data acquisition and signal processing

Non-invasive fetal ECG measurements were repeatedly performed antenatally. A non-invasive electrophysiological monitor for obstetrics (NEMO; Fig. 7.1a) was used to record and store the data. The device has less than 5 μV root mean square noise. The NEMO system was approved by the Medical Technical Service Department of the Máxima Medical Center. Recordings were performed at approximately 14, 18, 22, 24, 26, 30, 34, 36, 38, and 40 wG. Measurements were performed non-invasively using eight self-adhesive electrodes, one reference and one ground electrode on the maternal abdomen (Fig. 7.1b). Each recording session took place between 8:00 h and 18:00 h, with the woman lying comfortably in a bed in semi-recumbent position. During this time period, no important fluctuations in fetal HRV were expected [195]. The duration of recordings was approximately 45 min. Simultaneous ultrasound recordings were performed to assess the fetal rest–activity state.
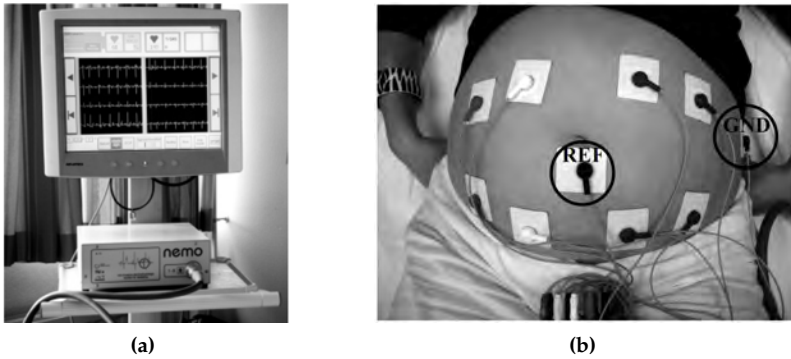
Figure 7.1: (a) Prototype of the NEMO system. (b) Electrode configuration for antepartum fetal ECG recording. ECG, electrocardiography; GN, ground electrode; REF, reference electrode.

The abdominal data were analyzed off-line. The eight input signals were recorded with a sample frequency of 1000 Hz. The signals were band-pass filtered between 1.5 and 70 Hz and a 50-Hz notch filter was used. The maternal ECG waveform was estimated and subtracted from the signals. This was done by means of weighted averaging of maternal ECG segments [120]. Fig. 7.2a shows an example of a filtered abdominal signal of a 24-week pregnant woman, containing both maternal and fetal ECG. Fig. 7.2b shows the signal after subtracting the maternal ECG. The eight resulting fetal ECG traces were processed to detect the beat-to-beat FHR. The signal-to-noise ratio of these signals is enhanced by spatially combining the signals [196]. The fetal ECG in the combined signal is further enhanced by using the length transformation [197]. R-peaks are detected in the transformed signal as peaks that exceed an adaptive threshold and the detected R-peaks are then used to create the fetal beat-to-beat heart rate signals [196].

Spectral information about fetal beat-to-beat heart rate was obtained using a Fourier Transform. Based on previous studies [106], as well as the physiological range of fetal heart and respiratory movement rate, the following frequency bands were chosen: total power (TP): 0.04– 1.5 Hz; LF: 0.04–0.15 Hz; HF: 0.4–1.5 Hz. Beat-to-beat RR-intervals were re-sampled at 4 Hz to obtain equidistantly distributed heart rates. To prevent aliasing, the Fourier Transform was calculated in intervals of 64 s (based on 0.04 Hz, the lowest frequency of interest) [87]. The direct current component was subtracted before calculating the Fourier Transform. To reduce spectral leakage, the signal was multiplied with a Parzen window function. After calculating the spectral power of fetal HRV, normalized values were calculated by dividing LF and HF by TP (denoted as LF_n and HF_n, respectively).
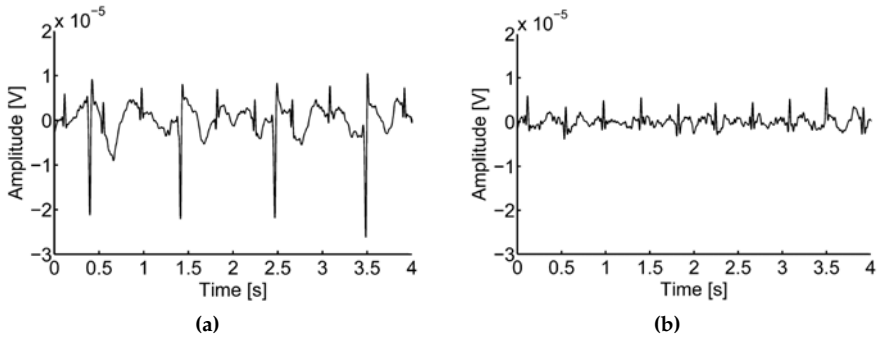
Figure 7.2: Filtered abdominal signal. (a) Signal that contains both the maternal and fetal ECG. (b) Fetal ECG after subtraction of the maternal ECG.

To prevent incorrect RR-intervals from dominating the spectrum, an RR-interval was automatically excluded if it exceeded the range of 0.2–1.3 s (46–300 beats per minute) or deviated more than 12% from preceding successive RR-intervals [32]. These incorrect RR-intervals were removed from the dataset and replaced by linear interpolation between the last preceding and the first succeeding correct RR-interval. From the beat-to-beat FHR data, 64-s segments were selected consecutively. To minimize the effect of artifact correction on the calculated spectral estimates, only segments with less than 5% artifact correction were included for analysis [168]. Visual inspection by an expert was performed to check for remaining artifacts, originating from mis-detection of fetal R-peak. When a segment still contained an artifact, it was excluded from further analysis.

For each selected 64-s segment of FHR data, the corresponding ultrasound segment was analyzed. All segments were divided into quiet sleep and active sleep. Assessment of fetal rest–activity states was based on the presence or absence of fetal body movements. When, after 34 wG, the fetal rest–activity state could not be determined by ultrasound, the behavioral state was determined based on visual inspection of the FHR pattern [87]. In healthy fetuses from this wG, the relationship between fetal movements and CTG pattern was so strong that the different states could be assessed reliably by visual identification of heart rate patterns alone [85].

7.2.2 Statistical methods

Statistical analysis were performed using SPSS software version 19 (IBM Corp., Armonk, NY, USA). For each woman, for all available 64-s segments of heart rate data per wG group, median values were calculated for the absolute and normalized spectral power in the LF and the HF band. It is known that fetal ECG measurements are extremely difficult to obtain around 30 wG due to the

presence of the vernix caseosa, which electrically shields the fetus from its surroundings [106]. Since changes in fetal HRV due to fetal rest–activity state only occur after 30 wG [85], data were analyzed separately for the periods below and above 30 wG. The median spectral estimates were plotted as a function of wG. Simple linear regression was used to study changes in spectral estimates over wG. For the group above 30 wG, analysis was repeated, restricted to fetal rest and activity to examine the effect of fetal rest–activity state on the relationship between spectral estimates and wG. In addition, for the group above 30 wG, the mean values of the median spectral estimates were compared during the active and quiet fetal state. An independent t-test was used to compare the active and quiet state. Statistical significance was assumed at an a-level of 0.05.

7.3   Results

A total of 40 women were studied longitudinally during pregnancy. Measurements were performed from January 2007 to August 2009. From the 40 participants under study, three women were excluded because pregnancy was complicated by pregnancy-induced hypertension. In addition, two women were excluded because of preterm labor. From the remaining data, 14% of all measurements contained one or more suitable data segments that could be used for spectral analysis. In total, 330, 64-s, segments of beat-to-beat heart rate data were retrieved, accounting for 3% of the data. Fig. 7.3 shows the percentage of usable segments for the different wG groups. The period until 21 wG was excluded for further analysis, since only five 64-s segments of heart rate data could be retrieved. Furthermore, no segment could be retrieved in the period between 30 and 34 wG. From the included 35 women, 10 were then excluded because good-quality fetal beat-to-beat heart rate could not be retrieved from the abdominal recordings. For the remaining 25 women included for analysis, a total of 213 abdominal measurements were performed, from which 325 segments could be used for analysis. The mean number of measurements per woman was nine (standard deviation, SD, 1.6). The mean duration of each measurement was 42 min (SD 9). All mothers delivered at term, and all neonates had a birth weight above the 10th percentile. All neonates had an Apgar score of at least 8 at 1 min and at least 9 at 5 min. All neonates had an umbilical artery pH>7.05 and an umbilical artery base deficit ⩽10. The characteristics of the women are given in Table 7.1.

Fig. 7.4 shows absolute LF and HF as a function of wG, for the period of 21-30 and 34-41 wG. Fig. 7.5 shows LF_n and HF_n as a function of wG, for the period of 21–30 and 34–41 wG. From the available segments below 30 wG, fetal rest–activity state could be determined based on ultrasound recordings for 85 segments (43%). Of these segments, 86% were retrieved during the active state and 14% during the quiet state. In the group of 34-41 wG, rest–activity state could be classified based on ultrasound recordings for 69 segments (54%). For

Table 7.1: Characteristics of the patients included for analysis.

	% or mean±STD
Maternal body mass index before pregnancy	23.6±4.0
Nulliparous	64%
Maternal age at birth (years)	32±4
gestational age at birth (days)	279±10
Birthweight (gram)	3561±543
Apgar score at 5 minutes	10±0.3
Umbilical artery pH at birth	7.22±0.08
Umbilical artery base deficit at birth	7.3±2.7
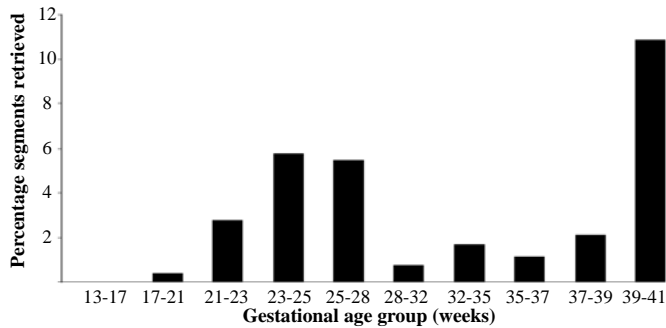
Figure 7.3: Percentage of 64-s segments of beat-to-beat FHR data, that could be retrieved for Fourier Transform for each wG group.

the remaining 58 segments (46%), the state was assessed based on FHR pattern. From the selected segments, 38% were retrieved during active sleep and 62% during quiet sleep. Table 7.2 displays the percentage of the selected segments in active sleep and quiet sleep for the different groups after 34 wG. Table 7.3 shows the mean values of median LF, HF, LF_n, and HF_n, for the active and quiet state, for 34–41 wG. To guarantee no bias was introduced by assessment of fetal rest–activity state by FHR pattern, the analysis was repeated for segments for which rest–activity state was solely assessed based on ultrasound. The results (data not shown) were highly comparable and remained significant. To study the effect of fetal behavior on spectral estimates, the association between spectral estimates and wG was studied for rest and activity separately, for the period above 34 wG. Fig. 7.6 shows the LF and HF as a function of wG for the active and quiet state.
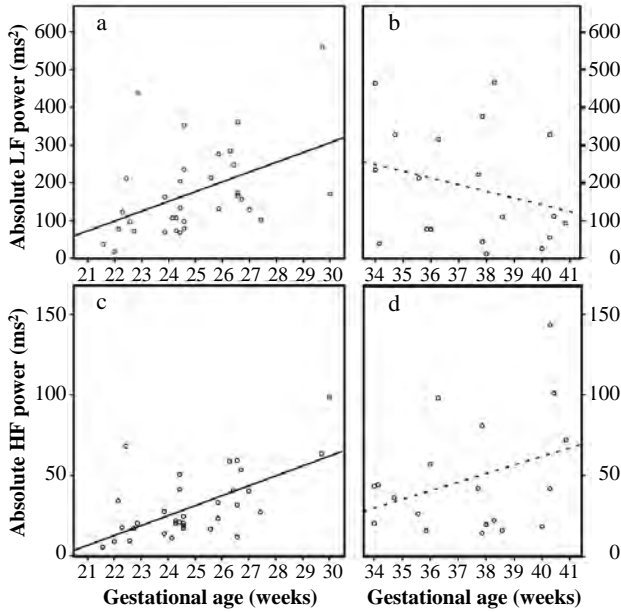
Figure 7.4: The association between LF and HF and wG, for the period of 21-30 and 34-41 wG. (a) R^2: 0.20 (P = 0.009), (b) R^2: 0.08 (P = 0.26), (c) R^2: 0.37 (P = 0.0004), and (d) R^2: 0.12 (P = 0.15).
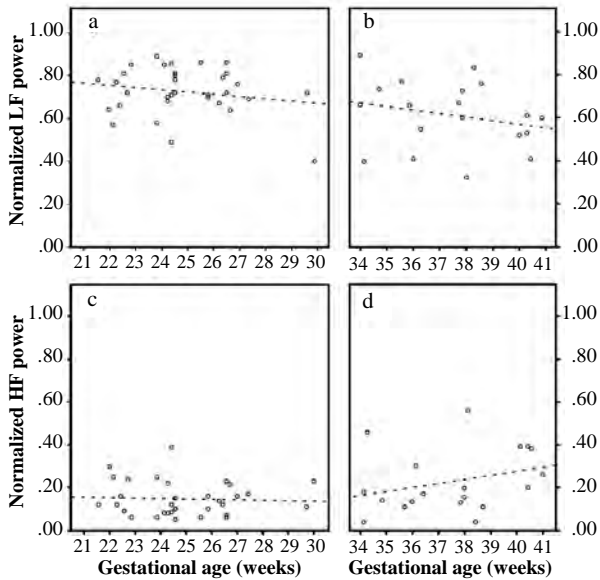
Figure 7.5: The association between LF_n and HF_n and wG, for the period of 21-30 and 34-41 wG. (a) R^2: 0.04 (P = 0.28), (b) R^2: 0.06 (P = 0.31), (c) R^2: 0.003 (P = 0.76), and (d) R^2: 0.09 (P = 0.21).

Table 7.2: Percentage of segments with the fetus in the active state and in rest, for the groups after 30 wG.

wG (weeks)	Active sleep (%)	Quiet sleep (%)
34-36	70	30
36-38	43	57
38-40	32	68
40-41	28	72

Table 7.3: Mean values of the median LF, HF, LF_n and HF_n for the active and quiet sleep state for the period of 34 to 41 wG.

	Active sleep	Quiet sleep	P-value
LF (ms²)	555	151	0.002
HF (ms²)	62	38	0.090
LF_n	0.77	0.59	0.005
HF_n	0.10	0.26	0.002
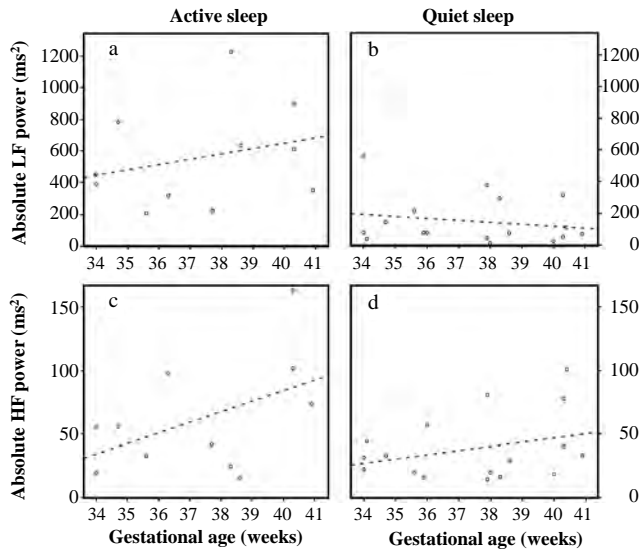
Figure 7.6: The association between LF and HF and wG, for the active and quiet sleep state, for the period of 34-41 wG. (a) R^2: 0.08 (P = 0.41), (b) R^2: 0.04 (P = 0.44), (c) R^2: 0.23 (P = 0.14), and (d) R^2: 0.10 (P = 0.22).

7.4 Discussion

Our group developed a new method for non-invasive fetal ECG measurements [120, 196]. This new method can be used during periods in pregnancy, in which other (invasive) techniques cannot be used for monitoring. Although Doppler ultrasound can also be used to obtain FHR non-invasively, ultrasound typically provides a FHR that is averaged over a few cardiac cycles. This averaging affects the spectral information in the high frequency domain, virtually yielding only reliable information for the low frequency domain [33]. In addition, ultrasound is sensitive to maternal and fetal movements and is therefore less suitable for prolonged measurements.

Our results in this study group showed that it is possible, although difficult, to retrieve fetal beat-to-beat heart rate from non-invasive abdominal fetal ECG measurements. Spectral analysis was feasible in 14% of all measurements; however, only 3% of the abdominal data was applicable for analysis. Due to the relatively large number of measurements without good-quality heart rate segments, we were unable to statistically analyze the development of the spectral estimates on a case-based level. Thus, it is evident that further improvements in signal processing need to be made. The signal quality was independent of body mass index (BMI), since no significant difference (p = 0.9) was found between BMI of women included in our analysis (Table 7.1; 23.6, SD 4.0) and BMI of women excluded due to poor signal quality (23.3, SD 5.2). We were not able to retrieve fetal beat-to-beat heart rate from the abdominal measurements before 18 and between 30 and 34 wG. Before 18 wG, this was probably due to the small size of the fetal heart. This results in a very low amplitude of the fetal ECG, rendering it undetectable on the maternal abdomen. Between 30 and 34 wG, the presence of the vernix caseosa, which electrically isolates the fetal heart [106], probably caused significant attenuation of the ECG signal. During the early preterm period (21–28 wG), approximately 5% of data was suitable for spectral analysis. At term, approximately 7% of data was suitable for spectral analysis. Probably, the disappearance of the vernix caseosa and the relatively large fetal heart, made it easier during the term period to detect the fetal signal from the combined fetal–maternal signals measured on the maternal abdomen.

For the early preterm period, we observed a significant increase in LF and HF of fetal HRV with progressing pregnancy. We hypothesize that this increase was due to increased sympathetic and parasympathetic modulation of the fetal heart, resulting from maturation of the fetal autonomic nervous system. This is in accordance with animal studies that showed an increase in sympathetic and parasympathetic cardiac modulation in premature fetuses, compared to immature fetuses [83].

It is unlikely that the observed changes in spectral estimates before 30 wG were due to changes in fetal breathing movements or rest–activity state. Although fetal breathing movements occurred as early as 10 wG [198], the HF peak that was observed during breathing at term [199] could not be observed

at 26 wG [200]. In addition, the incidence of fetal breathing movements did not change between 24 and 28 wG [201]. The incidence of fetal movements decreased as pregnancy progresses [202]. From 24 to 28 wG, a healthy fetus on average made 150–200 movements each hour [202]. Therefore, it was expected that most selected 64-s segments of heart rate data below 30 wG were measured during fetal activity, as was confirmed by our analysis of the corresponding ultrasound measurements. In addition, LF was high in term fetuses during the active state compared with quiescence [184]. Although short rest–activity cycles were first noticed at 23 wG, fetal HRV was similar during fetal activity and rest up to 30 wG [85] and behavioral states could not be observed [203].

The observed increase in absolute LF and HF was not reflected in the normalized values during the early preterm period. This might be due to a comparable relative increase in both LF and HF.

For the (near) term fetuses, a non-significant decrease in LF and a non-significant increase in HF were observed. A decrease in LF after 30 wG was also described by David et al. [79]. Fetal activity is known to increase fetal HRV from approximately 30 wG onwards [85], and a decrease in fetal movements with wG was reported [202]. Therefore, a LF decrease after 30 wG is expected to occur due to a decrease in fetal movements. Later in pregnancy, starting in the 34th week of gestation, fetal behavioral states appear [86]. As these states are partly defined on the basis of HRV, it seems relevant to consider them in the interpretation of HRV measures.

Furthermore, LF and LF_n were found to be significantly higher and HF_n significantly lower during fetal activity compared with at rest. A non-significant increase in HF was observed during the active state. These results were similar to those obtained with invasive measurements during labor at term [184].

If analysis was repeated with restriction to periods of fetal rest and activity (as shown in Fig. 7.6), LF increased non-significantly as a function of wG during activity, whereas LF decreased non-significantly during rest. Since for the selected segments the time spent in rest increased with wG during the (near) term period (as shown in Table 7.2), a decrease in fetal activity might explain the overall decrease in LF as pregnancy progresses.

In post term fetuses, an increase in both HF and HF_n was found in our previous studies with invasive measurements, in relation to the near term group [184]. We observed a similar trend towards increased HF and HF_n near term in the present study. Because this trend was independent of fetal rest–activity state, it cannot be explained by changes in fetal behavior. This trend might suggest continuing parasympathetic maturation during the term period and increasing influence of the vagal system. This is in line with Assali et al. [83] who found a marked rise in parasympathetic tone during the neonatal period, up until the adult state.

7.5 Conclusions

Our non-invasive fetal ECG method enables us to measure fetal HRV in frequency-domain during the early preterm and term period. Our results are in accordance with those seen in animal studies and with the previous literature regarding invasive measurements during labor. This is the first study that measures spectral estimates longitudinally and relates spectral estimates to fetal behavioral state. Further progress in signal processing will enable improved study of the relationship between spectral estimates and wG, allowing for longitudinal analysis.

8

THE INFLUENCE OF BETAMETHASONE ON FETAL HEART RATE VARIABILITY

Abstract - Background*: Betamethasone is widely used to enhance fetal lung matura-tion in case of threatened preterm labor. Fetal heart rate variability is one of the most important parameters to assess in fetal monitoring, since it is a reliable indicator for fetal distress. Aim: To describe the effect of betamethasone on fetal heart rate variability, by applying spectral analysis on non-invasive fetal electrocardiogram recordings.* Study design*: Prospective cohort study.* Subjects*: Patients that require betamethasone, with a gestational age from 24 weeks onwards.*Outcome measures*: Fetal heart rate variabil-ity parameters on day 1, 2, and 3 after betamethasone administration are compared to a reference measurement.* Results*: Following 68 inclusions, 12 patients remained with complete series of measurements and sufficient data quality. During day 1, an increase in absolute fetal heart rate variability values was seen. During day 2, a decrease in these values was seen. All trends indicate a return to pre-medication values on day 3. Normalised high- and low-frequency power show little changes during the study pe-riod.* Conclusions*: The changes in fetal heart rate variability following betamethasone administration show the same pattern when calculated by spectral analysis of the fetal electrocardiogram, as when calculated by cardiotocography. Since normalised spectral values show little changes, the influence of autonomic modulation is minor.*[1,2]

---

1 Results in this chapter were obtained with signal processing methods that date back to 2012. With the methods presented in chapters 3 and 4, the percentage of recordings with usable fetal heart increases from 60% to 86%.

2 This chapter has been accepted for publication as *Verdurmen K.M., Warmerdam G.J.J., Lempersz C., Hulsenboom O., Renckens J., Dieleman J., Vullings R., Van Laar J.O.E.H., Oei S.G., "The influence of betamethasone on fetal heart rate variability, obtained by noninvasive fetal electrocardiogram recordings".*

8.1 Introduction

Cardiotocography (CTG) is used for fetal monitoring worldwide. One of the most important parameters to assess in CTG monitoring is fetal heart rate variability (HRV). Normal fetal HRV is a reliable indicator of fetal wellbeing, while decreased fetal HRV is associated with poor neonatal outcome (acidosis, low Apgar score and death) [204]. The fetal heart rate (FHR), and thus HRV, is regulated by a complex interplay of the sympathetic and parasympathetic branches of the autonomic nervous system [66]. Spectral analysis of fetal HRV can be used to quantify these changes in autonomic regulation [31, 32, 184, 193, 205]. Low frequency power (LF) reflects baroreceptor reflex activity, and is both sympathetically and parasympathetically mediated [30]. High frequency power (HF) is associated with fetal respiration, and is solely parasympathetically mediated [30].

Antenatal betamethasone administration plays an important role in the clinical management of threatened preterm delivery between 24 and 34 weeks of gestation (wG). It enhances fetal lung maturation and results in a significant reduction in, amongst others, neonatal mortality and respiratory distress syndrome [206]. However, betamethasone can easily cross the placenta [207] and influence fetal autonomic modulation and thus fetal HRV. Since fetal HRV is an important marker for fetal distress, knowledge on the influence of betamethasone on autonomic regulation is needed to avoid misinterpretation of changes in fetal HRV following betamethasone administration, and therefore prevent unnecessary iatrogenic preterm delivery.

Results of previous studies describing the effect of betamethasone on fetal HRV indicate that fetal HRV increases during the first day, followed by a decrease during days 2-3 [191]. Values returned to baseline during day 4. However, these studies were performed using CTG and measured the FHR by Doppler-ultrasound. With CTG, the FHR is averaged over several heartbeats and therefore beat-to-beat information is lacking. As a consequence, it is not possible to perform reliable spectral analysis.

The aim of this study is to quantify the effects of maternally administered betamethasone on spectral values of fetal HRV. To perform a reliable calculation of LF and HF we extracted beat-to-beat FHR information from non-invasive abdominal fetal ECG recordings [208].

8.2 Materials and Methods

We performed a prospective, longitudinal cohort study at the Máxima Medical Center, Veldhoven, the Netherlands. This is a tertiary care teaching hospital for obstetrics. The study protocol was approved by the Medical Ethical Committee of the Máxima Medical Center. Participants were included after written informed consent.

8.2.1 Study population

As described in our study protocol, we aimed for at least 50 inclusions and expected to end with 10-20 complete sets of measurements due to the anticipated loss to follow-up in this study group. We were not able to perform a power calculation, since this is the first study describing a five-day follow-up period following betamethasone administration with non-invasive abdominal fetal ECG recordings. From March 2013 until July 2016, women with a singleton pregnancy, at risk for preterm delivery and admitted to the Obstetric High Care unit were asked to participate in this study. All women requiring betamethasone (Celestone Chrondose®, Schering AG, Berlin, Germany; 2 doses of 12mg intramuscularly, 24 hours apart) as part of standard clinical management were eligible to participate. In case of threatened preterm labor, co-administration of tocolytic drugs was allowed. Nifedipine was used to attenuate uterine contractions, occasionally complemented by indomethacin in case of continuous uterine contractions when betamethasone administration was not yet completed. In case of preterm prelabor rupture of membranes, patients also received antibiotics (erythromycin 250mg 4 times daily during 10 days) as part of the standard treatment protocol. Women were excluded in case of maternal age <18 years, multiple pregnancy, fetuses with a known congenital malformation, signs of intra-uterine infection or fetal growth restriction (defined as the estimated weight of the fetus below the 5th percentile for gestational age).

The following data were gathered prospectively: maternal gravidity and parity, indication for betamethasone administration, obstetrical and general medical history, gestational age at inclusion and administered medication during the study period. Follow-up measurements of study participants lasted from the date of informed consent until five days after the first measurement, discharge or delivery, whichever occurred first. Postpartum, neonatal charts were checked for any indications of congenital anomalies that might have influenced the measurements and for missed cases of growth restriction defined as birth weight below the 5th percentile (corrected for gestational age, parity and sex of the neonate).

8.2.2 Measurements

We performed series of measurements as visualised in Fig. 8.1. Recordings were obtained while the patient was lying in a semi-recumbent position, to prevent supine hypotension syndrome. To reduce the influence of diurnal variations, the timing of measurements within a series was fixed for each patient (between 20 and 28 hours after the previous measurement). In order to respect the patient's night rest, no measurements were performed between 24.00h and 7.00h.

Most patients were transferred from secondary care hospitals in the region. Since for these patients betamethasone treatment was initiated prior to transport, they had no baseline measurement (0-measurement, on day 0). Former research showed that all changes in FHR and fetal HRV returned to baseline values from
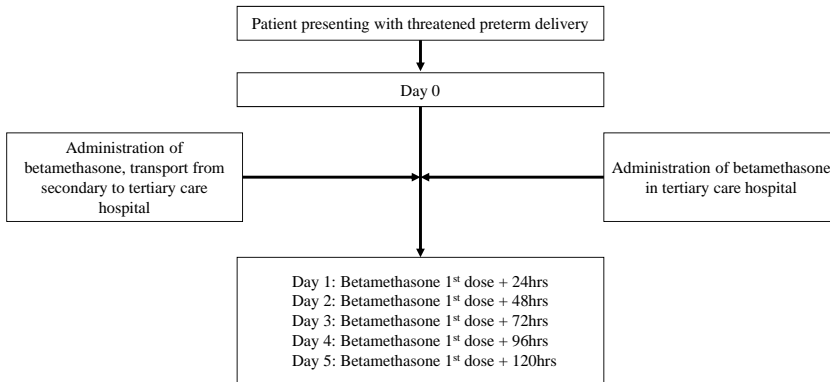
Figure 8.1: Flowchart of patient inclusion and timing of measurements.

day 4 onwards (96 hours after the first dose of betamethasone) [191]. Therefore, we included transferred patients if we were able to conduct a measurement during day 4 or 5 following the first dose of betamethasone. We used the median value of the measurements during day 0, and/or day 4, and/or day 5 as the "reference measurement". By means of a full range plot, we verified whether our reference measurement was comparable with the real 0-measurement in a separate subset of patients. Included cases with good quality measurements on day 0, and day 4, and/or day 5 were selected.

Complete series were defined as series including a reference measurement and measurements during at least days 1, 2, and 3. In case one or more of these measurements was missing, the patient was excluded. The duration of a measurement was approximately 30 minutes. The total measurement was divided in segments of 60 seconds, and per segment HRV parameters were calculated. The median value of all available segments was used for statistical analysis.

8.2.3 Data acquisition and signal processing

The fetal ECG was recorded on six channels, using a fixed configuration on the maternal abdomen as illustrated in Fig. 8.2. The abdominal signals were recorded by two non-invasive electrophysiological monitoring devices; the Nemo fetal monitor (Nemo Healthcare BV, Eindhoven, the Netherlands) and the Porti system (TMSi, Enschede, the Netherlands), operating at sampling rates of 500 Hz and 512 Hz, respectively. Both devices were approved by the Medical Technical Service Department of the Máxima Medical Center.

The recordings were analyzed offline. Recordings were first pre-processed to suppress the maternal ECG using a dynamic template subtraction technique [120]. The signals remaining after maternal ECG suppression were spatially combined to enhance the signal-to-noise ratio of the fetal ECG with respect to remaining electrophysiological interferences (e.g. muscle activity) [196, 209]. Finally, a
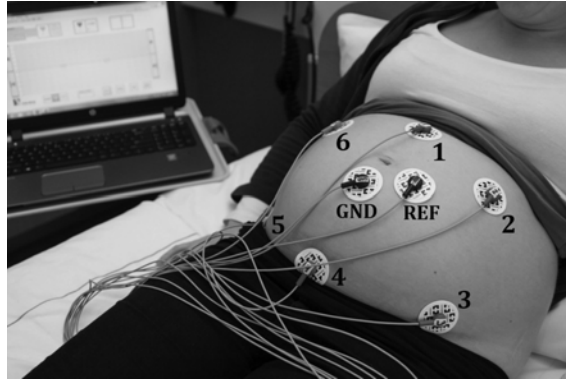
Figure 8.2: The six channel fetal electrocardiogram is recorded with electrodes on the maternal abdomen, placed in a fixed configuration. The ground (GND) and reference (REF) electrode are placed near the belly button. The electrodes are connected to a battery operated data acquisition system (Nemo Healthcare BV), which filters, amplifies, and digitises the data for further processing. This system is connected to a computer.

wavelet-based R-peak detection was performed to obtain a beat-to-beat FHR [150]. In case no R-peaks were detected using all six channels, channels with good quality fetal ECG were selected manually to avoid negative effects on the spatial combination of those channels that were dominated by interferences.

Prior to HRV analysis, the obtained heart rates were automatically analyzed for incorrect RR-intervals. RR-intervals shorter than 0.3 seconds or longer than 1.2 seconds (<50 or >200 bpm) were assumed to be incorrect [150]. Furthermore, if an RR-interval deviated more than 12% from a running average RR-interval, it was also assumed to be incorrect [168]. The incorrect RR-intervals were replaced by linear interpolation. To ensure reliable spectral analysis, only heart rate segments of 60 seconds were included with less than 20% interpolation and less than five seconds of consecutive interpolation [168]. We only included measurements with at least three segments that met the quality criteria.

8.2.4 Heart rate variability analysis

Fetal HRV was quantified using both time-domain features (short-term variability, STV, and long-term variability, LTV) and features from spectral analysis (LF and HF). The obtained heart rates were resampled at 4 Hz by linear interpolation, since spectral analysis requires equidistantly distributed signals.

Spectral analysis was performed using a continuous wavelet transform [166]. Based on previous studies, the following frequency bands were selected: 0.04-1.5 Hz for the total power (TP), 0.04-0.15 Hz for LF, and 0.4-1.5 Hz for HF [30, 32, 184, 210, 211]. LF and HF were expressed in absolute units (ms^2) and normalised units (LF_n = LF/TP, HF_n = HF/TP).

In addition to spectral powers, STV and LTV were calculated to compare our results to prior research performed with CTG measurements. LTV was calculated as the difference between the maximum and minimum RR-interval in every 60 seconds segment [34, 212]. STV was calculated as the mean of absolute differences between consecutive RR-intervals in every 60 seconds segment [34]. Note that in CTG (ultrasound) monitoring, STV is defined based on epochs (e.g. 1/16th of a minute) because FHR is not acquired beat-to-beat. However, since the gold standard for STV is beat-to-beat variation [212], we used the aforementioned ECG-based STV calculation.

8.2.5 Statistical analysis

Descriptive statistics were used to describe the study population and outcome measures. No further statistical analysis was performed. For each fetus a different number of segments were available during the study period, mainly due to variations in ECG signal quality. The result on each day was compared to the reference measurement.

8.3 Results

The inclusion process is depicted in Fig. 8.3. Initially, 68 women were included in this study. Three patients requested withdrawal from the study because of poor prognosis for an extreme premature child (1), technical issues (1) and inconvenient timing of measurements for the patient (1). In one patient unexpected intra-uterine fetal death occurred during the study period. Extensive evaluation revealed no evident cause. In 28 patients we were able to obtain a complete set of measurements, of which 16 were excluded due to insufficient data quality (less than three good quality segments per measurement) in one or more of the measurements. Eventually, 12 patients were included with a complete set of sufficient data quality. Table 8.2 shows the patient characteristics of the included cases. The amount of available segments for analysis is displayed in Table 8.1.

Measurements during day 0, and/or day 4, and/or day 5 were compared in five patients. In Fig. 8.4, LF, HF, LF_n, and HF_n are displayed. As expected, the absolute fetal HRV values showed some inter- and intra-patient variation, which can mainly be explained by variation in the segments that were recorded during active and quiet states and by variation in gestational age of the fetuses. LF_n and HF_n show better comparability during day 0, 4, and 5, since these normalised values are not masked by changes in total power. For instance, these values are not influenced by fetal activity states.

Our outcome of interest was fetal HRV. Descriptively, in Fig. 8.5 we see an increase in LTV and STV on day 1, and a decrease on day 2 and 3 as compared to the reference measurement. For LF and HF, we see the same trend. For LF_n and HF_n we see little changes during the study period.
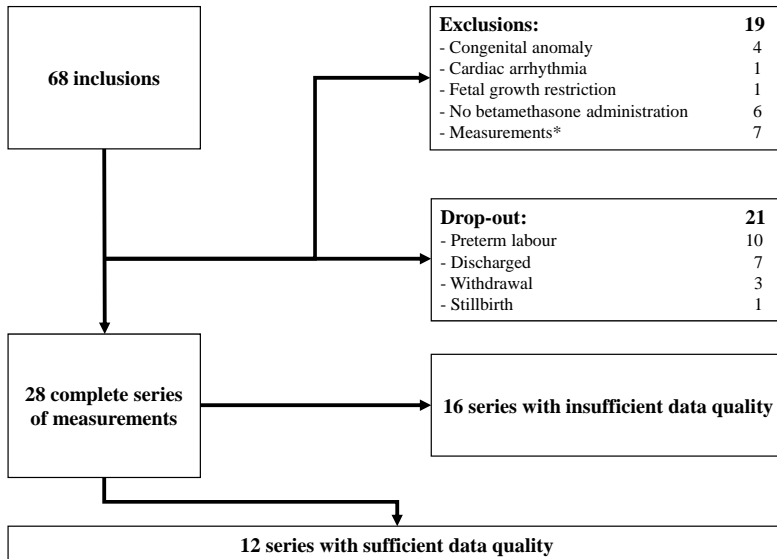
*Patients were excluded if the measurements were not performed within the time window (between 20 and 28 hours after the previous measurement), had one or more missing measurement in the series, or were insufficient in data quality.

Figure 8.3: Overview of the inclusion process.

Table 8.1: Amount of segments available for analysis.

	Segments for analysis/ total segments	Percentage of segments for analysis
Reference measurement		
Day 0[a]	103/110	94%
Day 4	201/305	66%
Day 5[b]	162/278	58%
Day 1	332/580	57%
Day 2	214/403	53%
Day 3	223/407	55%

[a] Day 0: measurements performed in 3 out of 12 patients.
[b] Day 5: measurements performed in 9 out of 12 patients.
On the other study days, measurements were performed in all 12 patients.

Table 8.2: Patient characteristics and pregnancy outcome.

case	Maternal gravidity, parity	Indication	Relevant history	wG at inclusion	Medication (not betamethasone)	wG at delivery	Birth weight percentile[a]	Apgar score 1´/5´	NICU admission
1	G1P0	TPL	-	24+4	Nifedipine,indomethacin, LMWH	25+4	50	7/8	Yes
2	G1P0	PE	May-Turner, thrombosis,	33+4	LMWH,methyldopa	34+3	5-10	9/10	No
3	G2P1	VBL	Gestational diabetes	31+1	Progesterone (vaginal), nifedipine, augmentin	33+5	50-80	9/10	No
4	G2P1	PPROM	-	33+0	Nifedipine, erythromycin	34+1	50-80	8/9	No
5	G2P1	TPL	-	26+2	Nifedipine,	39+5	50-80	5/9	No
6	G1P0	TPL	LEEP	29+2	Nifedipine,	40+1	80	9/10	No
7	G1P0	VBL	-	25+2	-	38+1	20-50	9/10	No
8	G2P1	TPL	Pre-existent hypertension	26+1	Nifedipine,labetalol, magnesium sulphate, indomethacin	36+6	50-80	8/10	No
9	G2P1	TPL	-	25+6	Nifedipine, progesterone (vaginal)	40+4	50	9/10	No
10	G2P1	VBL	-	33+0	Iron tablets	37+5	90-95	9/10	No
11	G1P0	TPL	-	30+6	Nifedipine	32+6	>97	9/10	No
12	G1P0	VBL	LEEP	26+6	-	33+5	50-80	?/10	No

[a] Birth weight percentile: percentiles are corrected for parity, gestational age at delivery and sex, and apply to the Dutch population. Source: Perined.

Abbreviations: LEEP = loop electrosurgical excision procedure of the cervix, LMWH = low molecular weight heparin, NICU = neonatal intensive care unit, PE = pre-eclampsia, PPROM = premature prelabor rupture of membranes, TPL = threatened preterm labor, VBL = vaginal blood loss.
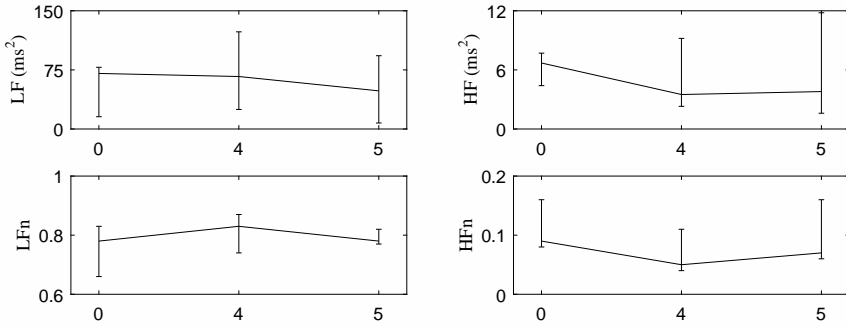
Figure 8.4: Verification of the reference measurement. Median value and full range plot of LF, HF, LF_n, and HF_n on days 0, and/or day 4, and/or day 5 for five patients.
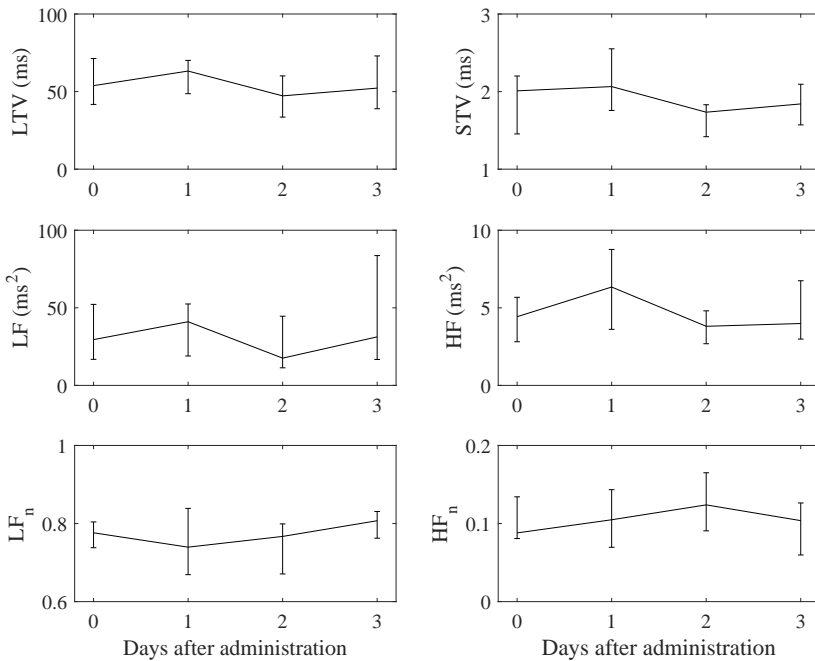
Figure 8.5: Changes in fetal HRV parameters during the study period. The x-axis shows the number of days after the first administration of betamethasone. Day 0 is the median value of the measurements during day 0, and/or day 4, and/or day 5. The outcomes are depicted as median values with interquartile ranges.

8.4 Discussion

Up to our knowledge, this is the first study on the influence of betamethasone on spectral estimates of fetal HRV measured by non-invasive fetal ECG recordings with electrodes on the maternal abdomen. As we anticipated, over 80% of our inclusions could not be used in the final analysis; we aimed for at least 50 inclusions and expected to end with 10-20 complete sets of measurements. This was mainly due to loss to follow-up and insufficient data quality. Insufficient data quality is a general problem encountered when studying HRV with spectral analysis [185, 190]. We applied a high standard for good signal quality; only measurements containing at least three segments with good signal quality per measurement were selected. Since we preferred data quality over data quantity, only a limited number of series (12) were available eventually. Therefore, we decided to describe our study results and not perform any statistical analysis. Hence, our study results should be interpreted with appropriate caution.

8.4.1 Heart rate variability outcomes

We found a similar trend in LTV and STV with fetal ECG analysis as compared to previous studies that used CTG analysis [191]. A more accurate way to evaluate autonomic modulation is spectral analysis of the beat-to-beat FHR. LF and HF are absolute spectral estimates, that relate to LTV and STV. As expected, the same trends are seen during the study period for these parameters.

Due to normalisation, relative changes in LF and HF are not masked by changes in total power. Both LF_n and HF_n show little changes during the study period. This indicates that the influence of autonomic modulation is minor.

8.4.2 Considerations

We defined the reference measurement as the median value of the measurements during day 0, and/or day 4, and/or day 5. Although relatively good comparability was seen for fetal HRV values, this remains second best with regard to a true baseline measurement.

The high number of measurements that had to be excluded due to poor signal quality, can mainly be explained by presence of vernix caseosa. This fatty layer surrounds the fetus and results in an electrical isolation, which diminishes the signal amplitude of the fetal ECG. Especially between 30 and 34 wG, this layer causes a poor signal-to-noise ratio [109, 190]. We do not expect any other major influencing factors on signal quality. Analysis of the data was mainly performed computerised. It is possible that failed registration results in selection bias, although the influence is expected to be minor.

As shown in Table 8.1, the mean amount of available segments per day was always more than 50%. One has to bear in mind that this is in selected series with sufficient quality of the performed measurements. There are no obvious

differences between the measurement days; the amount of available segments is steady between 52% and 57%. Only the measurements performed on day 0 show a higher percentage of available segments. However, only 3 out of 12 patients were eligible for a measurement during day 0.

By including patients receiving other pregnancy-related drugs rather than betamethasone, we aimed to obtain information that is applicable in daily clinical practice. Nifedipine and indomethacin seem to have no clinically important effect on fetal HRV, while magnesium sulphate can cause decreased fetal HRV and cases of bradycardia have been described [104]. In one case, magnesium sulphate was administered during days 1, 2 and 3 of the study period. Since magnesium sulphate was not administered during the reference measurement, this might have had some influence on the study results. In one case labetalol was administered to the patient; this was already started prior to the measurements and no changes in dosage occurred during the study period. Therefore, it is not likely that this had major influence on the study results. It is unlikely for amoxicillin-clavulanic acid, low-molecular weight heparin, methyldopa and progesterone to have any influence on fetal HRV parameters due to their mechanism of action.

Apart from pathological conditions, two major factors that one should consider when assessing FHR patterns are gestational age and fetal behavioural states [97]. Previous studies show that gestational age significantly affects the fetal HRV power spectrum, with a gradual increase in LF and HF during gestation [77, 79, 190]. In this study, the included fetuses had a gestational age varying from 24 to 33 wG. Since we studied fetuses on successive days and were interested in relative changes in fetal HRV parameters, the influence of the increase in LF and HF during gestation is likely to be minor. This study demonstrated an increase in time spent in the quiet state following betamethasone administration. This might be caused by disturbance of the maternal glucose metabolism [213], which is a known side effect of corticosteroids.

Fetal HRV and fetal movements are two parameters associated with fetal well-being. The reduction in both, due to betamethasone administration, can be misinterpreted as fetal deterioration and can therefore possibly lead to unnecessary iatrogenic preterm delivery [214, 215]. Most likely, the reduction in fetal movements is a direct effect of corticosteroid administration, possibly by occupying the glucocorticosteroid receptor in the central nervous system, suppressing neuronal activity and therefore reducing physical activity in the fetus [191]. No other signs of fetal hypoxia, like decelerations or abnormalities in Doppler flow velocity waveforms, have occurred after corticosteroid administration [214–218]. In addition, Shenhav et al. [219] demonstrated that reduced fetal HRV was not related to the fetal acid-base balance at birth when delivery occurred <48 hours following betamethasone administration. This study confirms these results, since the influence of autonomic modulation was found to be minor (reflected as no evident changes in normalised spectral powers during the study period). However, in fetal monitoring it is important to be aware of the side-effects, such as reduced fetal HRV and fetal movements.

8.5 Conclusion

The changes in fetal HRV following betamethasone administration show the same pattern when calculated by spectral analysis of the fetal ECG, as when calculated by Doppler-ultrasound CTG. Since normalised spectral values show little changes, the influence of autonomic modulation is minor.

9

DISCUSSION AND FUTURE DIRECTIONS

9.1 Discussion

Monitoring of the fetal condition and early recognition of fetal distress are of vital importance to ensure timely intervention. One of the most important features to assess in fetal monitoring is fetal heart rate variability (HRV) [7]. Since the autonomic nervous system (ANS) controls the fetal heart rate (FHR), changes in fetal HRV are indicative of ANS regulation and can indirectly provide information about fetal distress [29, 30]. Recent studies have shown interest in computerized analysis of fetal HRV for detection of fetal distress [31–39]. However, most clinicians currently use Doppler ultrasound (US) to monitor the FHR. Since FHR from Doppler US can only provide an averaged FHR, its use for computerized analysis of fetal HRV is limited. Instead of the averaged FHR from Doppler US, a beat-to-beat FHR can be obtained from the fetal electrocardiogram (ECG). Besides accurate FHR information, the fetal ECG also provides additional morphology information that could be used to assess the fetal condition [13, 15, 19, 47]. Unfortunately, in clinical practice the fetal ECG is currently only available via invasive measurement using a scalp electrode. Hence, the fetal ECG can only be obtained during labor after sufficient cervical dilation and after the fetal membranes have ruptured.

The fetal ECG can also be recorded non-invasively with electrodes on the maternal abdomen. However, the non-invasiveness comes at the expense of typically low signal to noise ratios (SNR) of the fetal ECG. In the first part of this thesis we focused on improving signal quality and reliability of FHR detection. In addition to these technical challenges, it is also necessary to study the physiological context in which the acquired FHR can be used for computerized HRV analysis. In the second part of this thesis we focused on the application of computerized analysis of fetal HRV for detection of fetal distress.

Before FHR detection can be performed, it is required to suppress the power line interference (PLI) from the abdominal recordings. Although PLI suppression is a mature domain, filtering PLI from ECG recordings remains a challenging task due to the overlap of the PLI frequency and the frequency content of the ECG [112]. Filtering PLI with classical fixed-bandwidth notch filters results in a ringing effect in the ECG [131]. Especially for the fetal ECG, ringing leads to significant distortions of the ECG waveform, because the frequency content of the fetal ECG is relatively high and it strongly overlaps with the PLI frequency.

Ringing distortion in the fetal ECG waveform may result in inaccuracies if the waveform information is used for further analysis, e.g. for morphology analysis or for the FHR detection that was described in Chapter 4. In **Chapter 3** a Kalman smoother with adaptive noise estimation was presented to suppress the PLI. All non-PLI signals (a.o. the ECG) in the Kalman smoother are represented by the observation noise term. During an ECG complex, the parameter adaptation of the Kalman smoother is reduced because the observation noise increases as the ECG amplitude increases. The combination of an adaptive smoothing filter and adaptive noise estimation resulted in minimal distortion of the ECG waveform. The proposed method outperformed other methods in the literature in terms of PLI suppression and step response settling time.

The abdominal signals that remain after PLI suppression contain the fetal ECG and interferences such as the maternal ECG, abdominal muscle activity, and activity from the uterine muscle [45]. The low amplitude of the fetal ECG with respect to these interferences makes FHR detection difficult. Moreover, the fetal position and orientation can change with respect to the abdominal electrodes during a recording. As a consequence, the fetal ECG waveform that is measured at the abdomen can vary, which further complicates FHR detection [48–50]. In **Chapter 4** a method was presented for FHR detection that uses predictive models of the fetal ECG waveform and the FHR. In this method the information of the FHR model is used to update an ECG waveform model. The information of the waveform model is subsequently used to detect the FHR and update the FHR model. To overcome a possible lack of convergence due to circular reasoning, the ECG waveform and FHR models are combined within an hierarchical Bayesian framework. As the fetal ECG is typically recorded by an array of electrodes that covers the maternal abdomen, the model is extended to a multi-channel approach. The developed method outperforms state-of-the-art methods that have been proposed in the literature in terms of detection accuracy. Our method works well even under low and varying SNR conditions.

In the second part of this thesis we focused on some of the challenges in using fetal HRV analysis for detection of fetal distress. Although several studies have shown that computerized analysis of fetal HRV provides information on fetal distress, these studies do not account for the strong influence of uterine contractions on the cardiovascular control and hence on fetal HRV, which limits the performance in these studies. In **Chapter 5** we hypothesised that separating contractions from rest periods improves the HRV analysis for detection of fetal distress during labor. To test our hypothesis, we used a case-control study in which we compared HRV features of 14 healthy fetuses to that of 14 fetuses with asphyxia. Several conventional HRV features were calculated that describe different properties of cardiovascular control. We did not find a significant difference for HRV features that were calculated without separating contractions and rest periods. In contrast, separating contractions from rest periods did result in significant differences for HRV features between cases and controls.

In **Chapter 6** we examined whether detection of fetal distress can be improved by combining HRV features that were calculated without distinguishing contractions and rest periods with contraction-dependent HRV features. In this study we also examined whether using contraction-dependent HRV features could lead to earlier detection of fetal distress. A dataset was used of 100 recordings, containing 20 cases of fetuses with asphyxia. We used a Genetic Algorithm to determine the most informative subset from an extensive set of HRV features. The classification performance of these feature subsets for detection of fetal distress was evaluated with Support Vector Machines (SVMs). We showed that combining HRV features calculated without distinguishing contractions with contraction-dependent HRV features improves the detection rate of fetal distress.

From the studies in Chapters 5 and 6, it appeared that in particular the ratio between HRV features calculated during contractions and during rest periods improved the HRV analysis. For healthy fetuses, the HRV features during contractions are relatively high, indicating a healthy response of the cardiovascular system to changes in external pressure. During rest periods a healthy fetus quickly recovers and the HRV features are relatively low. In contrast to healthy fetuses, distressed fetuses are unable to adequately respond to changes in pressure caused by contractions and the HRV features are relatively low during contractions. Besides, the oxygen concentration in the fetal blood is low after a contraction has ended and cardiovascular control is also required during rest periods, leading to relatively high HRV features during rest periods. As a consequence, we observed that the ratio of HRV features calculated during contractions and rest periods is higher for healthy fetuses compared to fetuses in distress.

In the studies in Chapters 5 and 6 we focused on term fetuses and we did not consider the influence of medication on fetal HRV. Effects of maturation and medication on fetal HRV should, however, be accounted for before computerized fetal HRV analysis can be used in clinical practice. Non-invasive fetal ECG recordings are required to study the effects of maturation and medication on beat-to-beat fetal HRV, because for measurements in these studies the fetal membranes are still intact and invasive recording of FHR is impossible. In **Chapter 7** we examined the influence of maturation on fetal HRV using a longitudinal study with measurements performed every two weeks. It was found that fetal HRV increases with gestation age, probably due to increased sympathetic and parasympathetic modulation because of maturation of the ANS. In **Chapter 8** the influence of administration of corticosteroids on fetal HRV was examined. Corticosteroids are often used in case of threatening preterm labor to expedite fetal lung maturation. A cohort study was performed with measurements during five successive days after administration of corticosteroids. During day 1 an increase in fetal HRV was seen, followed by a decrease during day 2. After day 3, HRV values returned back to normal. The change in fetal HRV following corticosteroid administration is likely to correspond to changes in quiet and active state of the fetus.

9.2   Future directions

The first documented attempt to record the fetal ECG was performed by Cremer in 1906 [43]. Since then, developments in fetal ECG monitoring lost momentum due to difficulties to extract a good quality fetal ECG. In the 1960s, the fetal ECG regained interest after the introduction of the invasive fetal ECG [13, 15, 19, 47, 102]. However, several drawbacks restrict its use in clinical practice, i.e. invasiveness and only single lead ECG information [103]. To overcome these limitations, a renewed interest has been shown in the non-invasive fetal ECG. With improvements in computational power, new processing techniques have become available that allow for more reliable extraction of the fetal ECG from the non-invasive recordings.

In spite of the efforts to enhance the signal quality of the non-invasive fetal ECG, there is still a lot to gain in this area. We hope that the methods that have been developed in this thesis will increase the chance that the non-invasive fetal ECG becomes a standard monitoring technique. Several improvements need to be made before our methods can be used in clinical practice. The most critical points are discussed below for each chapter.

The model that was used to describe the PLI in Chapter 3 assumes that variations in PLI phase and frequency are small. In most developed countries this approximation holds because the PLI is relatively stable. To use the method in countries where the PLI is less stable, it is necessary to extend the model to a non-linear model that also estimates the PLI phase and frequency. Another assumption of the PLI model is that the observation noise is white. However, the observation noise represents all non-PLI signals and thus also consists of correlated physiological noise. A whitening filter could be implemented to ensure that the observation noise is uncorrelated. The design of the whitening filter should account for the non-stationary frequency content of the observation noise (e.g. because the frequency content of the ECG varies over time).

One of the critical improvements for the FHR detection method in Chapter 4 is to adapt the method for online applications. Although the method works well even under low and varying SNR conditions, it can only be used for offline applications or for applications where a delay of at least one minute is allowed. For online bedside monitoring a delay of one minute would be too long for detection of fetal distress. Moreover, for online use the computational complexity of the method needs to be reduced. Besides improvements for online applications, the models used for the fetal ECG waveform and FHR are developed for normal conditions. The performance of the method is expected to reduce in case of an abnormal ECG waveform (e.g. congenital abnormalities) or abnormal FHR (e.g. during premature cardiac contractions or strong decelerations). For future work it would be interesting to extend our ECG and FHR model to include abnormal conditions.

In Chapters 5 and 6 we showed that combining contraction-dependent HRV features with regular HRV features improves the classification performance

for detection of fetal distress. To calculate the contraction-dependent HRV features we used visual annotation of uterine contractions. Not only is this a time-consuming process, it can also suffer from inter-observer variability. To use contraction-dependent HRV features in clinical practice, uterine contractions should be detected automatically. Besides, the number of cases with asphyxia that was used in these studies was relatively small, mainly due to the low incidence of fetuses with adverse outcome. To gain more insight into which combination of HRV features is the most informative, further study using a larger dataset is required. If a larger dataset is available, it would be interesting to use other clinical information in addition to the FHR as input for the classifier (e.g. gestational age, maternal age, or administered medication). In case (non-invasive) fetal ECG recordings are used, information from the fetal ECG waveform could also be included in the classifier. Finally, it would be interesting to explore the use of more model-based approaches such as point-process models to describe the FHR and fetal HRV.

From Chapters 7 and 8 it becomes clear that one of the major challenges to overcome for the non-invasive fetal ECG is the low percentage of data that is available for HRV analysis. It should be stressed that these studies were conducted with older signal processing methods and not with the methods that are presented in this thesis. When the recordings are analyzed with our newly developed methods the percentage of recordings with usable FHR for HRV analysis increases from 14% to 66% for the longitudinal study and 60% to 86% for the corticosteroid study. The percentage of usable recordings for the longitudinal study is lower because this also includes recordings that were performed before 20 weeks of gestation. With more available FHR data, the studies in Chapter 7 and 8 can be repeated, which hopefully leads to more conclusive results. Despite improvements in signal processing, it should be noted that in the period between 28 and 34 weeks of gestation the signal quality is reduced due to the presence of the vernix caseosa. Hence, further technological developments are required to improve the signal quality of the non-invasive fetal ECG during this period.

In recent years, the non-invasive fetal ECG has developed from a technique that was mostly used by researchers in controlled settings to a commercially available monitoring technique. Developments in both hardware and software have resulted in non-invasive and wireless applications. Currently, several commercial non-invasive fetal ECG monitors have found their way to the market. Yet, commercial applications for the non-invasive fetal ECG monitors are still in their infancy and we hope that the methods that were developed in this thesis will bring the non-invasive fetal ECG one step closer to clinical use.

BIBLIOGRAPHY

[1] A.K. Sundström, D. Rosén, and K.G. Rosén. "Fetal surveillance." In: *Gothenburg: Neoventa Medical AB* (2000).

[2] J. A. Low, B. G. Lindsay, and E. J. Derrick. "Threshold of metabolic acidosis associated with newborn complications." In: *American Journal of Obstetrics & Gynecology* 177.6 (1997), pp. 1391–1394.

[3] World Health Organisation. *Neonatal and perinatal mortality: country, regional and global estimates*. 2006.

[4] World Health Organisation. *Birth Asphyxia - Summary of the previous meeting and protocol overview*. 2007. URL: http://www.curoservice.com/health_professionals/news/pdf/10-09-2007_birth_asphyxia02.pdf.

[5] R.G. Kennedy. "Electronic fetal heart rate monitoring: retrospective reflections on a twentieth-century technology." In: *Journal of the Royal Society of Medicine* 91.5 (1998), p. 244.

[6] R.K. Freeman, T.J. Garite, M.P. Nageotte, and L.A. Miller. *Fetal heart rate monitoring*. Lippincott Williams & Wilkins, 2012.

[7] D. Ayres-de Campos, C.Y. Spong, and E. Chandraharan. "FIGO consensus guidelines on intrapartum fetal monitoring: Cardiotocography." In: *International Journal of Gynecology & Obstetrics* 131.1 (2015), pp. 13–24.

[8] K.B. Nelson, J.M. Dambrosia, T.Y.x Ting, and J.K. Grether. "Uncertain value of electronic fetal monitoring in predicting cerebral palsy." In: *New England Journal of Medicine* 334.10 (1996), pp. 613–619.

[9] Z. Alfirevic, D. Devane, and G.M.L. Gyte. "Continuous cardiotocography (CTG) as a form of electronic fetal monitoring (EFM) for fetal assessment during labour." In: *The Cochrane Database of Systematic Reviews* 3 (2006), p. CD006066.

[10] E. Blix, O. Sviggum, K.S. Koss, and P. Øian. "Inter-observer variation in assessment of 845 labour admission tests: comparison between midwives and obstetricians in the clinical setting and two experts." In: *BJOG: An International Journal of Obstetrics & Gynaecology* 110.1 (2003), pp. 1–5.

[11] P. van den Berg, S. Schmidt, J. Gesche, and E. Saling. "Fetal distress and the condition of the newborn using cardiotocography and fetal blood analysis during labour." In: *BJOG: An International Journal of Obstetrics & Gynaecology* 94.1 (1987), pp. 72–75.

[12] D. C. Young, J. H. Gray, E. R. Luther, and L. J. Peddle. "Fetal scalp blood pH sampling: its value in an active obstetric unit." In: *American Journal of Obstetrics & Gynecology* 136.3 (1980), pp. 276–281.

[13] K. G. Rosén and I. Kjellmer. "Changes in the fetal heart rate and ECG during hypoxia." In: *Acta Physiologica Scandinavica* 93.1 (1975), pp. 59–66.

[14] K.G. Rosén, A. Dagbjartsson, B.A. Henriksson, H. Lagercrantz, and I. Kjellmer. "The relationship between circulating catecholamines and ST waveform in the fetal lamb electrocardiogram during hypoxia." In: *American Journal of Obstetrics & Gynecology* 149.2 (1984), pp. 190–5.

[15] K. R. Greene, G. S. Dawes, H. Lilja, and K. G. Rosén. "Changes in the ST waveform of the fetal lamb electrocardiogram with hypoxemia." In: *American Journal of Obstetrics & Gynecology* 144.8 (1982), pp. 950–958.

[16] K. G. Rosén, K. H. Hökegård, and I. Kjellmer. "A study of the relationship between the electrocardiogram and hemodynamics in the fetal lamb during asphyxia." In: *Acta Physiologica Scandinavica* 98.3 (1976), pp. 275–284.

[17] K. H. Hökegård, B. O. Eriksson, I. Kjellmer, R. Magno, and K. G. Rosén. "Myocardial metabolism in relation to electrocardiographic changes and cardiac function during graded hypoxia in the fetal lamb." In: *Acta Physiologica Scandinavica* 113.1 (1981), pp. 1–7.

[18] J. Westgate, M. Harris, J.S.H. Curnow, and K.R. Greene. "Plymouth randomized trial of cardiotocogram only versus ST waveform plus cardiotocogram for intrapartum monitoring in 2400 cases." In: *American Journal of Obstetrics & Gynecology* 169.5 (1993), pp. 1151–1160.

[19] I. Amer-Wåhlin, C. Hellsten, H. Norén, H. Hagberg, A. Herbst, I. Kjellmer, H. Lilja, C. Lindoff, M. Månsson, L. Mårtensson, et al. "Cardiotocography only versus cardiotocography plus ST analysis of fetal electrocardiogram for intrapartum fetal monitoring: a Swedish randomised controlled trial." In: *The Lancet* 358.9281 (2001), pp. 534–538.

[20] K. Ojala, M. Vääräsmäki, K. Mäkikallio, M. Valkama, and A. Tekay. "A comparison of intrapartum automated fetal electrocardiography and conventional cardiotocography - a randomised controlled study." In: *BJOG: An International Journal of Obstetrics & Gynaecology* 113.4 (2006), pp. 419–423.

[21] C. Vayssière, E. David, N. Meyer, R. Haberstich, V. Sebahoun, E. Roth, R. Favre, I. Nisand, and B. Langer. "A French randomized controlled trial of ST-segment analysis in a population with abnormal cardiotocograms during labor." In: *American Journal of Obstetrics & Gynecology* 197.3 (2007), 299–e1.

[22] M.E. Westerhuis, G.H. Visser, K.G. Moons, E. van Beek, M.J. Benders, S.M. Bijvoet, H.J. van Dessel, A.P. Drogtrop, H.P. van Geijn, G.C. Graziosi, et al. "Cardiotocography plus ST analysis of fetal electrocardiogram compared with cardiotocography only for intrapartum monitoring: a randomized controlled trial." In: *Obstetrics & Gynecology* 115.6 (2010), pp. 1173–1180.

[23] M.A. Belfort, G.R. Saade, E. Thom, S.C. Blackwell, U.M. Reddy, J.M. Thorp Jr, A.T.N. Tita, R.S. Miller, A.M. Peaceman, D.S. McKenna, et al. "A randomized trial of intrapartum fetal ECG ST-segment analysis." In: *New England Journal of Medicine* 373.7 (2015), pp. 632–641.

[24] A. Kwee, A.H.S. Dekkers, H.P.J. van Wijk, C.W. van der Hoorn-van den Beld, and G.H.A. Visser. "Occurrence of ST-changes recorded with the STAN S21-monitor during normal and abnormal fetal heart rate patterns during labour." In: *European Journal of Obstetrics & Gynecology and Reproductive Biology* 135.1 (2007), pp. 28–34.

[25] I. Amer-Wåhlin, S. Arulkumaran, H. Hagberg, K. Marsál, and G H A. Visser. "Fetal electrocardiogram: ST waveform analysis in intrapartum surveillance." In: *BJOG: An International Journal of Obstetrics & Gynaecology* 114.10 (2007), pp. 1191–1193.

[26] A.A. Mahendru and C.C. Lees. "Is intrapartum fetal blood sampling a gold standard diagnostic tool for fetal distress?" In: *European Journal of Obstetrics & Gynecology and Reproductive Biology* 156.2 (2011), pp. 137–139.

[27] J.P. Neilson. "Fetal electrocardiogram (ECG) for fetal monitoring during labour." In: *The Cochrane Database of Systematic Reviews* 4 (2012), p. CD000116.

[28] T.P. Schaap, K.A. Moormann, J.H. Becker, M.E.M.H. Westerhuis, A. Evers, H.A.A. Brouwers, N.W.E. Schuitemaker, G.H.A. Visser, and A. Kwee. "Cerebrospinal fluid leakage, an uncommon complication of fetal blood sampling: a case report and review of the literature." In: *Obstetrical & Gynecological Survey* 66 (1 2011), pp. 42–46.

[29] S. Akselrod, D. Gordon, J. B. Madwed, N. C. Snidman, D. C. Shannon, and R. J. Cohen. "Hemodynamic regulation: investigation by spectral analysis." In: *American Journal of Physiology* 249.4 Pt 2 (1985), H867–H875.

[30] A.J. Camm, M. Malik, J.T. Bigger, B. Günter, S. Cerutti, and R. Choen. "Task force of the European Society of Cardiology and the North American Society of Pacing and Electrophysiology. Heart rate variability: standards of measurement, physiological interpretation and clinical use." In: *Circulation* 93.5 (1996), pp. 1043–1065.

[31] J.O.E.H. van Laar, C.H.L. Peters, R. Vullings, S. Houterman, J.W.M. Bergmans, and S. G. Oei. "Fetal autonomic response to severe acidaemia during labour." In: *BJOG: An International Journal of Obstetrics & Gynaecology* 117.4 (2010), pp. 429–437.

[32] J.O.E.H. van Laar, C.H.L. Peters, S. Houterman, P.F.F. Wijn, A. Kwee, and S.G. Oei. "Normalized spectral power of fetal heart rate variability is associated with fetal scalp blood pH." In: *Early Human Development* 87.4 (2011), pp. 259–263.

[33] J.O.E.H. van Laar, M.M. Porath, C.H.L. Peters, and S.G. Oei. "Spectral analysis of fetal heart rate variability for fetal surveillance: review of the literature." In: *Acta Obstetricia et Gynecologica Scandinavica* 87.3 (2008), pp. 300–306.

[34] G. Magenes, M.G. Signorini, and D. Arduini. "Classification of cardiotocographic records by neural networks." In: *Proceedings of the IEEE-INNS-ENNS International Joint Conference on Neural Networks* (2000).

[35] G. Georgoulas, D. Stylios, and P. Groumpos. "Predicting the risk of metabolic acidosis for newborns based on fetal heart rate signal classification using support vector machines." In: *IEEE Transactions on Biomedical Engineering* 53.5 (2006), pp. 875–884.

[36] H. Gonçalves, A.P. Rocha, D. Ayres-de Campos, and J. Bernardes. "Linear and nonlinear fetal heart rate analysis of normal and acidemic fetuses in the minutes preceding delivery." In: *Medical and Biological Engineering and Computing* 44.10 (2006), pp. 847–855.

[37] J. Spilka, V. Chudáček, M. Koucký, L. Lhotská, M. Huptych, P. Janků, G. Georgoulas, and C. Stylios. "Using nonlinear features for fetal heart rate classification." In: *Biomedical Signal Processing and Control* 7.4 (2012), pp. 350–357.

[38] P. Abry, S.G. Roux, V. Chudácek, P. Borgnat, P. Goncalves, and M. Doret. "Hurst exponent and intrapartum fetal heart rate: Impact of decelerations." In: *Computer-Based Medical Systems (CBMS), 2013 IEEE 26th International Symposium on*. IEEE. 2013, pp. 131–136.

[39] A. Georgieva, S. J. Payne, M. Moulden, and C.W.G. Redman. "Artificial neural networks applied to fetal monitoring in labour." In: *Neural Computing and Applications* 22.1 (2013), pp. 85–93.

[40] M. Peters, J. Crowe, J. F. Piéri, H. Quartero, B. Hayes-Gill, D. James, J. Stinstra, and S. Shakespeare. "Monitoring the fetal heart non-invasively: a review of methods." In: *Journal of Perinatal Medicine* 29.5 (2001), pp. 408–416.

[41] G.W. Lawson, R. Belcher, G.S Dawes, and C.W. Redman. "A comparison of ultrasound (with autocorrelation) and direct electrocardiogram fetal heart rate detector systems." In: *American Journal of Obstetrics & Gynecology* 147.6 (1983), pp. 721–722.

[42] J. Jezewski, J. Wrobel, and K. Horoba. "Comparison of Doppler ultrasound and direct electrocardiography acquisition techniques for quantification of fetal heart rate variability." In: *IEEE Transactions on Biomedical Engineering* 53.5 (2006), pp. 855–864.

[43] M. Cremer. "Über die direkte ableitung der aktionsströme des men-schlichen herzens vom oesophagus und über das elektrokardogramm des fötus." In: *Münchener Medizinische Wochenschrift* 53 (1906), pp. 811–813.

[44] R. Sameni. "Extraction of fetal cardiac signals from an array of maternal abdominal recordings." PhD thesis. Citeseer, 2008.

[45] R. Vullings. "Non-invasive fetal electrocardiogram: analysis and interpre-tation." PhD thesis. Technische Universiteit Eindhoven, The Netherlands, 2010.

[46] J. Behar, F. Andreotti, S. Zaunseder, J. Oster, and G.D. Clifford. "A prac-tical guide to non-invasive foetal electrocardiogram extraction and analy-sis." In: *Physiological Measurement* 37.5 (2016), R1.

[47] S.D. Larks and G.G. Larks. "Components of the fetal electrocardiogram and intrauterine electrical axis: quantitative data." In: *Neonatology* 10.3-4 (1966), pp. 140–152.

[48] R. Vullings, M. Mischi, S.G. Oei, and J.W.M. Bergmans. "Novel Bayesian vectorcardiographic loop alignment for improved monitoring of ECG and fetal movement." In: *IEEE Transactions on Biomedical Engineering* 60.6 (2013), pp. 1580–1588.

[49] M.J. Rooijakkers, C. Rabotti, H. de Lau, S.G. Oei, J.W.M. Bergmans, and M. Mischi. "Feasibility study of a new method for low-complexity fetal movement detection from abdominal ECG recordings." In: *IEEE Journal of Biomedical and Health Informatics* 20.5 (2016), pp. 1361–1368.

[50] H. Biglari and R. Sameni. "Fetal motion estimation from noninvasive car-diac signal recordings." In: *Physiological Measurement* 37.11 (2016), p. 2003.

[51] M. Romano, P. Bifulco, M. Cesarelli, M. Sansone, and M. Bracale. "Foetal heart rate power spectrum response to uterine contraction." In: *Medical and Biological Engineering and Computing* 44.3 (2006), pp. 188–201.

[52] M. Cesarelli, M. Romano, M. Ruffo, P. Bifulco, and G. Pasquariello. "Foetal heart rate variability frequency characteristics with respect to uterine contractions." In: *Journal of Biomedical Science and Engineering* 03.10 (2010), 1014–1021.

[53] A. Guyton and J. Hall. *Textbook of medical physiology, 11th.* Elsevier Inc., 2006.

[54] T.G. Laske, M. Shrivastav, and P.A. Iaizzo. *Handbook of Cardiac Anatomy, Physiology, and Devices: The cardiac conduction system.* Humana Press, 2005. Chap. 13.

[55] N.P. Depasquale and G.E. Burch. "The electrocardiogram, ventricular gra-dient, and spatial vectorcardiogram during the first week of life." In: *American Journal of Cardiology* 12 (1963), pp. 482–493.

[56] G. Mielke and N. Benda. "Cardiac output and central distribution of blood flow in the human fetus." In: *Circulation* 103.12 (2001), pp. 1662–1668.

[57] S. Yagel, N.H. Silverman, and U. Gemburch. *Fetal cardiology: embryology, genetics, physiology, echocardiographic evaluation, diagnosis and perinatal management of cardiac diseases*. 2nd ed. Informa Healthcare Inc, New York, USA, 2009.

[58] anatomybodysystem.com. URL: https://anatomybodysystem.com.

[59] D.B. Geselowitz. "Dipole theory in electrocardiography." In: *The American Journal of Cardiology* 14 (1964), pp. 301–306.

[60] H. C. Burger and J. B. Van Milaan. "Heart-vector and leads." In: *British Heart Journal* 8.3 (1946), pp. 157–161.

[61] E. Frank. "General theory of heat-vector projection." In: *Circulation Research* 2.3 (1954), pp. 258–270.

[62] J. Malmivuo and R. Plonsey. *Bioelectromagnetism principles and applications of bioelectric and biomagnetic fields*. Oxford University Press, New York, 1995.

[63] W. Einthoven. "Weiteres über das elecktrokardiogram." In: *Pflüger Arch ges Physiol* 122 (1908), pp. 517–48.

[64] D.A. Grant, J. Fauchère, K.J. Eede, J. Tyberg, A.M. Walker, et al. "Left ventricular stroke volume in the fetal sheep is limited by extracardiac constraint and arterial pressure." In: *The Journal of Physiology* 535.1 (2001), pp. 231–239.

[65] R.M. Berne and M.N. Levy. *The autonomic nervous system and its central control*. 4th ed. Mosby Inc., St Louis, USA, 1998.

[66] C.M. van Ravenswaaij-Arts, L.A. Kollée, J.C. Hopman, G.B. Stoelinga, and H.P. van Geijn. "Heart rate variability." In: *Annals of Internal Medicine* 118.6 (1993), pp. 436–447.

[67] D.R. Brown, J.D. Yingling, D.C. Randall, H.M. Aral, J.M. Evans, J.B. Charles, C.F. Knapp, R. Raisch, and C.E. Ott. "Angiotensin II does not contribute to rapid reflex control of arterial pressure." In: *American Journal of Physiology-Regulatory, Integrative and Comparative Physiology* 261.2 (1991), R473–R477.

[68] T. Kiserud and G. Acharya. "The fetal circulation." In: *Prenatal Diagnosis* 24.13 (2004), pp. 1049–1059.

[69] J.G. Nijhuis, G.G.M. Essed, H.P. van Geijn, and G.H.A. Visser. *Foetale bewaking*. Reed Business, 1998.

[70] C. Widmark, K. Lindecrantz, H. Murray, and K.G. Rósen. "Changes in the PR, RR intervals and ST waveform of the fetal lamb electrocardiogram with acute hypoxemia." In: *Journal of Developmental Physiology* 18.3 (1992), pp. 99–103.

[71] H. E. Cohn, E. J. Sacks, M. A. Heymann, and A. M. Rudolph. "Cardiovascular responses to hypoxemia and acidemia in fetal lambs." In: *American Journal of Obstetrics & Gynecology* 120.6 (1974), pp. 817–824.

[72] L. L. Peeters, R. E. Sheldon, MD Jones Jr, E. L. Makowski, and G. Meschia. "Blood flow to fetal organs as a function of arterial oxygen content." In: *American Journal of Obstetrics & Gynecology* 135.5 (1979), pp. 637–646.

[73] B. S. Richardson, L. Carmichael, J. Homan, L. Johnston, and R. Gagnon. "Fetal cerebral, circulatory, and metabolic responses during heart rate decelerations with umbilical cord compression." In: *American Journal of Obstetrics & Gynecology* 175.4 Pt 1 (1996), pp. 929–936.

[74] M. De Haan, J. S. Wyatt, S. Roth, F. Vargha-Khadem, D. Gadian, and M. Mishkin. "Brain and cognitive-behavioural development after asphyxia at term birth." In: *Developmental Science* 9.4 (2006), pp. 350–358.

[75] R. Victory, D. Penava, O. Da Silva, R. Natale, and B. Richardson. "Umbilical cord pH and base excess values in relation to adverse outcome events for infants delivering at term." In: *American Journal of Obstetrics & Gynecology* 191.6 (2004), pp. 2021–2028.

[76] A. Martín-Ancel, A. García-Alix, F. Gayá, F. Cabañas, M. Burgueros, and J. Quero. "Multiple organ involvement in perinatal asphyxia." In: *Journal of Pediatrics* 127.5 (1995), pp. 786–793.

[77] J. Karin, M. Hirsch, and S. Akselrod. "An estimate of fetal autonomic state by spectral analysis of fetal heart rate fluctuations." In: *Pediatric Research* 34.2 (1993), pp. 134–138.

[78] P. Van Leeuwen, D. Geue, S. Lange, W. Hatzmann, and D. Grönemeyer. "Changes in the frequency power spectrum of fetal heart rate in the course of pregnancy." In: *Prenatal Diagnosis* 23.11 (2003), pp. 909–916.

[79] M. David, M. Hirsch, J. Karin, E. Toledo, and S. Akselrod. "An estimate of fetal autonomic state by time-frequency analysis of fetal heart rate variability." In: *Journal of Applied Physiology* 102.3 (2007), pp. 1057–1064.

[80] D. Walker. "Functional development of the autonomic innervation of the human fetal heart." In: *Biology of the Neonate* 25.1-2 (1974), pp. 31–43.

[81] A.J. Pappano. "Ontogenetic development of autonomic neuroeffector transmission and transmitter reactivity in embryonic and fetal hearts." In: *Pharmacological Reviews* 29.1 (1977), pp. 3–33.

[82] B. Nuwayhid, C.R. Brinkman 3rd, C. Su, J. A. Bevan, and N. S. Assali. "Development of autonomic control of fetal circulation." In: *American Journal of Physiology* 228.2 (1975), pp. 337–344.

[83] N.S. Assali, C.R. Brinkman 3rd, J.R. Woods Jr, A. Dandavino, and B. Nuwayhid. "Development of neurohumoral control of fetal, neonatal, and adult cardiovascular functions." In: *American Journal of Obstetrics & Gynecology* 129.7 (1977), pp. 748–759.

[84] J. Itskovitz, E. F. LaGamma, and A. M. Rudolph. "Heart rate and blood pressure responses to umbilical cord compression in fetal lambs with special reference to the mechanism of variable deceleration." In: *American Journal of Obstetrics & Gynecology* 147.4 (1983), pp. 451–457.

[85] M. Pillai and D. James. "Behavioural states in normal mature human fetuses." In: *Archives of Disease in Childhood* 65.1 Spec No (1990), pp. 39–43.

[86] I.J. Nijhuis, J. ten Hof, J.G. Nijhuis, E.J. Mulder, H. Narayan, D.J. Taylor, and G.H. Visser. "Temporal organization of fetal behavior from 24-weeks gestation onwards in normal and complicated pregnancies." In: *Developmental Psychobiology* 34.4 (1999), pp. 257–268.

[87] J.G. Nijhuis, H.F.R. Prechtl, C.B. Martin Jr., and R.S.G.M. Bots. "Are there behavioural states in the human fetus?" In: *Early Human Development* 6.2 (1982), pp. 177–195.

[88] E. J. Mulder, G. H. Visser, D. J. Bekedam, and H. F. Prechtl. "Emergence of behavioural states in fetuses of type-1-diabetic women." In: *Early Human Development* 15.4 (1987), pp. 231–251.

[89] M.M. Wolf, G.A. Varigos, D. Hunt, and J.G. Sloman. "Sinus arrhythmia in acute myocardial infarction." In: *The Medical Journal of Australia* 2.2 (1978), pp. 52–53.

[90] F. Lombardi, G. Sandrone, S. Pernpruner, R. Sala, M. Garimoldi, S. Cerutti, G. Baselli, M. Pagani, and A. Malliani. "Heart rate variability as an index of sympathovagal interaction after acute myocardial infarction." In: *The American Journal of Cardiology* 60.16 (1987), pp. 1239–1245.

[91] G.A. Myers, G.J. Martin, N.M. Magid, P.S. Barnett, J.W. Schaad, J.S. Weiss, M. Lesch, and D.H. Singer. "Power spectral analysis of heart rate varability in sudden cardiac death: Comparison to other methods." In: *IEEE Transactions on Biomedical Engineering* 12 (1986), pp. 1149–1156.

[92] M. Malik and A.J. Camm. *Heart rate variability*. Futura Publishing Company, 1995.

[93] D.J. Ewing and B.F. Clarke. "Diagnosis and management of diabetic autonomic neuropathy." In: *British Medical Journal (Clinical Research ed.)* 285.6346 (1982), p. 916.

[94] A. Bravi, A. Longtin, and A.J. Seely. "Review and classification of variability analysis techniques with clinical applications." In: *Biomedical Engineering Online* 10.1 (2011), p. 90.

[95] A. Voss, S. Schulz, R. Schroeder, M. Baumert, and P. Caminal. "Methods derived from nonlinear dynamics for analysing heart rate variability." In: *Philosophical Transactions of the Royal Society of London A: Mathematical, Physical and Engineering Sciences* 367.1887 (2009), pp. 277–296.

[96] M.V. Kamath, M. Watanabe, and A. Upton. *Heart rate variability (HRV) signal analysis: clinical applications*. CRC Press, 2012.

[97] U. Schneider, E. Schleussner, A. Fiedler, S. Jaekel, M. Liehr, J. Haueisen, and D. Hoyer. "Fetal heart rate variability reveals differential dynamics in the intrauterine development of the sympathetic and parasympathetic branches of the autonomic nervous system." In: *Physiological Measurement* 30.2 (2009), 215–226.

[98] S.M. Pincus. "Approximate entropy as a measure of system complexity." In: *Proceedings of the National Academy of Sciences* 88.6 (1991), pp. 2297–2301.

[99] J.S. Richman and J.R. Moorman. "Physiological time-series analysis using approximate entropy and sample entropy." In: *American Journal of Physiology-Heart and Circulatory Physiology* 278.6 (2000), H2039–H2049.

[100] A.L. Goldberger, L.A.N. Amaral, J.M. Hausdorff, P.C. Ivanov, C.K. Peng, and H.E. Stanley. "Fractal dynamics in physiology: alterations with disease and aging." In: *Proceedings of the National Academy of Sciences* 99.suppl 1 (2002), pp. 2466–2472.

[101] C. Kittel, W.D. Knight, M.A. Ruderman, et al. "Mechanics, Berkeley Physics Course, Vol. 1." In: *Reverté* (1965).

[102] E.H. Hon. "Instrumentation of fetal heart rate and fetal electrocardiography. II. A vaginal electrode." In: *American Journal of Obstetrics & Gynecology* 86 (1963), pp. 772–784.

[103] R. Vullings, K.M.J. Verdurmen, A.D.J. Hulsenboom, S. Scheffer, H. de Lau, A. Kwee, P.F.F. Wijn, I. Amer-Wåhlin, J.O.E.H. van Laar, and S.G. Oei. "The electrical heart axis and ST events in fetal monitoring: A post-hoc analysis following a multicenter randomised controlled trial." In: *Plos One* 12.4 (2017), e0175823.

[104] K.M.J. Verdurmen, A.D.J. Hulsenboom, J.O.E.H. van Laar, P.F.F. Wijn, R. Vullings, and S.G. Oei. "Orientation of the electrical heart axis in mid-term pregnancy." In: *European Journal of Obstetrics and Gynecology and Reproductive Biology* 207 (2016), pp. 243–246.

[105] C. Rabotti. "Characterization of uterine activity by electrohysterography." In: *Technische Universiteit Eindhoven* (2010).

[106] T.F. Oostendorp, A. van Oosterom, and H.W. Jongsma. "The effect of changes in the conductive medium on the fetal ECG throughout gestation." In: *Clinical Physics and Physiological Measurement* 10 Suppl B (1989), pp. 11–20.

[107] J.T. Oldenburg and M. Macklin. "Changes in the conduction of the fetal electrocardiogram to the maternal abdominal surface during gestation." In: *American Journal of Obstetrics & Gynecology* 129.4 (1977), pp. 425–433.

[108] J.G. Stinstra and M.J. Peters. "The volume conductor may act as a temporal filter on the ECG and EEG." In: *Medical & Biological Engineering & Computing* 36.6 (1998), pp. 711–716.

[109] T.F. Oostendorp, A. Van Oosterom, and H.W. Jongsma. "The fetal ECG throughout the second half of gestation." In: *Clinical Physics and Physiological Measurement* 10.2 (1989), p. 147.

[110] T.F. Oostendorp. "Modeeling the foetal ECG." PhD thesis. K.U.Nijmegen, The Netherlands, 1989.

[111] S. Abboud and D. Sadeh. "Spectral analysis of the fetal electrocardiogram." In: *Computers in Biology and Medicine* 19.6 (1989), pp. 409–415.

[112] S.M.M. Martens, M. Mischi, S.G. Oei, and J.W.M. Bergmans. "An improved adaptive power line interference canceller for electrocardiography." In: *IEEE Transactions on Biomedical Engineering* 53.11 (2006), pp. 2220–2231.

[113] D. Devedeux, C. Marque, S. Mansour, G. Germain, and J. Duchêne. "Uterine electromyography: a critical review." In: *American Journal of Obstetrics & Gynecology* 169.6 (1993), pp. 1636–1653.

[114] M.J. Rooijakkers, S. Song, C. Rabotti, S.G. Oei, J.W.M. Bergmans, E. Cantatore, and M. Mischi. "Influence of electrode placement on signal quality for ambulatory pregnancy monitoring." In: *Computational and mathematical methods in medicine* 2014 (2014).

[115] M.W.C. Vlemminx, K.M.J. Thijssen, G.I. Bajlekov, J.P. Dieleman, M.B. Van der Hout-Van der Jagt, and S.G. Oei. "Electrohysterography for uterine monitoring during term labour compared to external tocodynamometry and intra-uterine pressure catheter." In: *European Journal of Obstetrics & Gynecology and Reproductive Biology* 215 (2017), pp. 197–205.

[116] M.J. Rooijakkers, C. Rabotti, S.G. Oei, R.M. Aarts, and M. Mischi. "Low-complexity intrauterine pressure estimation using the Teager energy operator on electrohysterographic recordings." In: *Physiological Measurement* 35.7 (2014), p. 1215.

[117] T.F. Oostendorp, A. van Oosterom, and H.W. Jongsma. "Electrical properties of tissues involved in the conduction of foetal ECG." In: *Medical & Biological Engineering & Computing* 27.3 (1989), pp. 322–324.

[118] S. Cerutti, G. Baselli, S. Civardi, E. Ferrazzi, A.M. Marconi, M. Pagani, and G. Pardi. "Variability analysis of fetal heart rate signals as obtained from abdominal electrocardiographic recordings." In: *Journal of Perinatal Medicine* 14.6 (1986), pp. 445–452.

[119] M. Ungureanu, J.W.M. Bergmans, S.G. Oei, and R. Strungaru. "Fetal ECG extraction during labor using an adaptive maternal beat subtraction technique." In: *Biomedizinische Technik* 52.1 (2007), pp. 56–60.

[120] R. Vullings, C.H.L. Peters, R.J. Sluijter, M. Mischi, S.G. Oei, and J.W.M. Bergmans. "Dynamic segmentation and linear prediction for maternal ECG removal in antenatal abdominal recordings." In: *Physiological Measurement* 30.3 (2009), pp. 291–307.

[121] B. Widrow, J.R. Glover Jr, J.M. McCool, J. Kaunitz, C.S. Williams, R.H. Hearn, J.R. Zeidler, E. Dong Jr, and R.C. Goodlin. "Adaptive noise cancelling: Principles and applications." In: *Proceedings of the IEEE* 63.12 (1975), pp. 1692–1716.

[122] P.P. Kanjilal, S. Palit, and G. Saha. "Fetal ECG extraction from single-channel maternal ECG using singular value decomposition." In: *IEEE Transactions on Biomedical Engineering* 44.1 (1997), pp. 51–59.

[123] L. De Lathauwer, B. De Moor, and J. Vandewalle. "Fetal electrocardiogram extraction by blind source subspace separation." In: *IEEE Transactions on Biomedical Engineering* 47.5 (2000), pp. 567–572.

[124] S.M.M. Martens, C. Rabotti, M. Mischi, and R.J. Sluijter. "A robust fetal ECG detection method for abdominal recordings." In: *Physiological Measurement* 28.4 (2007), p. 373.

[125] F. Andreotti, M. Riedl, T. Himmelsbach, D. Wedekind, N. Wessel, H. Stepan, C. Schmieder, A. Jank, H. Malberg, and S. Zaunseder. "Robust fetal ECG extraction and detection from abdominal leads." In: *Physiological Measurement* 35.8 (2014), p. 1551.

[126] M. Varanini, G. Tartarisco, L. Billeci, A. Macerata, G. Pioggia, and R. Balocchi. "An efficient unsupervised fetal QRS complex detection from abdominal maternal ECG." In: *Physiological Measurement* 35.8 (2014), p. 1607.

[127] J. Behar, J. Oster, and G.D. Clifford. "Combining and benchmarking methods of foetal ECG extraction without maternal or scalp electrode data." In: *Physiological Measurement* 35.8 (2014), p. 1569.

[128] J.A. Lipponen and M.P. Tarvainen. "Principal component model for maternal ECG extraction in fetal QRS detection." In: *Physiological Measurement* 35.8 (2014), p. 1637.

[129] W. Chen, C. Sonntag, F. Boesten, S.B. Oetomo, and L. Feijs. "A design of power supply for neonatal monitoring with wearable sensors." In: *Journal of Ambient Intelligence and Smart Environments* 1.2 (2009), pp. 185–196.

[130] S.C. Pei and C.C. Tseng. "Elimination of AC interference in electrocardiogram using IIR notch filter with transient suppression." In: *IEEE Transactions on Biomedical Engineering* 42.11 (1995), pp. 1128–1132.

[131] P.S. Hamilton. "A comparison of adaptive and nonadaptive filters for reduction of power line interference in the ECG." In: *IEEE Transactions on Biomedical Engineering* 43.1 (1996), pp. 105–109.

[132] J.R. Glover Jr. "Adaptive noise canceling applied to sinusoidal interferences." In: *IEEE Transactions on Acoustics, Speech and Signal Processing* 25.6 (1977), pp. 484–491.

[133] Y.Z. Ider and H. Köymen. "A new technique for line interference monitoring and reduction in biopotential amplifiers." In: *IEEE Transactions on Biomedical Engineering* 37.6 (1990), pp. 624–631.

[134] A.K. Ziarani and A. Konrad. "A nonlinear adaptive method of elimination of power line interference in ECG signals." In: *IEEE Transactions on Biomedical Engineering* 49.6 (2002), pp. 540–547.

[135] R. Sameni. "A linear kalman notch filter for power-line interference cancellation." In: *Artificial Intelligence and Signal Processing (AISP), 2012 16th CSI International Symposium on*. IEEE. 2012, pp. 604–610.

[136] P.K. Dash, R.K. Jena, G. Panda, and A. Routray. "An extended complex Kalman filter for frequency measurement of distorted signals." In: *IEEE Transactions on Instrumentation and Measurement* 49.4 (2000), pp. 746–753.

[137] S. Butterworth. "On the theory of filter amplifiers." In: *Wireless Engineer* 7.6 (1930), pp. 536–541.

[138] J. Stinstra et al. "Multicenter study of fetal cardiac time intervals using magnetocardiography." In: *BJOG: An International Journal of Obstetrics & Gynaecology* 109 (2002), pp. 1235–1243.

[139] D.G. Fink and H.W. Beaty. *Standard handbook for electrical engineers*. McGraw-Hill, 1987.

[140] A. Gelb. *Applied optimal estimation*. MIT press, 1974.

[141] M. Niedźwiecki. "Generalized adaptive notch smoothing revisited." In: *Signal Processing, IEEE Transactions on* 58.3 (2010), pp. 1565–1576.

[142] B.D.O. Anderson and J.B. Moore. *Optimal Filtering.* 1979.

[143] J.F.G. de Freitas, M. Niranjan, and A.H. Gee. *Hierarchical Bayesian-Kalman models for regularisation and ARD in sequential learning*. Tech. rep. Cambridge University, 1998.

[144] R.E. Kalman. "A new approach to linear filtering and prediction problems." In: *Journal of basic Engineering* 82.1 (1960), pp. 35–45.

[145] B. Köhler, C. Hennig, and R. Orglmeister. "The principles of software QRS detection." In: *IEEE Engineering in Medicine and Biology Magazine* 21.1 (2002), pp. 42–57.

[146] F. Gustafsson. "Determining the initial states in forward-backward filtering." In: *IEEE Transactions on Signal Processing* 44.4 (1996), pp. 988–992.

[147] T.T Tay, I. Mareels, and J.B. Moore. *High performance control*. Birkhäuser, 1997.

[148] R. Sameni and G.D. Clifford. "A review of fetal ECG signal processing; issues and promising directions." In: *The Open Pacing, Electrophysiology & Therapy Journal* 3 (2010), p. 4.

[149] I. Silva, J. Behar, R. Sameni, T. Zhu, J. Oster, G.D. Clifford, and G.B. Moody. "Noninvasive fetal ECG: the PhysioNet/computing in cardiology challenge 2013." In: *Computing in Cardiology Conference*. IEEE. 2013, pp. 149–152.

[150] M.J. Rooijakkers, C. Rabotti, S.G. Oei, and M. Mischi. "Low-complexity R-peak detection for ambulatory fetal monitoring." In: *Physiological Measurement* 33.7 (2012), pp. 1135–1150.

[151] P.E. McSharry, G.D. Clifford, L. Tarassenko, and L.A. Smith. "A dynamical model for generating synthetic electrocardiogram signals." In: *IEEE Transactions on Biomedical Engineering* 50.3 (2003), pp. 289–294.

[152] R. Sameni, M.B. Shamsollahi, C. Jutten, and G.D. Clifford. "A nonlinear Bayesian filtering framework for ECG denoising." In: *IEEE Transactions on Biomedical Engineering* 54.12 (2007), pp. 2172–2185.

[153] H. Akaike. "Fitting autoregressive models for prediction." In: *Annals of the institute of Statistical Mathematics* 21.1 (1969), pp. 243–247.

[154] M. Arnold, X.H.R. Milner, H. Witte, R. Bauer, and C. Braun. "Adaptive AR modeling of nonstationary time series by means of Kalman filtering." In: *IEEE Transactions on Biomedical Engineering* 45.5 (1998), pp. 553–562.

[155] J.M. Leski. "Robust weighted averaging [of biomedical signals]." In: *IEEE Transactions on Biomedical Engineering* 49.8 (2002), pp. 796–804.

[156] J. Pan and W.J. Tompkins. "A real-time QRS detection algorithm." In: *IEEE Transactions on Biomedical Engineering* 32.3 (1985), pp. 230–236.

[157] A.L. Goldberger, L.A.N. Amaral, L. Glass, J.M. Hausdorff, P.C.H. Ivanov, R.G. Mark, J.E. Mietus, G.B. Moody, C. Peng, and H.E. Stanley. "Physiobank, physiotoolkit, and physionet." In: *Circulation* 101.23 (2000), e215–e220.

[158] R. Barbieri, E.C. Matten, A.A. Alabi, and E.N. Brown. "A point-process model of human heartbeat intervals: new definitions of heart rate and heart rate variability." In: *American Journal of Physiology-Heart and Circulatory Physiology* 288.1 (2005), H424–H435.

[159] G. Valenza, L. Citi, E.P. Scilingo, and R. Barbieri. "Point-process nonlinear models with laguerre and volterra expansions: Instantaneous assessment of heartbeat dynamics." In: *IEEE Transactions on Signal Processing* 61.11 (2013), pp. 2914–2926.

[160] S. Šprager and D. Zazula. "Optimization of heartbeat detection in fiber-optic unobtrusive measurements by using maximum a posteriori probability estimation." In: *IEEE Journal of Biomedical and Health Informatics* 18.4 (2014), pp. 1161–1168.

[161] FIGO. "Intrapartum surveillance: recommendation on current practice and overview of new developments." In: *International Journal of Gynecology & Obstetrics* 49 (1995), p. 213.

[162] X. Li, D. Zheng, S. Zhou, D. Tang, C. Wang, and G. Wu. "Approximate entropy of fetal heart rate variability as a predictor of fetal distress in women at term pregnancy." In: *Acta Obstetricia et Gynecologica Scandinavica* 84.9 (2005), pp. 837–843.

[163] M. Ferrario, M.G. Signorini, G. Magenes, and S. Cerutti. "Comparison of entropy-based regularity estimators: application to the fetal heart rate signal for the identification of fetal distress." In: *IEEE Transactions on Biomedical Engineering* 53.1 (2006), pp. 119–125.

[164] M.G. Signorini, A. Fanelli, and G. Magenes. "Monitoring fetal heart rate during pregnancy: contributions from advanced signal processing and wearable technology." In: *Computational and Mathematical Methods in Medicine* 2014 (2014).

[165] V. Chudacek, J. Andén, S. Mallat, P. Abry, and M. Doret. "Scattering transform for intrapartum fetal heart rate variability fractal analysis: A case-control study." In: *IEEE Transactions on Biomedical Engineering* 61.4 (2014), pp. 1100–1108.

[166] C.H.L. Peters, R. Vullings, M.J. Rooijakkers, J.W.M. Bergmans, S.G. Oei, and P.F.F. Wijn. "A continuous wavelet transform-based method for time-frequency analysis of artefact-corrected heart rate variability data." In: *Physiological Measurement* 32.10 (2011), pp. 1517–1527.

[167] P.S. Addison. *The illustrated wavelet transform handbook: introductory theory and applications in science, engineering, medicine and finance*. CRC press, 2002.

[168] C.H.L. Peters, R. Vullings, J.W.M. Bergmans, S.G. Oei, and P.F.F. Wijn. "The effect of artifact correction on spectral estimates of heart rate variability." In: *Conference Proceedings of the IEEE EMBC* 2008 (2008), pp. 2669–2672.

[169] C.K. Peng, S. Havlin, H.E. Stanley, and A.L. Goldberger. "Quantification of scaling exponents and crossover phenomena in nonstationary heartbeat time series." In: *Chaos: An Interdisciplinary Journal of Nonlinear Science* 5.1 (1995), pp. 82–87.

[170] E.A.F. Ihlen. "Introduction to Multifractal Detrended Fluctuation Analysis in Matlab." In: *Frontiers in Physiology* 3.141 (2012), pp. 1–19.

[171] A. Eke, P. Herman, L. Kocsis, and L.R. Kozak. "Fractal characterization of complexity in temporal physiological signals." In: *Physiological Measurement* 23.1 (2002), R1.

[172] J.D. Gibbons and S. Chakraborti. *Nonparametric statistical inference*. Springer, 2011.

[173] E. Heintz, T.H. Brodtkorb, N. Nelson, and L.Å. Levin. "The long-term cost-effectiveness of fetal monitoring during labour: a comparison of cardiotocography complemented with ST analysis versus cardiotocography alone." In: *BJOG: An International Journal of Obstetrics & Gynaecology* 115.13 (2008), pp. 1676–1687.

[174] E. d'Aloja, M. Müller, F. Paribello, R. Demontis, and A. Faa. "Neonatal asphyxia and forensic medicine." In: *The Journal of Maternal-Fetal & Neonatal Medicine* 22.sup3 (2009), pp. 54–56.

[175] P.C. Bakker, M. Zikkenheimer, and H.P. van Geijn. "The quality of intrapartum uterine activity monitoring." In: *Journal of Perinatal Medicine* 36.3 (2008), pp. 197–201.

[176] T.Y. Euliano, M.T. Nguyen, S. Darmanjian, S.P. McGorray, N. Euliano, A. Onkala, and A.R. Gregg. "Monitoring uterine activity during labor: a comparison of 3 methods." In: *American Journal of Obstetrics & Gynecology* 208.1 (2013), 66–e1.

[177] A. Fleischer, H. Schulman, N. Jagani, J. Mitchell, and G. Randolph. "The development of fetal acidosis in the presence of an abnormal fetal heart rate tracing. I. The average for gestational age fetus." In: *American Journal of Obstetrics & Gynecology* 144.1 (1982), pp. 55–60.

[178] B. Richardson, R. Natale, and J. Patrick. "Human fetal breathing activity during electively induced labor at term." In: *American Journal of Obstetrics & Gynecology* 133.3 (1979), pp. 247–255.

[179] L. Xu, C.W.G. Redman, S.J. Payne, and A. Georgieva. "Feature selection using genetic algorithms for fetal heart rate analysis." In: *Physiological Measurement* 35.7 (2014), 1357–1371.

[180] P. Warrick, E.F. Hamilton, D. Precup, and R.E. Kearney. "Classification of normal and hypoxic fetuses from systems modeling of intrapartum cardiotocography." In: *IEEE Transactions on Biomedical Engineering* 57.4 (2010), pp. 771–779.

[181] G.J.J. Warmerdam, R. Vullings, J.O.E.H. Van Laar, M.B. Van der Hout-Van der Jagt, J.W.M. Bergmans, L. Schmitt, and S.G. Oei. "Using uterine activity to improve fetal heart rate variability analysis for detection of asphyxia during labor." In: *Physiological Measurement* 37.3 (Feb. 10, 2016), p. 387.

[182] M. Mitchell. *An introduction to genetic algorithms*. MIT press, 1998.

[183]   J. Shawe-Taylor and N. Cristianini. *An Introduction to Support Vector Machines and Other Kernel-based Learning Methods*. Cambridge University Press, 2000, pp. 93–112.

[184]   J.O.E.H. van Laar, C.H.L. Peters, R. Vullings, S. Houterman, and S.G. Oei. "Power spectrum analysis of fetal heart rate variability at near term and post term gestation during active sleep and quiet sleep." In: *Early Human Development* 85.12 (2009), pp. 795–798.

[185]   G.D. Clifford, A. Shoeb, P.E. McSharry, and B.A. Janz. "Model-based filtering, compression and classification of the ECG." In: *International Journal of Bioelectromagnetism* 7.1 (2005), pp. 158–161.

[186]   A. Georgieva, A.T. Papageorghiou, S.J. Payne, M. Moulden, and C.W.G. Redman. "Phase-rectified signal averaging for intrapartum electronic fetal heart rate monitoring is related to acidaemia at birth." In: *BJOG: An International Journal of Obstetrics & Gynaecology* 121.7 (2014), pp. 889–894.

[187]   J.W. Kantelhardt, A. Bauer, A.Y. Schumann, P. Barthel, R. Schneider, M. Malik, and G. Schmidt. "Phase-rectified signal averaging for the detection of quasi-periodicities and the prediction of cardiovascular risk." In: *Chaos: An Interdisciplinary Journal of Nonlinear Science* 17.1 (2007), p. 015112.

[188]   B.D. Fulcher, A.E. Georgieva, C.W.G. Redman, and N.S. Jones. "Highly comparative fetal heart rate analysis." In: *Conference proceedings : ... Annual International Conference of the IEEE Engineering in Medicine and Biology Society. IEEE Engineering in Medicine and Biology Society. Annual Conference* 2012 (2012), pp. 3135–3138.

[189]   H. He and E.A. Garcia. *Learning from imbalanced data*. 2009.

[190]   J.O.E.H. van Laar, G.J.J. Warmerdam, K.M.J. Verdurmen, R. Vullings, C.H.L. Peters, S. Houterman, P.F.F. Wijn, P. Andriessen, C. Pul, and S.G. Oei. "Fetal heart rate variability during pregnancy, obtained from non-invasive electrocardiogram recordings." In: *Acta Obstetricia et Gynecologica Scandinavica* 93.1 (2014), pp. 93–101.

[191]   K.M.J. Verdurmen, J. Renckens, J.O.E.H. van Laar, and S.G. Oei. "The influence of corticosteroids on fetal heart rate variability: a systematic review of the literature." In: *Obstetrical & Gynecological Survey* 68.12 (2013), pp. 811–824.

[192]   M.B. van der Hout-van der Jagt, G.J.L.M. Jongen, P.H.M. Bovendeerd, S.G. Oei, et al. "Insight into variable fetal heart rate decelerations from a mathematical model." In: *Early Human Development* 89.6 (2013), pp. 361–369.

[193] S.M. Siira, T.H. Ojala, T.J. Vahlberg, J.O. Jalonen, I.A. Välimäki, K.G. Rosén, and E.M. Ekholm. "Marked fetal acidosis and specific changes in power spectrum analysis of fetal heart rate variability recorded during the last hour of labour." In: *BJOG: An International Journal of Obstetrics & Gynaecology* 112.4 (2005), pp. 418–423.

[194] G.H.A. Visser, P.H.C. Eilers, P.M. Elferink-Stinkens, H.M.W.M. Merkus, and J.M. Wit. "New Dutch reference curves for birthweight by gestational age." In: *Early Human Development* 85.12 (2009), pp. 737–744.

[195] S. Lange, P. Van Leeuwen, D. Geue, W. Hatzmann, and D. Grönemeyer. "Influence of gestational age, heart rate, gender and time of day on fetal heart rate variability." In: *Medical and Biological Engineering and Computing* 43.4 (2005), pp. 481–486.

[196] R. Vullings, C.H.L. Peters, M.J.M. Hermans, P.F.F. Wijn, S.G. Oei, and J.W.M. Bergmans. "A robust physiology-based source separation method for QRS detection in low amplitude fetal ECG recordings." In: *Physiological Measurement* 31.7 (2010), pp. 935–951.

[197] F. Gritzali, G. Frangakis, and G. Papakonstantinou. "Detection of the P and T waves in an ECG." In: *Computers and Biomedical Research* 22.1 (1989), pp. 83–91.

[198] J. I. de Vries, G. H. Visser, and H. F. Prechtl. "The emergence of fetal behaviour. I. Qualitative aspects." In: *Early Human Development* 7.4 (1982), pp. 301–322.

[199] M.Y. Divon, S. Yeh, E.Z. Zimmer, L.D. Platt, E. Paldi, and R.H. Paul. "Respiratory sinus arrhythmia in the human fetus." In: *American Journal of Obstetrics & Gynecology* 151.4 (1985), pp. 425–428.

[200] E. Ferrazzi, G. Pardi, P.L. Setti, M. Rodolfi, S. Civardi, and S. Cerutti. "Power spectral analysis of the heart rate of the human fetus at 26 and 36 weeks of gestation." In: *Clinical Physics and Physiological Measurement* 10.4B (1989), p. 57.

[201] R. Natale, C. Nasello-Paterson, and G. Connors. "Patterns of fetal breathing activity in the human fetus at 24 to 28 weeks of gestation." In: *American Journal of Obstetrics & Gynecology* 158.2 (1988), pp. 317–321.

[202] J. Ten Hof, I.J.M. Nijhuis, E.J.H. Mulder, J.G. Nijhuis, H. Narayan, D.J. Taylor, P. Westers, and G.H.A. Visser. "Longitudinal study of fetal body movements: nomograms, intrafetal consistency, and relationship with episodes of heart rate patterns A and B." In: *Pediatric Research* 52.4 (2002), pp. 568–575.

[203] A.P. Drogtrop, R. Ubels, and J.G. Nijhuis. "The association between fetal body movements, eye movements and heart rate patterns in pregnancies between 25 and 30 weeks of gestation." In: *Early Human Development* 23.1 (1990), pp. 67–73.

[204] R.H. Paul, A.K. Suidan, S. Yeh, B.S. Schifrin, and E.H. Hon. "Clinical fetal monitoring. VII. The evaluation and significance of intrapartum baseline FHR variability." In: *American Journal of Obstetrics & Gynecology* 123.2 (1975), pp. 206–210.

[205] G.S. Dawes, M. Moulden, and C.W.G. Redman. "Improvements in computerized fetal heart rate analysis antepartum." In: *Journal of Perinatal Medicine* 24.1 (1996), pp. 25–36.

[206] D. Roberts, J. Brown, N. Medley, and S.R. Dalziel. "Antenatal corticosteroids for accelerating fetal lung maturation for women at risk of preterm birth." In: *The Cochrane Library* (2006).

[207] M.C. Petersen, R.L. Nation, J.J. Ashley, and W.G. McBride. "The placental transfer of betamethasone." In: *European journal of clinical pharmacology* 18.3 (1980), pp. 245–247.

[208] C.H.L. Peters, J.O.E.H. van Laar, R. Vullings, S.G. Oei, and P.F.F. Wijn. "Beat-to-beat heart rate detection in multi-lead abdominal fetal ECG recordings." In: *Medical Engineering & Physics* 34.3 (2012), pp. 333–338.

[209] G.J.J. Warmerdam, R. Vullings, C. Van Pul, P. Andriessen, S.G. Oei, and P.F.F. Wijn. "QRS classification and spatial combination for robust heart rate detection in low-quality fetal ECG recordings." In: *Engineering in Medicine and Biology Society (EMBC), 2013 35th Annual International Conference of the IEEE*. IEEE. 2013, pp. 2004–2007.

[210] N.A.M. De Beer, P. Andriessen, R.C.M. Berendsen, S.G. Oei, P.F.F. Wijn, and S.B. Oetomo. "Customized spectral band analysis compared with conventional Fourier analysis of heart rate variability in neonates." In: *Physiological Measurement* 25.6 (2004), p. 1385.

[211] S. Min, H. Ko, and C. Kim. "Power spectral analysis of heart rate variability during acute hypoxia in fetal lambs." In: *Acta Obstetricia et Gynecologica Scandinavica* 81.11 (2002), pp. 1001–1005.

[212] J. Pardey, M. Moulden, and C.W.G. Redman. "A computer system for the numerical analysis of nonstress tests." In: *American Journal of Obstetrics & Gynecology* 186.5 (2002), pp. 1095–1103.

[213] N. Michaan, Y. Baruch, M. Topilsky, S. Amzalag, I. Iaskov, A. Many, and S. Maslovitz. "The effect of glucose administration on perceived fetal movements in women with decreased fetal movement, a double-blinded placebo-controlled trial." In: *Journal of Perinatology* 36.8 (2016), pp. 598–600.

[214] J.B. Derks, E.J.H. Mulder, and G.H.A. Visser. "The effects of maternal betamethasone administration on the fetus." In: *BJOG: An International Journal of Obstetrics & Gynaecology* 102.1 (1995), pp. 40–46.

[215]   D. Subtil, P. Tiberghien, P. Devos, D. Therby, G. Leclerc, P. Vaast, and F. Puech. "Immediate and delayed effects of antenatal corticosteroids on fetal heart rate: a randomized trial that compares betamethasone acetate and phosphate, betamethasone phosphate, and dexamethasone." In: *American Journal of Obstetrics & Gynecology* 188.2 (2003), pp. 524–531.

[216]   B.J. Cohlen, R.H. Stigter, J.B. Derks, E.J.H. Mulder, and G.H.A. Visser. "Absence of significant hemodynamic changes in the fetus following maternal betamethasone administration." In: *Ultrasound in Obstetrics & Gynecology* 8.4 (1996), pp. 252–255.

[217]   E.J.H. Mulder, J.B. Derks, and G.H.A. Visser. "Antenatal corticosteroid therapy and fetal behaviour: a randomised study of the effects of betamethasone and dexamethasone." In: *BJOG: An International Journal of Obstetrics & Gynaecology* 104.11 (1997), pp. 1239–1247.

[218]   M.V. Senat, S. Minoui, O. Multon, H. Fernandez, R. Frydman, and Y. Ville. "Effect of dexamethasone and betamethasone on fetal heart rate variability in preterm labour: a randomised study." In: *BJOG: An International Journal of Obstetrics & Gynaecology* 105.7 (1998), pp. 749–755.

[219]   S. Shenhav, M. Volodarsky, E.Y. Anteby, and O. Gemer. "Fetal acid–base balance after betamethasone administration: relation to fetal heart rate variability." In: *Archives of Gynecology and Obstetrics* 278.4 (2008), pp. 333–336.

DANKWOORD

Met het afronden van dit proefschrift komt er voor mij een einde aan een periode van enkele jaren onderzoek. Het proefschrift is het resultaat van vele samenwerkingen met anderen, zonder wiens hulp afronding niet mogelijk was geweest. Graag wil ik hier een aantal mensen persoonlijk bedanken.

In de eerste plaats wil ik mijn promotoren, prof. Jan Bergmans en prof. Guid Oei, bedanken voor de mogelijkheid die ze mij hebben gegeven om aan dit onderzoeksproject deel te nemen. Jan, ik ben bijzonder dankbaar voor je persoonlijke betrokkenheid bij mijn onderzoek, juist op de momenten dat het nodig was. Ik heb veel gehad aan je input over onderzoeksvragen, het bespreken van resultaten en het corrigeren van manuscripten. Naast je inhoudelijke kennis gaf het me een prettig gevoel dat ik altijd even binnen kon lopen voor advies. Beste Guid, ik wil je bedanken voor de energie en het niet-aflatende enthousiasme waarmee je onderzoek doet. Jouw houding heeft een motiverende werking op je omgeving en de creativiteit waarmee je lopende onderzoeken verder helpt en nieuwe onderzoeken opzet is bewonderenswaardig.

De totstandkoming van dit proefschrift was nooit gelukt zonder de bijdrage van mijn beide copromotoren dr. Rik Vullings en dr. Judith van Laar. Jullie waren al bij mijn afstuderen betrokken als begeleiders en mede dankzij jullie ben ik begonnen aan dit mooie promotietraject. Rik, ik wil je in de eerste plaats bedanken voor je vertrouwen om me tijdens mijn promotie mijn eigen weg te laten kiezen. Ik heb altijd respect gehad voor je vermogen om ingewikkelde technieken begrijpelijk te verwoorden en voor de snelheid waarmee je nieuwe informatie in een juiste context weet te plaatsen. Ik ben ervan overtuigd dat veel van wat ik van je geleerd heb goed van pas zal komen in mijn verdere carrière, al had ik je ervaringen van 'een-periode-thuis-zitten-na-een-ongeluk' liever niet overgenomen. Ik wil je ook bedanken voor alle gezelligheid naast het werk. Je hebt altijd wel wat te melden, al is dit soms beperkt tot het opsommen van 'bekende' mensen uit Venray. Judith, jou wil ik bedanken voor je bijdrage aan dit proefschrift op klinisch gebied. Met jouw kennis over het foetale ECG heb je altijd kunnen helpen met de interpretatie van resultaten. Om er zeker van te zijn dat mijn werk fysiologisch correct was, kon ik het altijd naar jou doorsturen. Mede door onze meetings ben ik me bewuster geworden van mijn eigen positie ten opzichte van mensen met een andere achtergrond. I also thank dr. Lars Schmitt for his contributions in our monthly meetings at Philips and for evaluating my manuscripts from an industrial point of view.

I thank prof. Riccardo Barbieri, prof. Diogo Ayres-del-Campos, and dr. Pieter Harpe for the efforts they made in reading the thesis and for sitting on the committee at the PhD defense.

The research project that resulted in this thesis was funded by the IMPULS-project. I gratefully acknowledge the support given by the project and would like to express my gratitude to all supervisors involved who made this collaboration possible. In particular, I like to thank my fellow PhD's from IMPULS; Deedee, Germaine, Jan, Janne, Mark, and Rohan for the so-called PIMP-meetings, and, in particular, Paul for the great trip we made in Florida.

That brings me to my valued colleagues in the Signal Processing Systems group. First of all I want to thank Massimo for organizing the Bm/d events, which are a great way to get to know your colleagues outside the office. Many thanks also go to my other colleagues with whom I had the pleasure of working with directly, such as Pierre, Lin, Salvatore, Aline, Eleni, Gabriele, Linda, Marina, and Michiel. In this regard I also want to thank Chiara, Libertario, Ruud, Simona, Anastasiia, Celine, Federica, Nienke, and Rogier for all these years of pleasant lunches, fun at the Bm/d events, and other after-work drinks we shared together. Ook wil ik Carla en Marieke bedanken die altijd klaarstaan om te helpen en zelfs een koffie-momentje hebben ingelast om, voor wie wil, op een gezellige manier wat Nederlands bij te leren.

Mijn dank ook aan alle onderzoekers en semi-artsen die hebben geholpen met het uitvoeren van de metingen en natuurlijk ook aan alle moeders die aan het onderzoek hebben deelgenomen. In het bijzonder wil ik Kim bedanken voor onze samenwerking aan hoofdstuk 8. Ik vind het knap hoe je naast je werk als arts-assistent en bouw van je eigen huis toch zo vlot je promotie hebt kunnen doorlopen. Beatrijs en Olenka wil ik bedanken voor hun bijdrage aan de datasets die gebruikt zijn in hoofdstukken 5 en 6. Beste collega-onderzoekers uit de groep FUNdamentele Perinatologie, ook jullie wil ik bedanken voor alle gezellige en inspirerende avonden tijdens de FUN-meetings bij Guid thuis. De laagdrempelige omgang geeft een unieke mogelijkheid voor multidisciplinaire samenwerking. Nanette, bedankt voor de gastvrije ontvangst en alle etentjes tijdens de FUN-meetings.

Tijdens het laatste jaar van mijn promotie is het werk dat ik voor Nemo Health-care heb gedaan een welkome afwisseling geweest van het schrijven van papers en het proefschrift. Ik ben Rik, Chris, Bas en Hans dan ook erg dankbaar dat ze me de kans hebben gegeven om mijn kennis gelijk in de praktijk te kunnen toepassen. Verder ook dank aan alle andere collega's; Michiel, René, Anne, Aron, Ilza, Joni en Nenad (ofwel Jonad), Marc-Antony en Ralph voor de gezellige tijd samen bij Nemo. Het is mooi om te merken dat met goede samenwerking zo veel mogelijk is in zo weinig tijd.

Het is natuurlijk fijn om leuke collega's te hebben, maar het leven is nog leuker dankzij alle vrienden en familie die me de afgelopen jaren de nodige afleiding hebben gegeven van mijn werk. Om te beginnen wil ik Ronald bedanken voor de mooie reizen de we hebben gemaakt, van verloren Inka-steden tot Tibetaanse hutten. Daarnaast wil ik Henk, Steven en Tim bedanken voor de welkome avondjes speciaalbier-drinken! Ook mijn studievrienden uit Nijmegen, Bas, Frank, Guus, Han, Martijn, Remco en Sjoerd wil ik bedanken voor alle top

avonden en de weekendjes om iedereen door heel Europa op te zoeken. Spelers, oud-spelers en stafleden van mijn voetbalteam bij Trekvogels wil ik bedanken voor alle zaterdagmiddagen en -avonden, weekendjes en vele activiteiten, die maken dat ik werk in het weekend even volledig los kan laten.

Margo, Bert en Jes, ik heb het maar getroffen met jullie als schoonfamilie. Zuid-zuid-zuid Limburg voelt als een tweede thuis en de weekenden bij jullie en op zondag bij de Oma zijn voor mij momenten om even bij te komen. Dankzij jullie heb ik naast theoretische kennis ook mijn praktische vaardigheden bijgespijkerd!

Lieve pap en mam, ik heb veel aan jullie te danken. Ik ben opgegroeid met jullie onvoorwaardelijke steun. Ook ben ik dankbaar voor de nooit ontbrekende interesse in waar ik mee bezig ben. Met jullie kan ik het inhoudelijk over alles in de wereld hebben, zodat ik zeker weet dat ik voor advies bij iemand terecht kan. En Maud, als grote zus heb je me altijd op sleeptouw genomen en ik hoop dat onze kinderen net zo met elkaar kunnen spelen. Wat fijn dat jij, Hugo en grote zus Vita zo om de hoek wonen!

Lieve lieve Chan, als laatst maar eigenlijk op de eerste plaats wil ik jou bedanken voor de afgelopen jaren die we samen hebben gedeeld. Ik ben je erg dankbaar voor je steun tijdens mijn promotie onderzoek en vooral ook voor je geduld in de laatste drukke maanden tijdens het afronden van dit proefschrift. Wat hebben we in al die jaren veel meegemaakt: van verre reizen, tot weekendjes weg of gewoon een dagje toeren, ik had het voor geen goud willen missen. De afgelopen twee jaar is er veel veranderd, eerst een huis gekocht en opgeknapt, daarna de geboorte van onze kleine Mesam. Lieve Mesam, jouw vrolijke lach brengt ons onbeschrijfelijk veel geluk! Wat ben ik trots op ons gezinnetje en ik vind het dan ook heel bijzonder dat ik jullie hartsignalen voor de kaft van mijn proefschrift heb kunnen gebruiken. Ik kijk uit naar de jaren die voor ons liggen en wat we nog allemaal samen gaan beleven.

- Guy Warmerdam

ABOUT THE AUTHOR

Guy Warmerdam was born in Nijmegen, the Netherlands, in 1988. He received his BSc. degree in Physics from the Radboud University Nijmegen in 2009. After receiving his bachelor, he started his master Applied Physics at the Eindhoven University of Technology, where he received the MSc. degree with distinction cum laude in 2012. Since 2013 he has been a PhD student within the IMPULS project, a joint project between the Eindhoven University of Technology, the Máxima Medical Center, and Philips Research Eindhoven. The results of his PhD project are described in this dissertation. Since April 2017 he has worked as a signal processing specialist for Nemo Healthcare B.V., where he worked on the development of an unobtrusive fetal monitoring system. In Februari 2018 he started as a medical physicist in training at the department of radiation oncology in the Radboudumc Nijmegen.